Czech Technical University in Prague

Faculty of Mechanical Engineering

Department of Automotive, Combustion Engine and Railway Engineering

Master Thesis

Design of rear wheel suspension for a city car sharing vehicle

Supervisor: Ing. Václav Jirovský, Ph.D.

Bc. Petr Vácha

2019

Task

Annotation

Author:	Bc. Petr Vácha
Title:	Design of rear wheel suspension for a city car sharing vehicle
Academic year:	2018/2019
Programme:	Master of Automotive Engineering
Major:	Advanced Powertrains
Department:	Department of Automotive, Combustion Engine and Railway Engineering
Supervisor:	Ing. Václav Jirovský, Ph.D.
Abstract:	This thesis consists of research on small city vehicles and prototypes, calculations of longitudinal dynamics of a vehicle and design calculations of a foldable rear suspension system. It also includes a CAD model of the rear suspension made in Catia V5 and dynamic tests in CarMaker.
Keywords:	Electric car, suspension, design, vehicle dynamics, foldable car
Number of pages:	111
Number of pictures:	159
Number of tables:	26

Guideline:

Car sharing can be seen as a partial solution for decrease of congestion in cities. For achieving such goal, not only car sharing could be a solution, but vehicle used in car sharing system shall match specific requirements. One of such requirements is the optimum size of the vehicle, which shall not occupy same space as current vehicles in all driving situations – when parked or when driving at maximum city speeds. Therefore, the vehicle has to be short enough to fit in a single parking space width, and narrow enough to fit two vehicles in single driving lane one next to another. Design of the vehicle has to implement some folding-like mechanism, which would allow shortening overall vehicle's length when parked but will not negatively influence vehicle's stability when driving. Perform a literature research aiming on visions of small city vehicles including but not limited to powertrain, package, driving specifics and suspension design. Design a concept of rear driven suspension powered by an electric motor with focus on i.e. folding the vehicle into smaller parking space, while maintaining acceptable driving characteristics in speeds up to 100 km/h.

Declaration

I hereby declare that I have completed this thesis independently and that I have listed all the literature and publication used in accordance with the methodological guidelines about adhering to ethical principles in the preparation of the final thesis.

In Prague.....

Bc. Petr Vácha

Acknowledgements

I would like to thank my supervisor Ing. Václav Jirovský Ph.D. for patient help with the thesis and my family for support during all my studies.

Table of Content

1. Introduction

Many big cities all around the world are facing a serious problem with overcrowding nowadays. According to research is fifty per cent of the world population living in urban areas and this number should increase to about two-thirds by the year 2050. [33] This fact can bring many issues, especially with traffic. Although there is a well-developed public transportation system especially in Europe, there will still be some need for personal mobility. As a solution to this situation could be car sharing. This concept has been already implemented in many towns including Prague. It can reduce the demand of people to have their own car as they can use shared one only when they actually need it. This can help to solve an issue of lack of parking spaces, but this programme is still in its beginning and it must be more widely used to notice a significant difference. However, we also have to think about our environment. Exhaust gases produced by vehicles powered by internal combustion engines form in higher concentrations so-called smog which covers skies of polluted cities. In this case, the breathing of this air can cause many health issues. Some of the cities of Europe are going to ban entry of ICE-powered cars (especially with diesel engines). The electric powertrain is able to produce locally zero emissions and at the moment it can be seen as the only one to satisfy future limits of emissions in city centres.

The task of this thesis gave fundamental properties of a future city vehicle which is suitable for a car sharing programme. It should be small enough to save space when it is parked. The objective is to keep the length of the vehicle shorter than is the width of a single parallel parking space. This can allow the vehicle to park into parallel parking space perpendicularly to the road. It also should be narrow enough that two of these vehicles can fit next to each other in only one lane in case of traffic jams. Required top speed should reach at least 100 km/h. Having taken these requirements into an account, it won't be possible to combine the short dimensions with dynamic stability. The vehicle has to be equipped with a folding mechanism to satisfy both requirements. While parking, the car will be shortened to save space and before the ride, it will be prolonged to get longitudinal stability necessary for high velocities on a highway. According to planned environmental regulations, it should be powered by an electric motor. As this vehicle is meant to be homologized as a quad in LE category, it mustn't exceed the maximal rated power of 15 kW. [5] The latest research in automotive engineering focuses on autonomous driving which would be implemented in this vehicle too. This feature would widen a range of possible usage of this car. The user would decide if he wants to drive or let the car drive on its own. For example, after being driven by a user, the car can go to another one or it can park itself at the most convenient location. In autonomous mode, it could work as a delivery service or taxi. There are varieties of possible applications. However, autonomous driving has been being developed by car manufacturers for many years but they are still postponing its application into production car for technical and legal reasons. It is not possible to determine at the moment when it will be available in production cars. The main task of this thesis is to design a rear suspension system of such a city vehicle of the future. The rear axle will be driven by an electric motor placed in the rear. The conception of the folding mechanism will be determined to set constraints for a rear suspension system. Research on production and prototype city cars will be made to study different types of rear suspension. Kinematics of the designed suspension will be imported to vehicle dynamics test software to verify the dynamic stability of the vehicle during the ride.

2. Research of small city vehicles

At the beginning of the project, it was necessary to make research on production vehicles and project cars. We needed to know what is offered at the market to be able to design a vehicle that is better in as many aspects as possible. This section is divided into two parts. At first, we are going to have a look at production cars which are currently available at the market. Each of them represents a slightly different point of view of a small city car and we are also going to show different types of rear suspension used in this segment. The second part will show us project cars which never have been produced. As there never has been a foldable car available at the market, we need to get a source of inspiration across concept cars.

2.1. Production city cars

2.1.1 Renault Twizy

In 2012, before an electric boom in the automotive industry, *Renault Twizy* was introduced to the market and opened a new category of city cars. This vehicle is the closest mass-produced car to our concept and is the main source of inspiration for this project. Its conception still matches requirements for a city car in all aspects. It offers space for one driver and one passenger, seated behind the driver. The passenger put his legs around driver's seat which is similar to a motorcycle seating. This architecture helped to keep the overall length of this vehicle as short as possible. Side doors are only an optional accessory and usually, they aren't equipped with any windows. It also doesn't have any heating or air condition which makes it as cheap as possible. The basic version of *Renault Twizy* called *Expression* costs in the UK 6690 £ (exclude mandatory battery hire which costs 45-67 £ per month, depends on conditions of hire). [19] It is not sold in the Czech Republic anymore, but it used to be offered from 319 900 Kč (tax incl.). [55]

Its rear axle is driven by an asynchronous induction electric motor produced by *Iskra* (now is part of *Mahle*) and delivers 12.5 kW of maximum power and 57 Nm of torque, while supplied by a voltage of 20V (there is also a low power version of *Twizy* with the limited velocity of 45 km/h). This power flows then through a transmission with a reduction gear with a gear ratio of 9.23. With this configuration, *Twizy* can reach up to 80 km/h and accelerate from 0 to 45 km/h in 6.1 seconds. Electric energy is stored in a Li-Ion battery with a capacity of 6.1 kWh and a voltage of 58 V. It weighs approximately 75kg and according to a brochure, it should result in a theoretical range of 100km. According to some reviews the real range reaches around 70 – 80 km. [55] The weight of *Twizy* is 474 kg. [19]

Figure 1 – Renault Twizy (2012). [18]

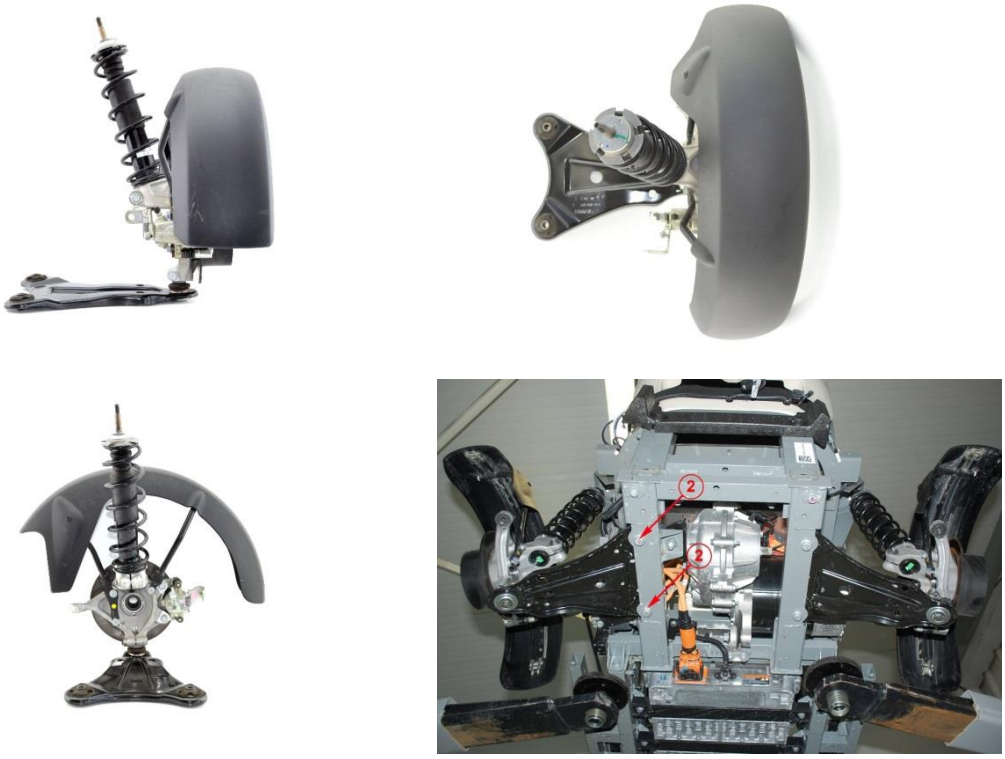

Figure 2 – Rear MacPherson suspension of Renault Twizy. [18]

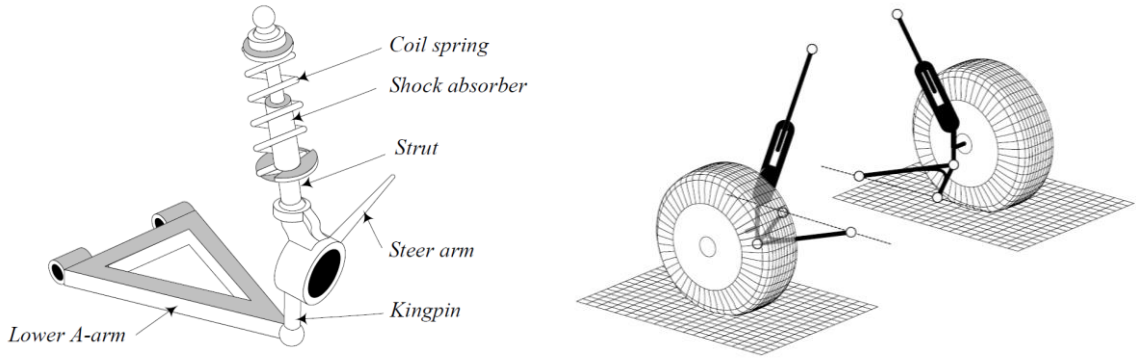

Figure 3 – MacPherson suspension. [4]

The suspension system was made in respect of the lowest cost. In front and rear, it uses a **MacPherson** suspension and they share some of the parts. MacPherson strut is currently the most used front suspension across many categories of cars. It is quite rare to see this kind of suspension in the rear because of the high vertical space requirement and limitation of boot volume. MacPherson suspension was derived from double wishbone suspension, but the upper arm was replaced with a linear joint which allows getting additional interior space. The lower arm is usually mounted to the chassis with rotational joints. At the other side of the lower arm, there is a spherical joint with a steering knuckle to be able to perform steering. A damper is usually combined with a spring and it is mounted to the chassis and to the steering knuckle. It also works as a guidance of the wheel. In comparison with normal dampers, it must have stronger construction as it has to bear transversal loads. In the contact of piston-cylinder and rod-guidance there could be higher friction while braking, accelerating or cornering. It could lead to blockage of the damper. Sometimes the spring is put a little tilted to reduce transversal forces. If this suspension is used in front it also has to have an axial bearing at contact place with chassis. This helps to avoid an additional torsional load of the spring as the wheels are turning. Both MacPherson suspensions in *Twizy* are equipped with antiroll bars which help to roll stability of the vehicle in corners. [1]

Figure 4 – Rear antiroll bar (stabilizer) of Twizy. [18]

2.1.2 Jiayuan City Spirit

As the Chinese automotive industry is rapidly evolving, we should be aware of cheap competition products coming from this Asian country. As an example of such a vehicle is *Jiayuan City Spirit*. This car is used by a Czech car sharing company called *Re.volt* which operates in Prague. It can be easily rented by a smartphone application for a fixed price of 6 Kč/min. Even in the city centre, parking is simple because electric cars are also allowed to park for free in zones for local residents. It has space for two people, seated side by side and a small boot. It's equipped with accessories like air condition, rear parking camera, Bluetooth handsfree or heating. It could be bought in the Czech Republic and the price for the more powerful version with 7.5 kW motor is 309 800,- Kč (tax included) with acid-lead batteries or 399 800 Kč (tax included) with Li-ion batteries. [21], [22]

Figure 5 – Jiayuan City Spirit.

The powertrain contains an electric asynchronous motor with the power of 7.5 kW which should be enough to go 80 km/h. There are two battery options. The first is a lead-acid accumulator or the second is a Li-ion battery. It provides a charge of 140Ah, a voltage of 72 V and the resulting capacity of 10.1 kWh. Theoretically, according to manufacturer it should be enough to travel 120 km per one charge, but *Re.volt* reckons with about 70km. [20], [22]

The front suspension is a standard MacPherson strut without any stabilizer. Rear suspension type is a **trailing arm**. This is another type of the rear independent suspension. In this case, it also doesn't use any stabilizer (according to the manufacturer's website [20], the standard rear suspension is a torsional strut and a trailing arm is optional). As both front and rear suspension systems aren't equipped with any stabilizer, a doubtful question could be asked about overall vehicle stability. It consists of two longitudinal trailing arms which are independently moving around two rotational joints. The axis of movement of the arms is perpendicular to the direction of drive. This suspension saves space and can keep the floor of the boot very low. It has a disadvantage of higher tilting of the chassis while cornering. [1]

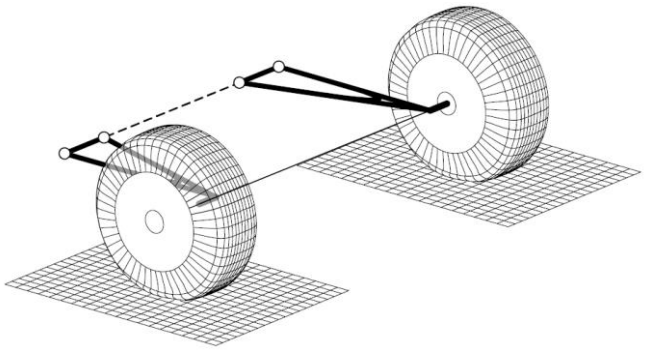

Figure 6 – Trailing arm suspension. [4]

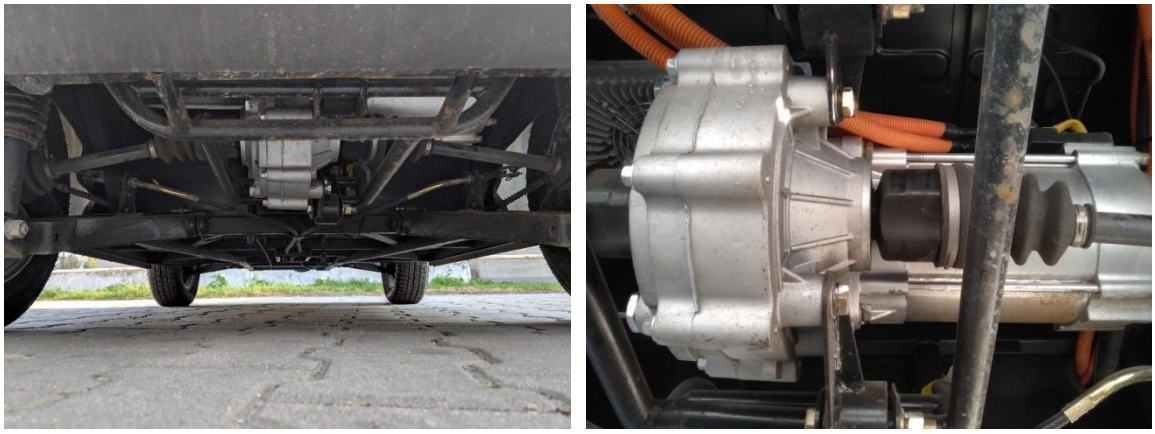

Figure 7 - Jiayuan City Spirit, left: rear suspension overview, right: detail on a motor and differential.

Figure 8 - Jiayuan City Spirit, left: rear left trailing arm suspension detail, right: front left MacPherson suspension.

To get also practical experience with a small city vehicle, we rented it using the *Re.volt* application. The car provides surprisingly high acceleration from the stall which could be useful at crossroads. However, as it gets some speed it becomes very lazy. It could be practically used up to velocities around 50 km/h which can be relatively easily achieved. We couldn't get to the maximum speed of 80 km/h in a reasonable time. Sometimes there are some noticeable noises and vibrations coming from the suspension system. The steering is quite imprecise and misses some feedback from the road. While cornering the vehicle tilts a lot and it is not safe to drive in corners at higher speeds than approx. 30 km/h. Brake test proofed absence of ABS (Anti-lock Brake System). In summary of the driving test, the vehicle is easy to drive, provides enough acceleration till city speed limit of 50 km/h. The suspension system is quite soft which could be beneficial in terms of cushioning, but there are still some strong surges and vibrations coming to the chassis. Cornering ability is very poor with high tilting at higher speeds and can surprise a driver who is used to a standard car. An additional stabilizer at least in front or ideally in both axles would significantly help with the rolling stability of this vehicle.

2.1.3 Smart ForTwo

The first generation of *Smart ForTwo* was introduced to the market in 1998 and made a revolution in small city cars. At that time, it was the smallest mass-produced car with a length of 2.5 meters. [25] Since 2015, the third generation has been sold and it has been produced in cooperation with *Renault* to help to reduce the cost. Many parts of *Smart ForTwo* and *Renault Twingo* are shared. It can be bought with gasoline naturally aspirated three-cylinder 1.0 engine with a power of 52 kW (this version was used for benchmarking), gasoline turbocharged three-cylinder 0.9 engine with a power of 66 kW or with an electric powertrain. [24], [23]

Figure 9 – Smart ForTwo 1.0 (2015). [18]

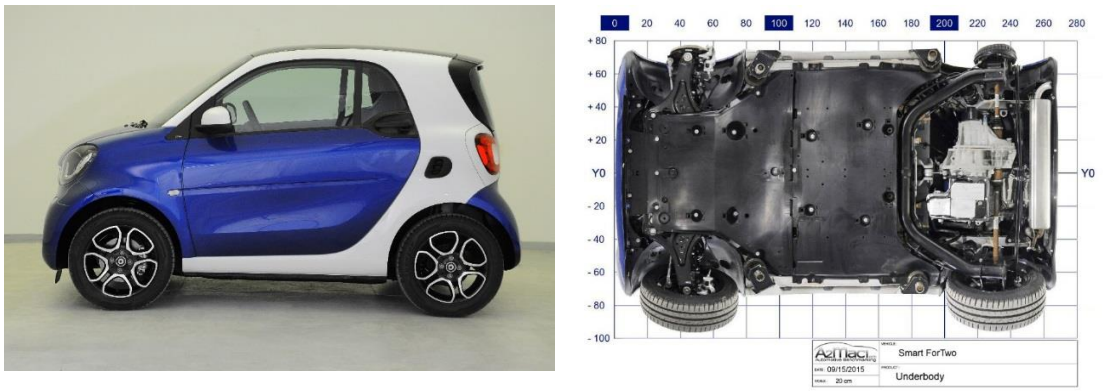

Figure 10 – Smart ForTwo 1.0 (2015). [18]

The electric version is called *Smart EQ ForTwo* and has a synchronous electric motor with permanent magnets with a nominal power of 41 kW (could be overloaded to 60 kW) and maximal torque of 160 Nm. There is a Li-ion accumulator with a capacity of 17.6 kWh which is declared to be enough to go up to 160 km. It the Czech Republic it's offered from the price of 470 165 Kč (tax included). [23]

Smart's rear wheels are driven, and the powertrain is placed in the rear, under the boot. For this architecture was implemented a rare type of a rear suspension system called **De-Dion**. It was a dominating rear suspension system is Formula 1 series in the '50s and was also popular in *Alfa Romeo* cars in the '80s. It is a special type of a rear dependent suspension system. In this suspension, both wheels are linked together with a rigid axle. It keeps both wheels in the same position related to each other. As both wheels are linked, when disturbance comes to one wheel, the second one is affected too. The simplest type of dependent suspension is a live axle. It is still used for a rear suspension of pickups, vans or off-road vehicles, because of its simplicity and durability. Its main part is a solid heavy axle linking both rear wheels, sprung by coil springs or leaf springs. The torque from the engine is coming to the differential which is housed in the live axle. Opposite reaction torque is arising and causes a lift to one wheel. It leads to unequal behaviour of the vehicle in left and right curves while applying power. The main advantage of De-Dion over the simple live axle is reduced unsprung mass. This has a positive influence to ride comfort and grip. The differential and even brakes could be mounted directly to the frame which also eliminates the torque reaction. The rigid axle of De-Dion is mounted to the frame using a spherical joint. To guide the axle in vertical direction there could be for example Watt's linkage. In *Smart's* case, there is a cheaper mechanism consisted of two arms and a beam. Both arms have rotational joints with the beam, but left arm's joint is mounted to the groove which allows also a linear motion. It requires the usage of quite expensive CV (constant velocity) joints as the wheels are relatively moving to the differential. [1]

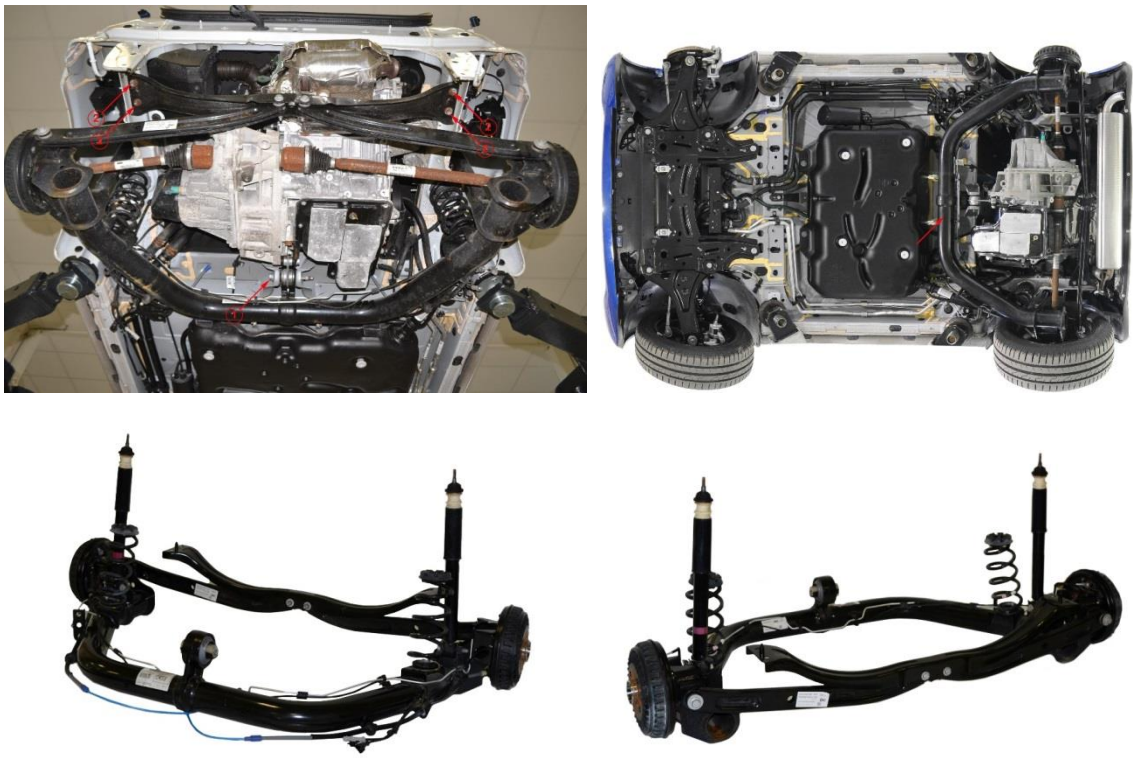

Figure 11 – Smart ForTwo 1.0: Rear De-Dion suspension. [18]

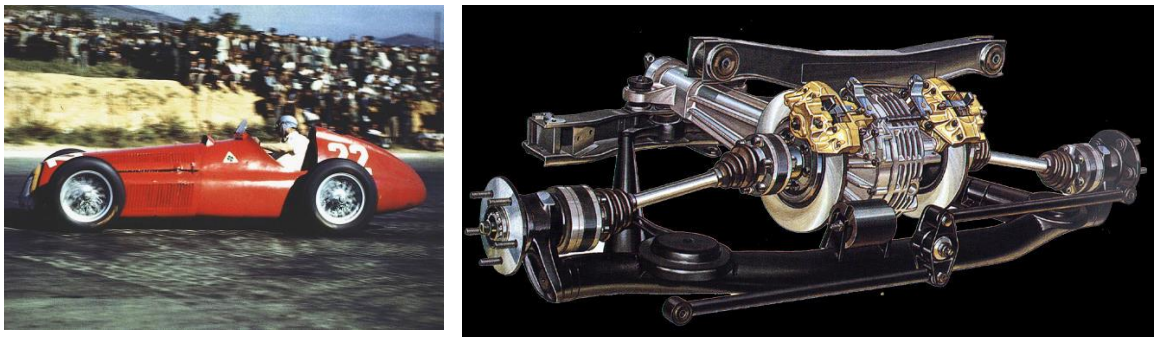

Figure 12 – left: Alfa Romeo 159 (1950) [26], right: Alfa Romeo De-Dion rear suspension from the '80s. [28]

Figure 13 – Live axle with leaf springs. [27]

2.1.4 Volkswagen e-UP!

As a representant of 5-door small standard-sized cars was taken *Volkswagen e-UP!*. Engineers from Wolfsburg took the standard *VW UP!* driven by a gasoline one-litre engine and rebuild it to an electric vehicle. The permanent magnet synchronous motor with the power of 60 kW and power electronics is located under the bonnet instead of the engine. Battery with a capacity of 18.7 kWh was placed in the floor, middle tunnel and fuel tank position. Currently, it is not available anymore at the Czech market, but it was offered for the price of 599.900 Kč (tax included). [29]

Figure 14 - Volkswagen e-UP! [18]

The suspension system in this vehicle is a standard for small cars, hatchbacks and even cars from the lower middle class. Front suspension is a MacPherson strut, and, in the rear, there is a **torsion beam suspension**. It is classified as a semi-independent suspension. Actually, it consists of two trailing arms and one torsional beam. Left and right wheel can move in respect to each other, but they are connected with a torsional soft beam (but with high bending stiffness) which works as a stabilizer and control mutual displacements. This suspension is also easy to manufacture as it contains only two rotational joints (with transversal axis) mounted to the frame. It makes it easy to assemble and cheap to maintain. The build-in space requirement is quite low what can result in a more spacious interior. Weight of the unsprung mass is reasonably low. As it contains a torsion beam there is no need for any additional stabilizer. [1]

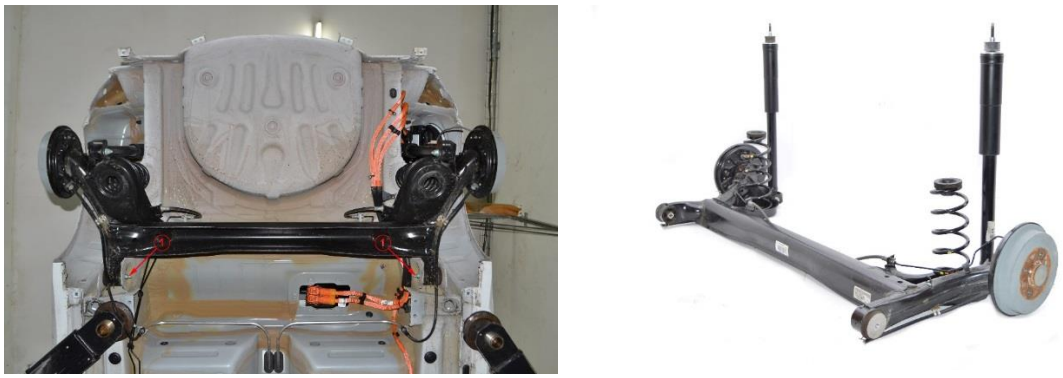

Figure 15 – Torsion beam suspension of VW e-UP! [18]

Usually, a torsional strut is not used as a driven axle. If the engine is located in the rear, the space for it is very limited. It also requires CV joints which can compensate displacements of wheels caused by deformation of the axle. If the engine is laid in the front, there is an issue of finding a way for driveline shaft to the rear. In figure 16 there is an exception of a driven torsional strut suspension in *Suzuki Vitara 4WD*. It is obvious that this solution has to pay the price of limiting of inner space as the mounts to frame must be located higher. However, it saves costs in comparison with a multilink suspension. [31]

Figure 16 - Suzuki Vitara - driven rear torsion beam suspension. [31]

2.2 Concept cars

2.2.1 Hiriko

In 2003, *Massachusetts Institute of Technology* came up with a project called *CityCar*. It showed an idea of a shared city vehicle of the future that should have solved an issue with overcrowded traffic. Lately, in 2012 the real size prototype was built by a Spanish company called *Hiriko Driving Mobility* according to the MIT design. This project was supported by foundations of EU and government of Spain, but unfortunately, the company collapsed for corruption reasons and it ended with only one prototype. [34]

Figure 17 – Hiriko. [35]

Figure 18 – Hiriko. [35]

Hiriko is an electric foldable car with space for two people seated side-by-side. The front windshield can be opened and allows the driver and passenger to get in and out. The length can be changed in a range from 1.5 metres to 2.5 metres. This helps to fit three of these vehicles to a single parking space. It is powered by four in-wheel electric motors. Overall nominal power reaches 15 kW and it boasts acceleration from 0 to 50 km/h in just 4 seconds. The maximum velocity is electronically limited to 60 km/h. The theoretical range with a full battery can reach up to 120 km. All of the wheels are steerable which allows it to spin at one spot or to move sideways. This feature makes it really easy to park everywhere. It weighs only 450 kg and satisfies the homologation for a quad as well as for example *Renault Twizy*. [32], [33]

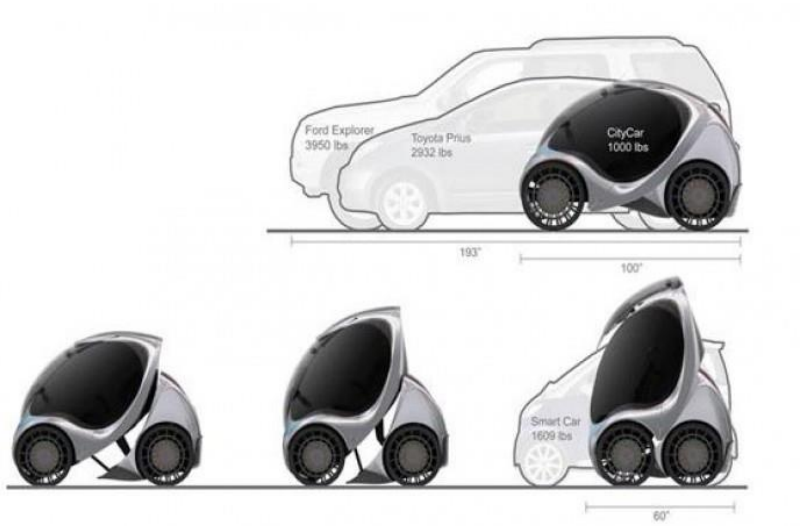

Figure 19 – Folding mechanism of Hiriko. [33]

2.2.2 Renault Zoom

Renault Zoom is a concept car made by *Renault* and *Matra* and was introduced at the Paris Motor Show in 1992. There was no intention to bring this project to production, but it came up with some possible ideas for a future city car. It has a foldable rear axle with a change in length from 230 cm to 265 cm. It has space for a driver and a passenger. There is a pair of scissor doors to make it easy to get in or off in the tightest parking spaces. There is an electric motor with a power of 25 kW which results in acceleration 0-50 km/h in 6 seconds and a top speed of 120 km/h. Nickel-Cadmium battery promises a range of 150 km and it weighs 300 kg. Total weight of the vehicle is 800 kg. [36], [37], [38]

Figure 20 – Renault Zoom. [36]

2.2.3. EvoCare

EvoCare is a concept of a foldable three-wheeler which was made by *Graz University of Technology* in 2016. [39] It uses an unconventional architecture of a cabin for three people, two of them seated side by side in the front and the last one behind them. There are two wheels in the front and one in the rear. The rear wheel is driven and connected to a propulsion module which also contains a battery, electric traction motor, gearbox and suspension. This module can be folded which results in a change of overall length from 3100 mm in a driving mode to 2100 mm in a parking mode. The aim was to design a low-cost and robust solution without any additional actuators. This required the development of a smart kinematics system, which is actuated by the electric traction motor. The folding process is started by braking of the front wheels and unlocking the propulsion module. The rear wheel is powered by the electric motor and the propulsion module moves forward, lifting the cabin up until it reaches the fixation spot for the parking mode. Figure 21 shows the components of the vehicle and its three modes: driving, folding and parking.

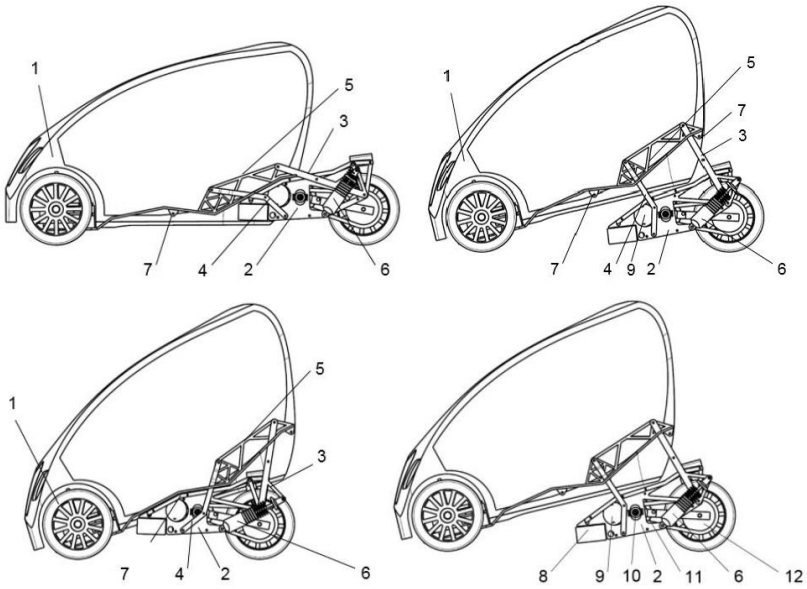

Figure 21 - EvoCare modes and components: cabin (1), propulsion module (2), linkages (3 and 4), main carrier (5), spring and damper (6), spots for fixation (7), battery (8), electric traction motor (9), gearbox (10), drive belt (11), rear wheel (12). [39]

For this kind of folding mechanism, the most crucial thing is the sufficient traction of all tires. According to the equation, the traction force F_x from tires to the road depends on multiplication of normal force F_y acting on the tire and coefficient of friction μ.

$$F_x = F_y \cdot \mu$$

During the folding, a normal force acting on tires is changing as the weight distribution is changing. The vehicle was intended to be able to fold itself with a different number of occupants which also significantly changes the weight distribution. A multibody simulation was calculated to prove whether this mechanism could work (cabin 340 kg, propulsion module: 350 kg, weight per

person: 80 kg). In figure 22 there is a dependency of the longitudinal force F_x and the normal forces F_z (for front and rear wheels) during the folding. In figure 23, on the left side, there is a minimum required coefficient of friction at front wheels. As we can see, the required coefficient increases to high values up to 1.4 which couldn't be normally achieved. Because of that, an additional spring was implemented to the mechanism (figure 27) and on the right side of figure 23, there is a graph of reduced force F_x. Finally, in figure 24 there are minimum required traction coefficients for the front pair of wheels and the rear wheel. With a maximum occupancy of 3 persons, the maximum required coefficient of friction is 0.46 at the rear wheel and 0.57 at front wheels. This means that this folding mechanism can reliably work even on wet tarmac (figure 28). According to the concept, a prototype in scale 1:5 was build and approved the theory (figure 26).

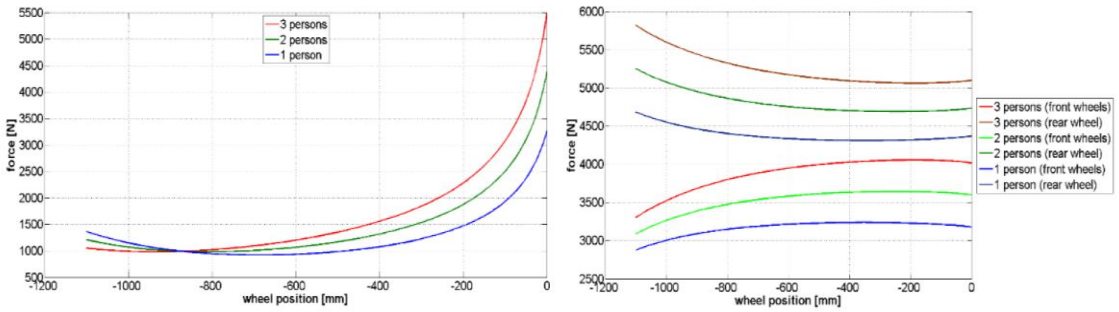

Figure 22 – Left: longitudinal force F_x for folding, right: normal force F_z acting on the 2 front wheels and the rear wheel. [39]

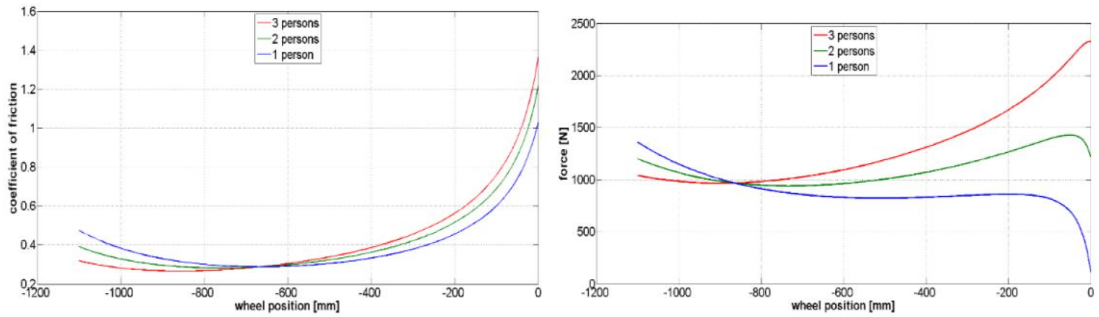

Figure 23 – Left: required minimum coefficient of friction at front wheels, right: reduced force F_x because of spring support in the kinematics mechanism. [39]

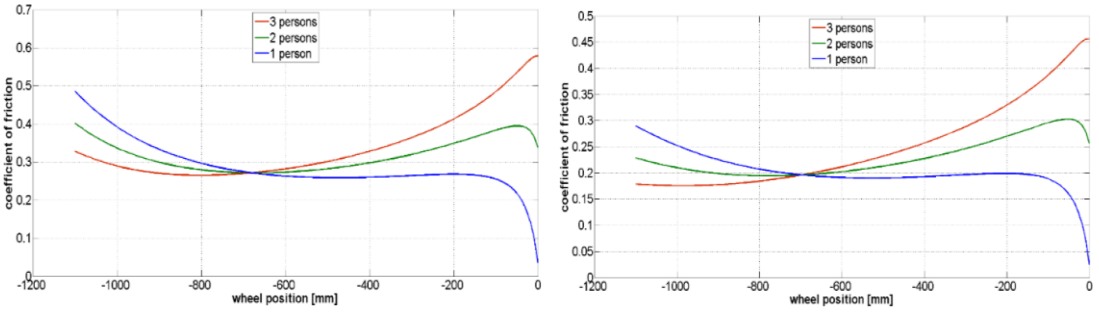

Figure 24 – Required minimum coefficients of friction for successful folding. Left: front wheels, right: rear wheel. [39]

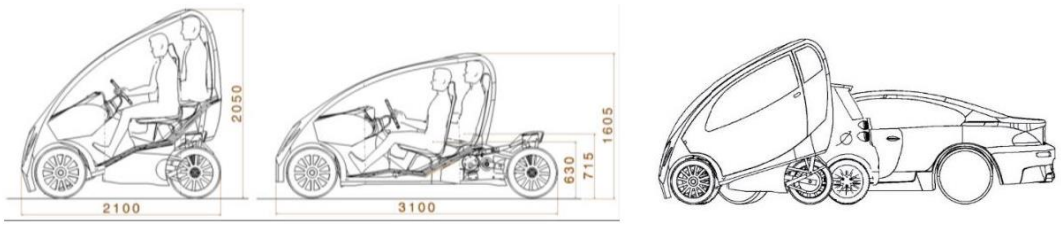

Figure 25 – External dimensions (in mm) and size comparison with Smart ForTwo 2007 and BMW E63 Coupe 2010. [39]

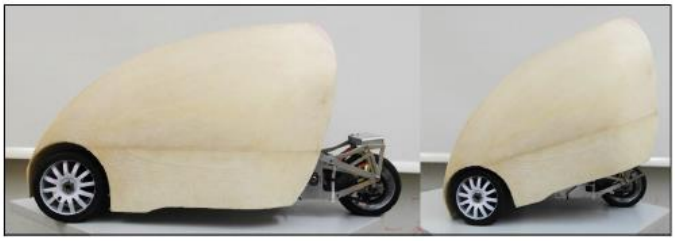

Figure 26 – EvoCare prototype in scale 1:5. [39]

Vehicle Specifications	
Vehicle mass (kg)	751
Lenght (mm)	3133
Lenght shortenend (mm)	2191
Width (mm)	1600
Height shortenend (mm)	2163
Performance (kW)	19,75
Max. speed (km/h)	100
Battery capacity (kWh)	12
Number of seats	3
Luggage space (l)	110

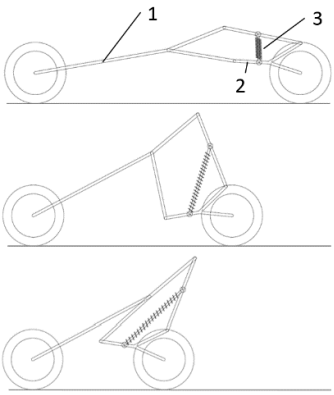

Figure 27 – Initial kinematic scheme of folding mechanism: cabin (1), propulsion module (2), supporting spring (3). [39]

Road Conditions [13]	Bachmann [14]	Mundl [15]	Gustafsson [16]	Mitschke [17]	PC Crash [18]	Barace [19]
Asphalt, dry Concrete, dry Cobblestone, dry	1.05 – 1.2	1.05 - -	1 - -	0.88-1.15 -	0.7 - 0.9	0.9 – 1.2
Gravel, dry	-	0.5[a]	0.5	-	-	0.5
Asphalt, wet Concrete, wet	0.73 – 0.81 0.66 – 0.8	0.85 -	0.7 -	0.7 – 0.95	0.5 – 0.7 (wet) 0.4 – 0.5 (very wet)	0.7 – 0.9 0.65 – 0.8
Asphalt, sandy	-	-	-	-	-	0.5[b]
Asphalt, snow Asphalt, ice (scattered) Asphalt, ice	- 0.18 – 0.38[c] -	0.2 - 0.1	0.3 - 0.1	0.07 – 0.02	0.1 – 0.5 0.05 – 0.25	0.2 – 0.3 0.1 – 0.2

[a] Mean value for loose gravel
[b] Assumed to be in the range of gravel
[c] Harsh ice

Figure 28 – Ranges of friction coefficient on different road conditions, based on a literature review. [39]

2.2.4 Seat Minimó

In 2019 *Seat* introduced an electric concept car *Minimó* which should mix the best of a car and a motorcycle. It looks very similar to *Renault Twizy* and technically it shouldn't be very different. It promises maximum speed of 90 km/h, space for two passengers (seated longitudinally in a line) and a range of 100 km. What is new in comparison with *Twizy* is an autonomous driving and swappable batteries. These features make this vehicle suitable for future car sharing programme as *Seat* also proclaims. Battery swapping makes sense in sharable vehicles and reduces the time to get the full state of charge again. It can also help to avoid fast charging which may be harmful to the battery and requires high power from the electrical grid. [40]

Figure 29 – Seat Minimó. [40]

2.2.5 Casple Podadera

This project of a concept car came from cooperation of Spanish business group *Casple* which is an important supplier for the automotive industry and Spanish renowned designer *Francisco Podadera*. This two-seated vehicle can change its length from 2.3 meters to 1.9 meters. There are not any closer technical details available, but it still can be an inspiration for our project. [41], [42]

Figure 30 – Casple Podadera. [41], [42]

3. Longitudinal dynamics

3.1 Powertrain

In accordance with the Czech act no. 56/2001 [5], the vehicle homologized in category LE mustn't exceed a maximal nominal power of 15 kW. According to the research on production electric city cars, there are mostly used two types of AC electric motors: asynchronous induction motor and synchronous motor with permanent magnet (PMSM).

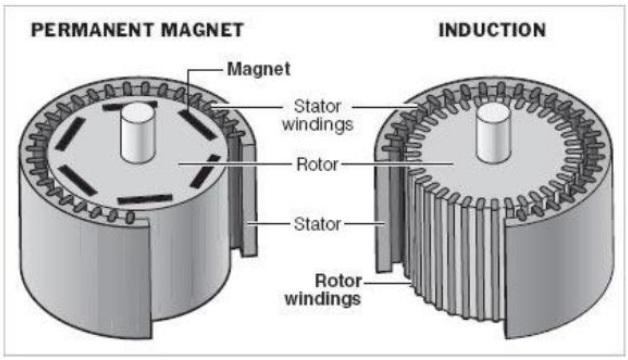

Figure 31 – Construction difference between an induction motor and PMSM [2]

Czech act no. 56/2001:

LE – motored three-wheelers:

- motored three-wheelers – a vehicle with three wheels located symmetrically to the central longitudinal plane, exceeding parameters (volume of cylinders or velocity) of the three-wheeled moped,
- quads different than light ones – the weight in the unloaded state (in case of electric powertrain without batteries) up to 400 kg, in case of cargo vehicle 550 kg, maximal nominal power up to **15 kW**.

Induction motor

An induction (asynchronous) motor consists of two main parts: stator and rotor. The stator has three coil windings (one for each phase) which are based in slots of steel laminations. The rotor is sometimes called "squirrel cage" because its design reminds that.

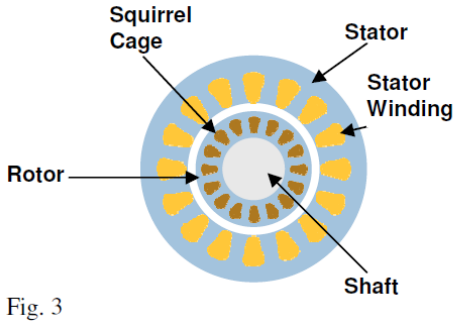

Figure 32 – Parts of an induction motor. [43]

The basic principle behind the functioning of the induction motor is electromagnetic induction. The stator is supplied by AC voltage which produces a rotating magnetic field. Because of Faraday's law of electromagnetic induction, there is induced a current in the rotor. As there is the current flowing in the rotor and it is situated in the magnetic field, Lorentz force starts the rotor to rotate. The synchronous speed of the rotor (speed of rotating magnetic field) can be calculated according to the following formula:

$$n = \frac{60f}{p}$$

Where n is synchronous speed in rpm, f supply AC voltage frequency and p number of pole-pairs. However, in the motor regime, the motor works in a slightly lower speed than is synchronous one. The difference between these speeds is expressed in percentage by slip. In generator regime, the speed of the rotor is higher than synchronous speed.

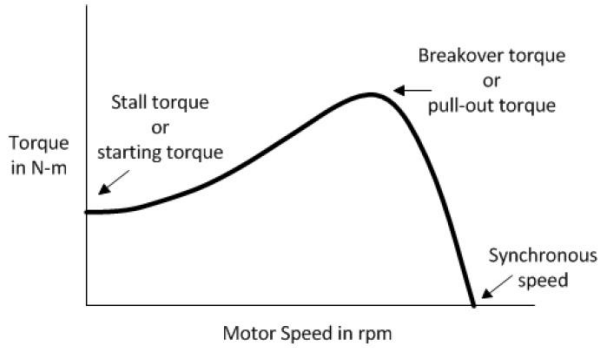

Figure 33 – Characteristics of an induction motor, while supplied by the constant frequency input voltage. [2]

The basic characteristics of an induction motor for single input voltage frequency, as it could be seen in figure 33, is not convenient for a traction motor of an electric vehicle. Because of that, we need a DC-AC inverter (as battery output is DC) with the ability to change its output voltage frequency, thus changing the speed of the rotating magnetic field and varying the speed of the rotor. With this electronic

device, we get a perfect characteristic for a traction motor as it is depicted in figure 34. An induction motor is very popular in the industry for its high reliability and low cost, but it provides lower torque density than PMSM and there are heat losses, hence lowering the total efficiency to about 92 – 93% (figure 35). The advantages and disadvantages are summarized in table 1.

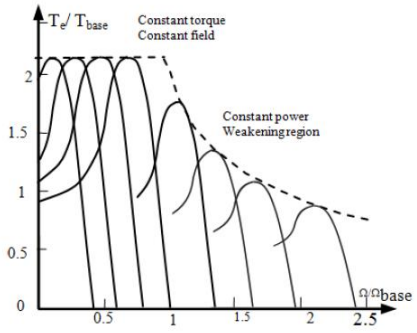

Figure 34 - Characteristics of an induction motor, while supplied by different frequency input voltages. [2]

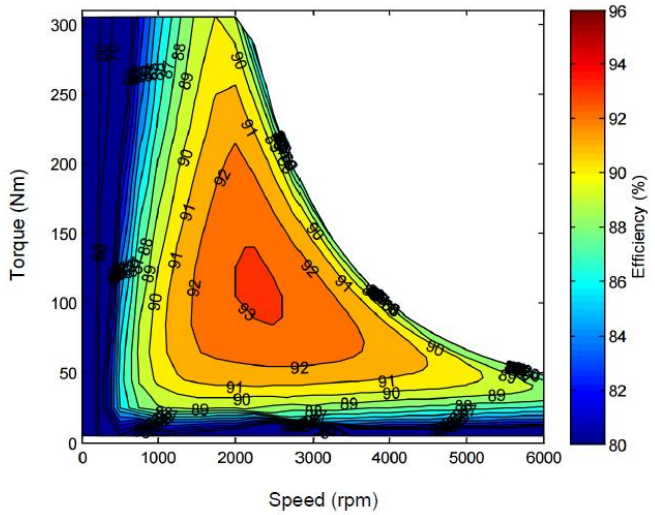

Figure 35 – Efficiency map (motor regime) of asynchronous induction motor with copper rotor cage. [2]

Table 1 – Advantages and disadvantages of an induction motor. [43]

Advantages:
+ high max. speed, high range of field weakening
+ low current at no load and part load operation
+ no rare earth metals necessary
+ robust design
+ no hazardous material, easy recycling
+ high safety with low effort
+ low production costs
Disadvantages:
- small torque density higher weight bigger volume
- high current at constant torque
- high power losses in the rotor (hot rotor)

Permanent magnet synchronous motor

The stator of PMSM is built in a similar way as the one of an induction motor. However, the rotor design makes a difference. It consists of permanent magnets which are producing an almost constant magnetic field. Because of the interaction of the rotating magnetic field of stator and rotor's magnetic field, the rotor begins to rotate. In motor regime, the rotor rotates at synchronous speed, because the rotor's magnetic field and rotating magnetic field of the stator are magnetically locked together.

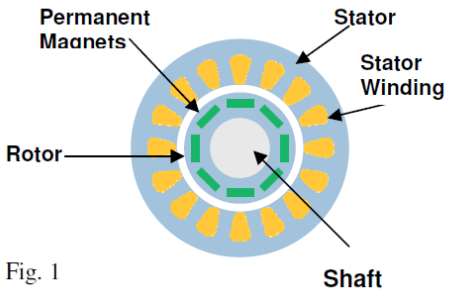

Figure 36 – Parts of PMSM. [43]

PMSM is more expensive, because of the price of rare elements used for permanent magnets. The temperature of permanent magnets must be controlled and kept under the temperature of beginning demagnetization; otherwise, it would significantly affect its function. On the other hand, it works with high efficiency reaching up to 96% (figure 37). In comparison with a similarly powerful induction motor, the PMSM is small and lighter; hence it has higher torque density. It is controlled like the induction motor. These advantages make PMSM popular for usage in modern hybrid vehicles.

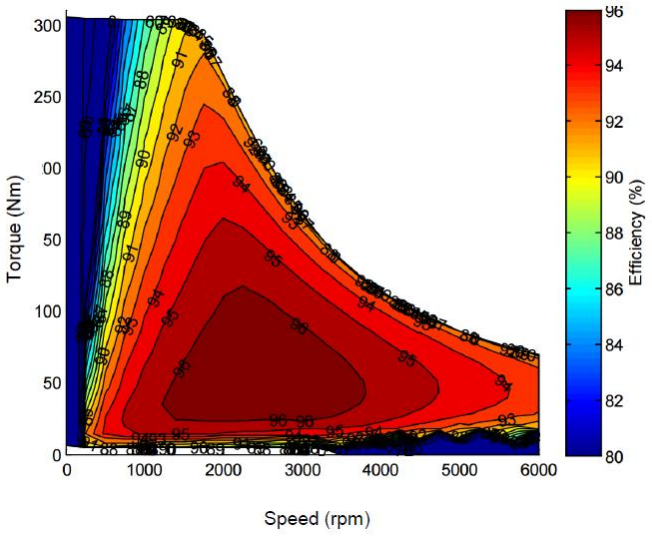

Figure 37 – Efficiency map (motor regime) of PMSM. [2]

Table 2 – Advantages and disadvantages of PMSM [43]

Advantages:
+ high torque density
+ high continuous torque
+ high efficiency
+ low power losses cool rotor temperature up to rated power
+ wide range of constant power
Disadvantages:
- high costs because of rare earth magnets
- efforts in field weakening necessary(field weakening current)
- high induced voltage when operating as a generator
- safety aspects of hazardous material (magnets) higher efforts in manufacturing, service, recycling
- identification of the rotor position necessary
- higher system costs

Motor Decision

Taking into an account all the advantages and disadvantages of both possible electric motors, it seems more suitable to use an asynchronous motor for our purpose. The main reason for this decision is lowering the costs of the vehicle. Both *Twizy* and *Jiayuan* (or even for example *Tesla S*) are using induction motors and both of those cars were made in respect to the lowest manufacturing costs. However, induction motor still can be run with decent efficiency and because of its simple design, it can provide a highly reliable operation. Let's make a comparison of two contrasting induction motors which can meet our requirements. The first one is an unnamed motor from a Chinese company and the second one is produced by a renowned German company, *Bosch*.

We would choose the *Bosch* motor for several reasons. It provides higher rated torque and significantly higher maximum speed (7000 rpm vs 12000 rpm). This can be beneficial for setting a higher gear ratio in a gear reduction transmission, thus getting higher output torque over all speeds of the motor.

Motor Alibaba

Figure 38 – Chinese electric motor. [44]

Table 3 – Properties of a Alibaba motor [44]

Model	GLMI15A4
Rated power [kW]	15
Peak power [kW]	30
Rated torque [Nm]	43
AC supply voltage [V]	144
Max. speed [rpm]	7000
Dimensions (diameter x length) [mm]	230 x 304
Weight [kg]	48

Motor Bosch 1MB160F-4B

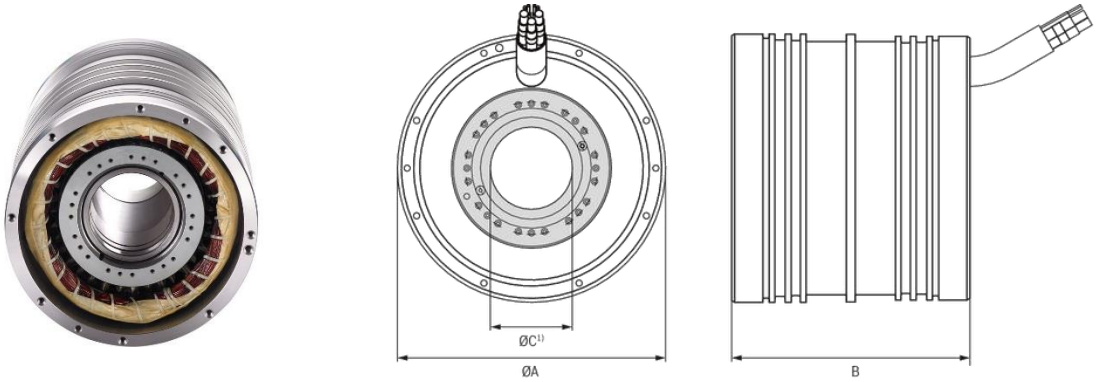

Figure 39 – Bosch 1MB160F-4B. [45]

Table 4 – Properties of Bosch 1MB160F-4B. [45]

Model	1MS160F-4B
Rated motor speed [rpm]	3000
Maximum speed [rpm]	12000
Rated torque [Nm]	48
Rated power [kW]	15
Nominal voltage [V]	285
Dimensions (diameter/length) [mm]	180 x 255
Weight (stator + rotor) [kg]	26

3.2. Longitudinal dynamics calculation

Since the electric motor has been chosen, we can continue to an evaluation of expected longitudinal dynamic properties of the vehicle. The task was to achieve a maximum velocity of 100 km/h. However, we are restricted by homologation LE for this vehicle, which limits the maximum rated power of the motor. Following calculations can prove, if such a goal is realistic. Moreover, we will be able to compare acceleration abilities with competition vehicles.

The basic calculation is made according to Newton's second law of motion. [3]

$$(m\delta + m_d)a = F_t - F_r - F_d$$

Where m is mass of the vehicle, δ is coefficient of rotating masses, m_d is mass of a driver (70 kg), a is acceleration, F_t is a tractive force, F_r is rolling resistance and F_d is air drag. Let's get a detailed look at every term in this equation.

Inertia

The single term on the left side represents inertial forces. Coefficient of rotating masses δ simply implements the influence of all rotating masses (e.g. rotor, transmission, driveline, wheels) to the overall acceleration of the vehicle. Its value of 1.2 was estimated according to [3], assuming the lowest value, because of the usage of small motor and wheels. The weight of the vehicle is taken the same as *Twizy's* (474 kg). [19]

Rolling resistance

Rolling resistance can be simply calculated using the following formula:

$$F_r = F_N f$$

Where F_r is rolling resistance, F_N is a normal force acting on the wheels and f is rolling resistance coefficient. Rolling resistance coefficient is sometimes considered as constant is some simplified calculations. However, in reality, the coefficient increases in velocity, thus we are going to suppose the quadratic model of the rolling resistance coefficient. [4]

$$f = f_0 + f_1 v^2$$

$$f_0 = 0.015$$

$$f_1 = 7 \cdot 10^{-6}\ s^2/m^2$$

Air drag

Air drag crucially influences the maximum velocity, as it has a quadratic dependence with respect to velocity. The calculation is made according to the following equation: [3]

$$F_d = 0.5 c_x S \rho v^2$$

Where c_x is drag coefficient, S is cross-sectional area, ρ is the density of the air and v is velocity. During the research of small city vehicles, it was found that drag coefficient of *Smart ForTwo II* is c_x = 0,38 [48] and of *Renault Twizy* is c_x = 0,64 [46]. Such a high drag coefficient of *Twizy* is caused by the absence of side windows in the doors. It was also not meant to go much faster than city limits, so there wasn't a strict priority to keep it really low. In the following calculations, we will assume air drag coefficient c_x = 0.5 which is somewhere between *Smart's* and *Twizy's* values. Cross-sectional area was taken from *Twizy*. [19]

Tractive force

In figure 40 there is a dependency of torque and rpm for chosen motor from *Bosch* with the maximal rated torque of 48 Nm and the rated power of 15 kW. An induction motor can be overloaded for a short time which can result in even better acceleration performance. However, the duration of the overloading depends on the effectiveness of the cooling. As we don't know at this stage of development how the motor will be cooled, we will assume just nominal available power and torque.

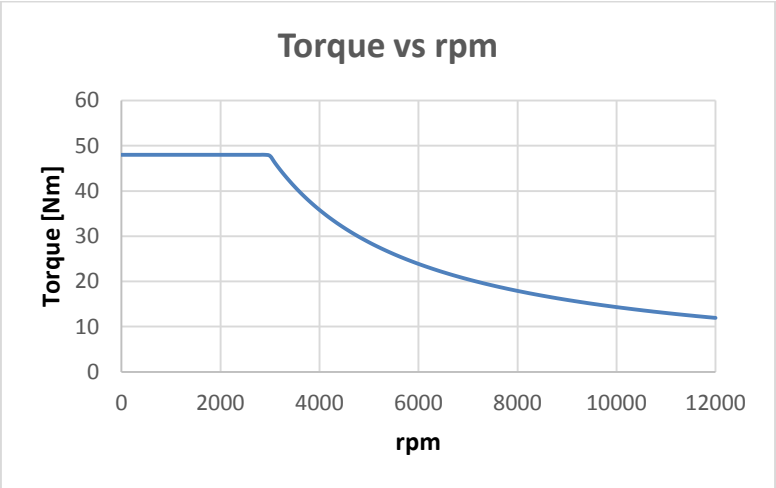

Figure 40 – The chosen Bosch motor characteristics.

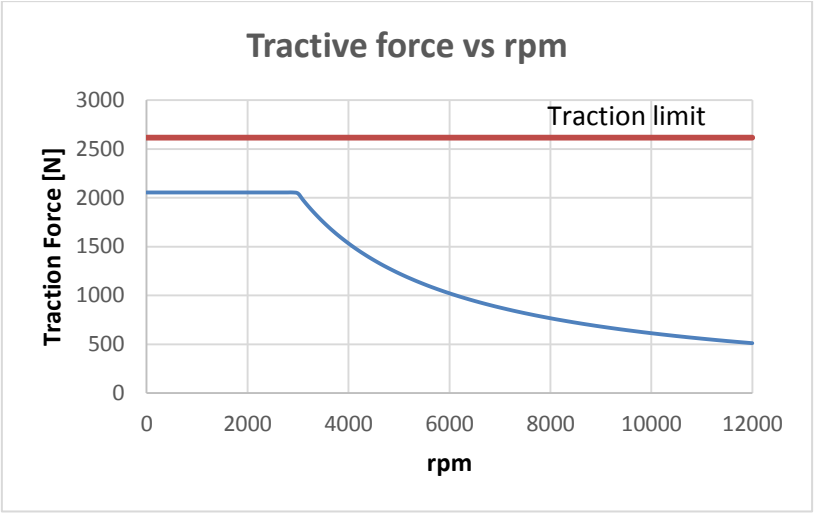

Figure 41 – Tractive force vs rpm, the red line symbolizes a traction limit of driven tires.

To get the tractive force on wheels we need to use the following equation:

$$F_t = \frac{Ti\eta_t}{r_d}$$

Where F_t is a tractive force, T is torque from the motor, i is a gear reduction ratio, η_t is the efficiency of the transmission and driveline and r_d is the kinematic radius of the tires. The gear ratio i was evaluated from the estimation of maximal velocity. The power delivered to the wheels equals the multiplication of resistance forces and velocity. From this assumption, we will get a cubic equation with the velocity as an unknown value.

$$P\eta_t = (F_d + F_r)v$$

$$P\eta_t = [F_N(f_0 + f_1 v^2) + 0.5cS\rho v^2]v$$

$$(F_N f_1 + 0.5cS\rho)v^3 + (F_N f_0)v - P\eta_t = 0$$

The only real solution is $\boldsymbol{v}$ **= 28.77 ms^{-1} (103.59 km/h)** which proves a satisfaction of the required maximum speed of the vehicle. The gear ratio is calculated according to the condition, that at the maximum velocity, the motor should be running at the maximal speed.

$$v = \omega_m r = \frac{2\pi n}{60}\frac{r_d}{i}$$

$$i = \frac{2\pi n}{60}\frac{r_d}{v}$$

In these equations ω_m is the angular velocity of the motor, n is the speed of the motor in rpm, r_d is the kinematic radius of a tire and i is the gear ratio. The final resulting gear ratio equals to $\boldsymbol{i}$ **= 11.87**.

The tractive force effort can be limited by maximal transmissible force by tires; we can evaluate this limit using the following formula:

$$F_{t\,max} = F_{N\,rear} f_{t\,max} = m_{rear} g f_{t\,max}$$

Where $F_{t\,max}$ is a maximal transmissible force by tires, $F_{n\,rear}$ is a normal force acting on rear-driven tires and $f_{t\,max}$ is the maximal coefficient of friction. $F_{N\,rear}$ is established according to the weight distribution of *Twizy*. [19] Coefficient of friction is taken from figure 28 where we assumed the lowest values because we are going to use narrow tires. Let's now summarize all input values for the calculation of longitudinal dynamic properties in table 5. At first, from resulting forces was calculated acceleration and it was numerically integrated to obtain velocity and distance in time.

Table 5 – Input parameters for calculation of longitudinal dynamical properties.

Curb weight [19]	m	474 kg
Weight of driver	m_d	70 kg
Weight on rear wheels (with driver) [19]	m_{rear}	268 kg + 70kg/2 = 303 kg
Coefficient of rolling resistance [4]	f_0	0.015
Drag coefficient	c_x	0.5
Cross-sectional area [46]	S	1.61 m^2
Kinematic radius of tire (chapter 5.3.1)	r_d	0.2717 m
Gear ratio	i	11.87
Coefficient of adhesion [39]	$f_{t\,max}$	0.88
Efficiency of driveline	η_t	0.98
Coefficient of rotational masses [3]	δ	1.2
Air density	ρ	1.2 $kg.m^{-3}$
Gravitation constant	g	9.81$m.s^{-2}$

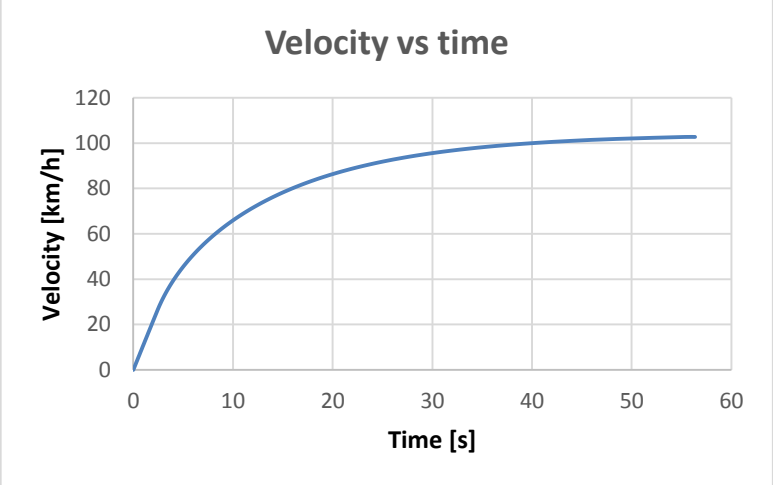

Figure 42 – Velocity vs time.

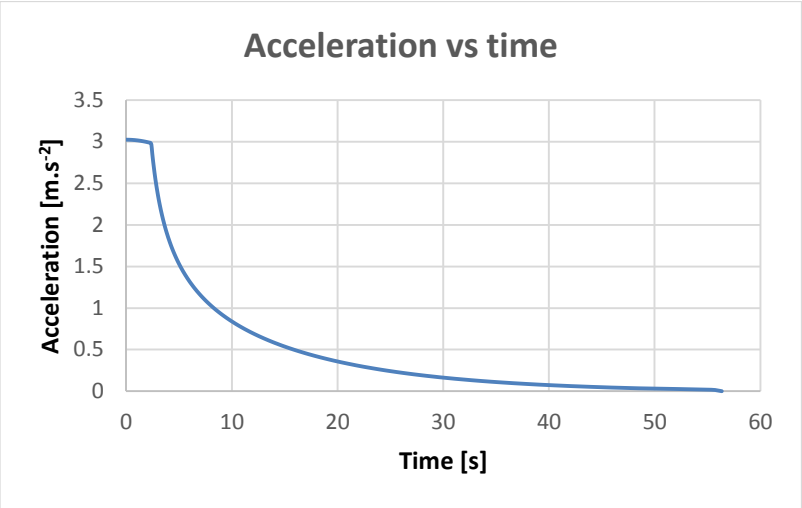

Figure 43 – Acceleration vs time.

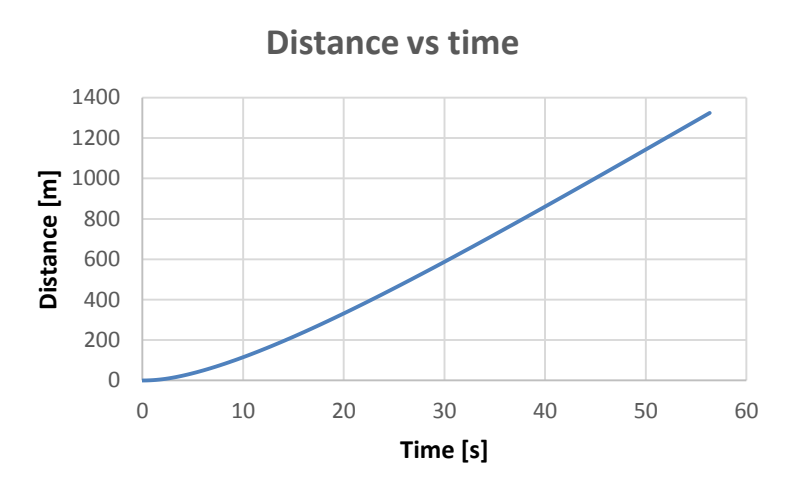

Figure 44 – Distance vs time.

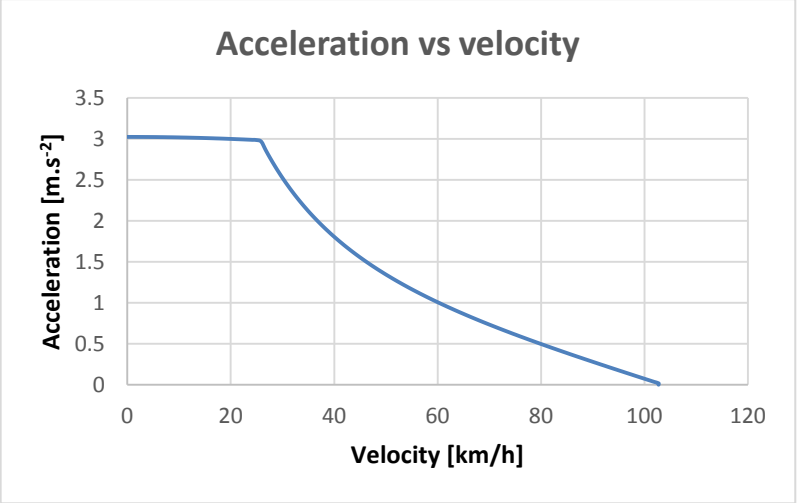

Figure 45 – Acceleration vs velocity.

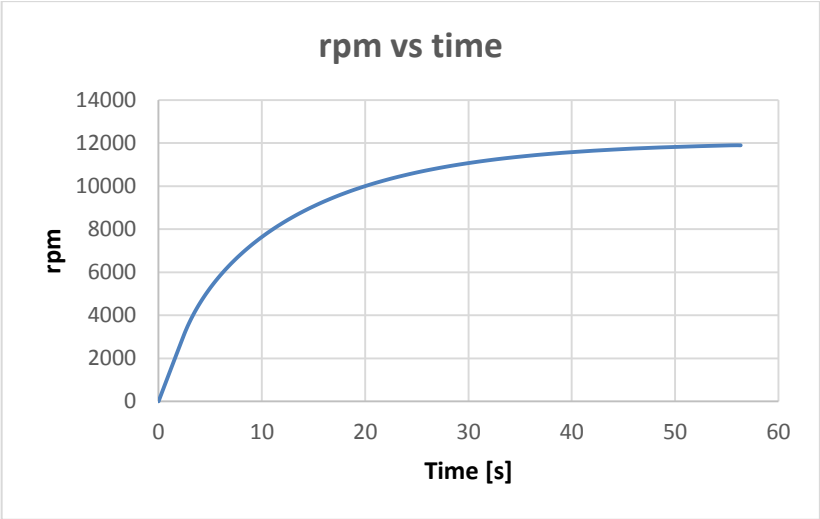

Figure 46 – rpm vs time.

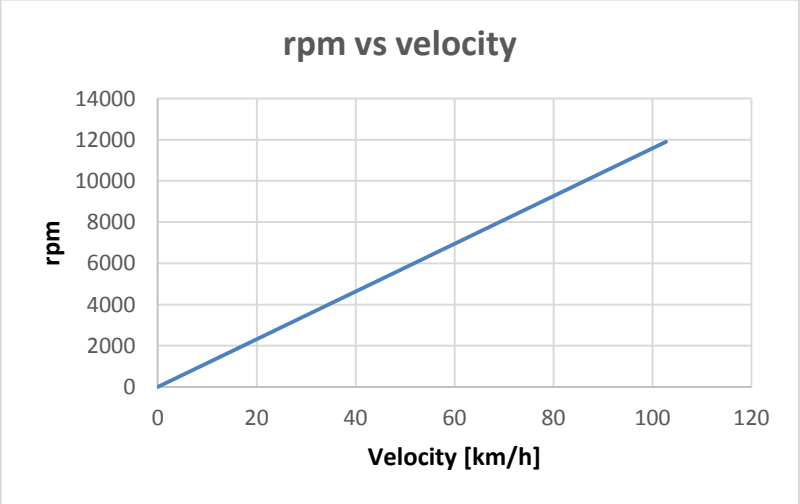

Figure 47 – rpm vs velocity.

Table 6 – Comparison of dynamic properties of our vehicle and *Renault Twizy* according to the numerical calculation. [46]

	Our vehicle	Renault Twizy
0-50 km/h	5.7 s (4.9 s; 0-45 km/h)	6.1 s (0-45 km/h)
0-80 km/h	15.6 s	-
0-100 km/h	37.8 s	-
30-60 km/h	5.4 s	8.1 s
0-50 m	6.1 s	6.6 s
Top speed	102.7 km/h	80 km/h

4. Folding mechanism

Our city vehicle should meet strict requirements in terms of its dimensions. It should be short enough to fit in a width of a parallel parking space. It has to provide decent ride stability up to its maximal velocity around 100 km/h. The width of the car should be small enough to fit two cars side by side in a single lane. To meet these requirements it was decided to design a folding mechanism for this car. Let's summarize the main reasons for this technical solution:

- Save space while it is parked.
- Get better stability of ride and confident handling at high speeds.
- Get an additional boot space by elongation of the vehicle.

Before determining a range of the rear axle folding mechanism, it is necessary to look through dimensions of competition vehicles. Figures illustrate exterior dimensions of *Renault Twizy*, *Volkswagen e-Up!* and *Smart ForTwo III*.

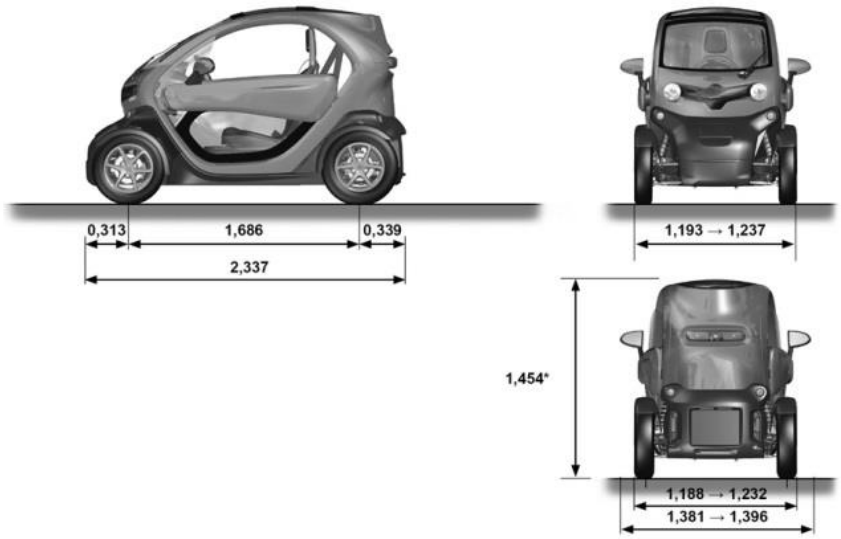

Figure 48 – Renault Twizy dimensions. [46]

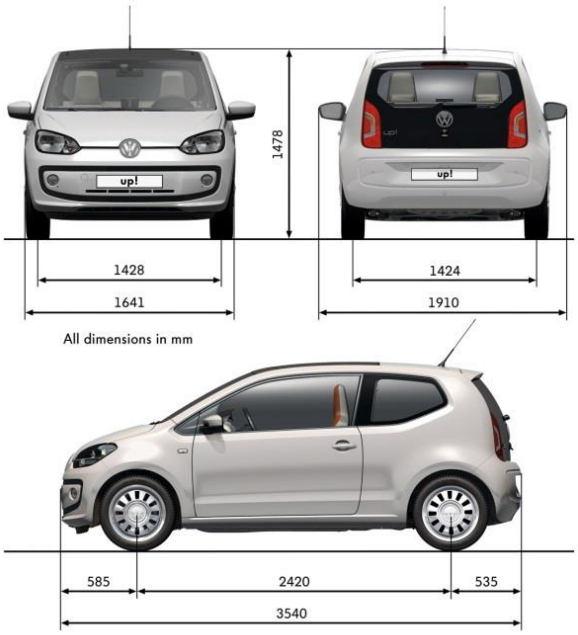

Figure 49 – Volkswagen e-Up! dimensions. [29]

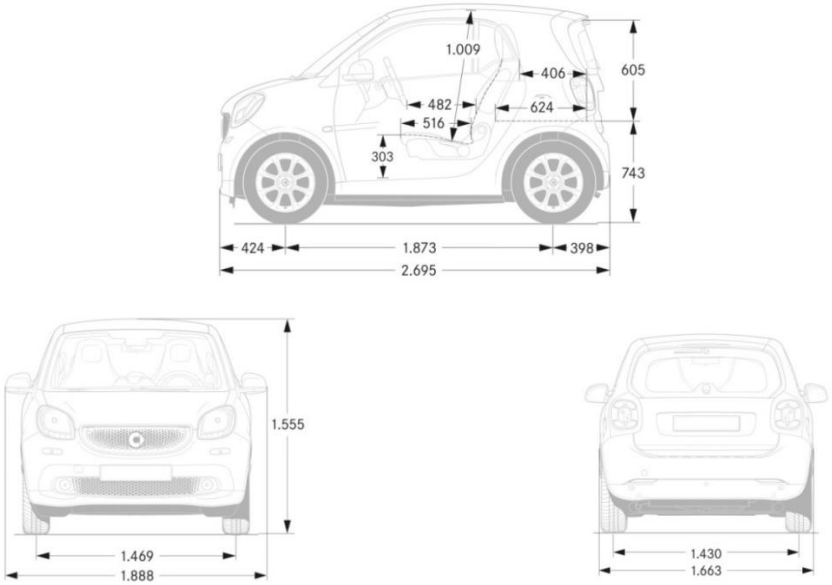

Figure 50 – Smart ForTwo III dimensions. [47]

The next step of the research is to find out dimensions of parking spaces. According to the Czech standard ČSN 73 6056 [6], the parallel parking space for small and middle passenger cars has a length of 5.5 m and width of 2 m, and for large passenger cars, it is 2.2 m wide and 6.5 m long. That means the parked length of the vehicle shouldn't exceed **2 metres**. Another Czech standard ČSN 73 6101 [7] defines the width of a lane on the roads. For single lane road (one way) the width has to be 3 metres. Two-lane road width (with both directions of traffic) can vary, because of different designed speed, from 2.75 metres (traffic density less than 1000 vehicles per day), through 3 metres (design speed 50, 60 and 70 km/h), up to 3.5 metres (design speed up to 90 km/h). Four-lane road (with both directions of traffic) should be 3.25 metres wide (design speed 70, 80, 90 km/h) or 3.50 metres (design speed 70, 80, 100km/h)

or 3.75 metres for highways. Let's assume the minimal lane width of **3 metres**; therefore to be able to fit two vehicles in one lane (in case of a traffic jam) the vehicle has to be narrower than **1.5 metres** (with mirrors). Because of that, the width of the track of the vehicle was set to **1100 mm**.

Table 7 – Dimensions of parallel parking spaces according to ČSN 73 6056. [6]

Parallel parking space	Width [m]	Length [m]
Passenger cars	**2**	5.5
Large passenger cars	2.2	6.5

Table 8 – Width of lane according to ČSN 73 6101; * Density of traffic is less than 1000 vehicles per 24 hours. [7]

Number of lanes	Designed speed [km/h]	Width of lane [m]
1	40; 30	**3**
2	60; 50	2.75*
	70; 60; 50	**3**
	80; 70; 60	3.5
	90; 80; 70	3.5
4	90; 80; 70	3.25
	100; 80; 70	3.50
	120; 100; 80	3.75

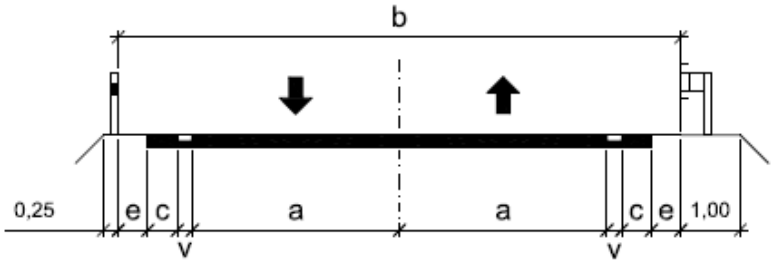

Figure 51 – Lane width (a) according to ČSN 73 6101 shown on a two-lane road. [7]

In summary, the vehicle should be **shorter than 2 metres** and **narrower than 1.5 metres** (with mirrors). Wheelbase should be definitely longer than *Twizzy's* (figure 48; 1.686 mm) to get higher comfort of the ride. According to standard ČSN 73 6058 for garage parking, the height of the vehicle shouldn't exceed 1.9 metres, but we are not going to approach this limit, as the height won't be more than approximately 1.5 metres.

4.1 Design and calculation of the folding mechanism

Respecting the requirement to keep manufacturing costs at a minimum, the folding mechanism also has to be designed as simple as possible. To avoid the usage of additional actuators, we can use the traction electric motor. The basic idea is to lock the front wheels by brakes and drive the rear wheels, thus folding the rear axle as the rear wheels are moving. The crucial part of this concept makes the coefficient of friction of all wheels. Because of that, we need to design a kinematical concept of the folding mechanism and perform calculations to prove the functionality of this system.

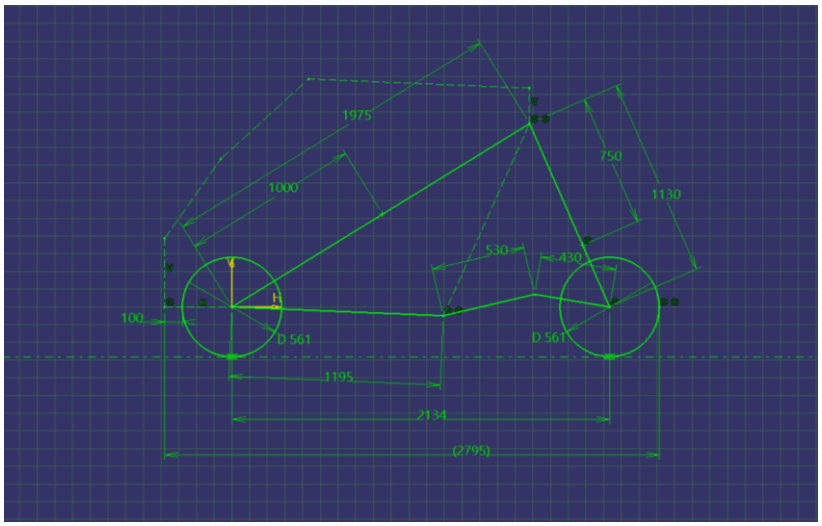

Figure 52 – Sketch of the folding mechanism in Catia.

The scheme of the mechanism is depicted in figure 53. It consists of chassis (*A*), upper arm (*B*), rear wheel (*C*) and lower arms (*E, D*). For the calculation model, we assume the front wheels and chassis as one part, because the front wheels are locked during the folding. Numbers, from 1 to 5, point rotational joints of the parts. Notice that joints number 2 and 3 are in the same position, representing a double rotational joint. F_{g1} is a gravitational force of chassis and F_{g2} is a gravitational force of the upper arm. Position of these forces was only estimated as we don't have any information about the detailed structure of the vehicle. In this case, the horizontal position of gravitational forces is the only one important, that's why they are located on the lines for simplification. The lower arms *D* and *E* were supposed as weightless in this task. The only resistance taken into the account was rolling resistance of the rear wheel (rolling resistance coefficient $f = 0.015$). In figure 52 there is a sketch of mechanism which was used to design this mechanism and to validate its geometrical properties. This mechanism was solved as a static case, getting forces and torque necessary for equilibrium condition. Force and torque equilibrium equations were derived for every single part of the mechanism. In table 9 there are input dimensions and parameters. Then a matrix form calculation was performed to obtain results.

Table 9 – Input parameters of the calculation of the folding mechanism

Position of F_{g1}	a	1 m
Distance: front wheel – joint 1	b	1.975 m
Distance: front wheel – joint 5	c	1.195 m
Length of upper arm	d	1.13 m
Position of F_{g2}	e	0.75 m
Length of lower arm D	g	0.43 m
Length of lower arm E	h	0.53 m
Gravitational force of chassis	F_{g1}	3668.94 N
Gravitational force of upper arm	F_{g2}	981 N
Rolling resistance coef.	f	0.015
Kinematic radius of tire	r	0.2717 m
Coefficient of friction	f_t	0.7

$$DOF = 3(6-1) - 5ROT - 2ROLL = 15 - 14 = 1°$$

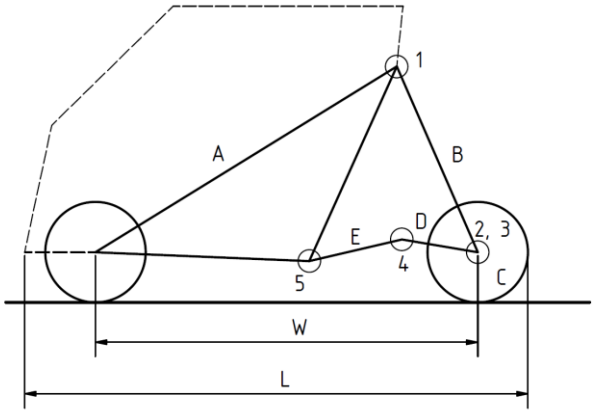

Figure 53 – Folding mechanism calculation model.

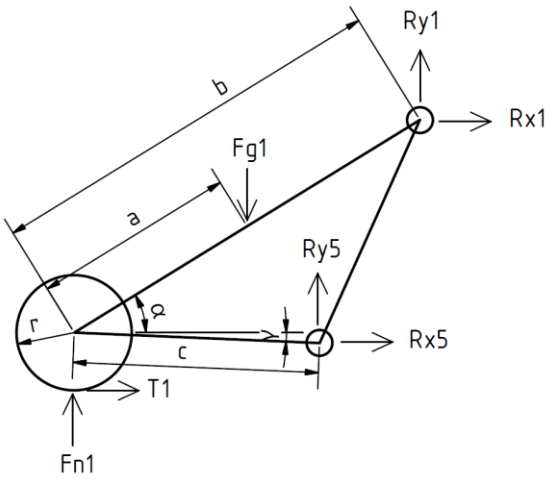

Figure 54 – Chassis (*A*).

$$R_{x1} + R_{x5} + T_1 = 0$$

$$R_{y1} + R_{y5} + F_{N1} - F_{G1} = 0$$

$$T_1 r - F_{G1} a \cos\alpha + R_{y1} b \cos\alpha - R_{x1} b \sin\alpha + R_{y5} c \cos\gamma + R_{x5} c \sin\gamma = 0$$

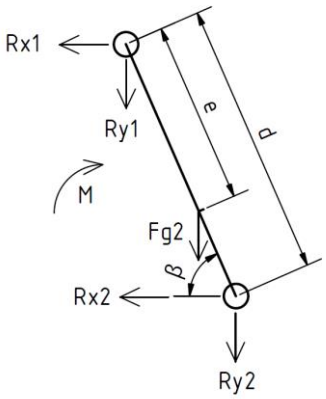

Figure 55 – Upper arm (*B*).

$$R_{x1} + R_{x2} = 0$$

$$R_{y1} + F_{G2} + R_{y2} = 0$$

$$R_{y2} d \cos\beta + R_{x2} d \sin\beta + F_{G2} e \cos\beta + M = 0$$

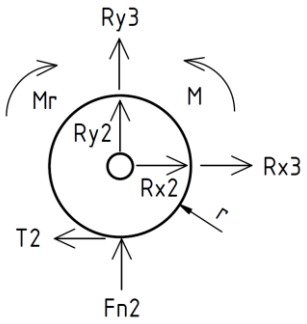

Figure 56 – Rear wheel (*C*).

$$R_{x2} + R_{x3} - T_2 + F_x = 0$$

$$R_{y2} + R_{y3} + F_{N2} + F_z = 0$$

$$M - M_v - T_2 r = 0$$

$$M_v = F_{N2} f$$

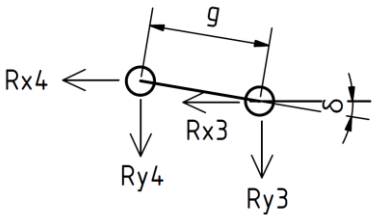

Figure 57 – Lower arm (*D*).

$$R_{x4} + R_{x3} = 0$$

$$R_{y4} + R_{y3} = 0$$

$$R_{y3} g \cos\delta + R_{x3} g \sin\delta = 0$$

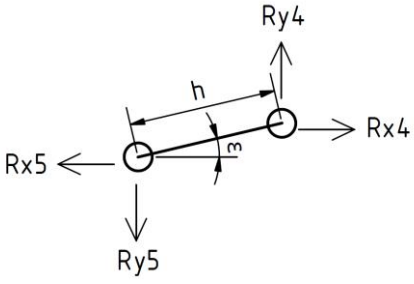

Figure 58 – Lower arm (*E*).

$$R_{x4} - R_{x5} = 0$$

$$R_{y4} - R_{y5} = 0$$

$$-R_{x4} h \sin\varepsilon + R_{y4} h \cos\varepsilon = 0$$

The most crucial forces for this calculation are traction forces on all wheels. In figure 59 there is a relationship between traction force and a wheelbase of the vehicle. The required traction forces on the front and rear wheels are the same in magnitude. T_{1max} and T_{2max} represent the maximal traction forces of the front and rear wheels. It was derived according to the following formula.

$$T_{1max} = F_{n1} f_t$$

$$T_{2max} = F_{n2} f_t$$

These limits of traction are changing, as the weight distribution between the front and rear is changing during the folding. The coefficient of friction f_t was chosen 0.7 which is a value for wet asphalt (figure 28) because we want to guarantee proper functionality of the mechanism also in wet conditions. A wheelbase range was determined from 1337 mm to 2134 mm. This results in 797mm of variable wheelbase length. The forces T_1 and T_2 are in the positive values in the interval from approx. 1700 mm to fully extended 2134 mm. However, when wheelbase is shorter than 1700 mm, the forces T_1 and T_2 are negative. This means, that the direction of forces T_1 and T_2 is changing. Achieving the shortest wheelbase 1337 mm, the front wheels are coming to its limit of traction. That's why it can't be folded any shorter. The maximum wheelbase doesn't reach the limits of traction, so theoretically it can be even longer. However, because of the lateral stiffness of the vehicle, its maximal wheelbase should be set reasonably. It exceeds the wheelbase of *Smart ForTwo III* (1873 mm) which can go up to 155km/h, so in terms of longitudinal stability, the chosen value of wheelbase should be sufficient. In figure 60 there is a dependency of required torque M delivered to the rear wheels by the electric motor. The red line symbolizes the maximum deliverable torque. As we can see, the required torque is safely below this threshold which can save energy during the folding. As the folding reach the length of the wheelbase of 1650 mm, the rear wheels don't need to be powered anymore. The mechanism achieves there equilibrium and from that point, it will be shortened automatically thanks to the gravitational force. Reversely, during the extending, it needs to be powered in reverse only till the same point of 1650 mm and after that, it can go on its own. Reaction forces R_{x3}, R_{y3}, R_{x4}, R_{y4}, R_{x5}, R_{y5} equal to zero. This means, that the lower arms are not participating during the folding and they also don't affect the kinematics of folding. Their role comes when the vehicle rides. They significantly help to get sufficient overall torsional and bending stiffness of the vehicle.

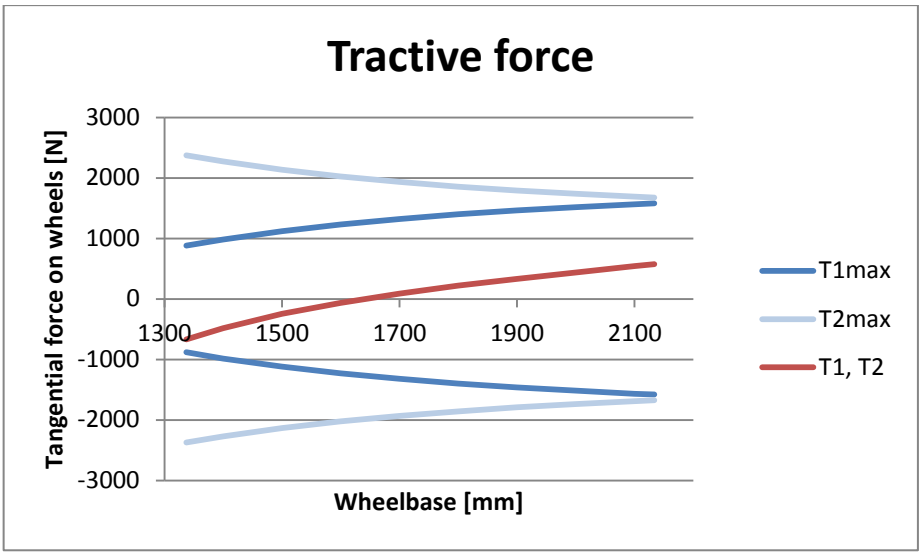

Figure 59 – Required force on tires (T_1, T_2) and limits of traction for the front (T_{1max}) and rear tires (T_{2max}).

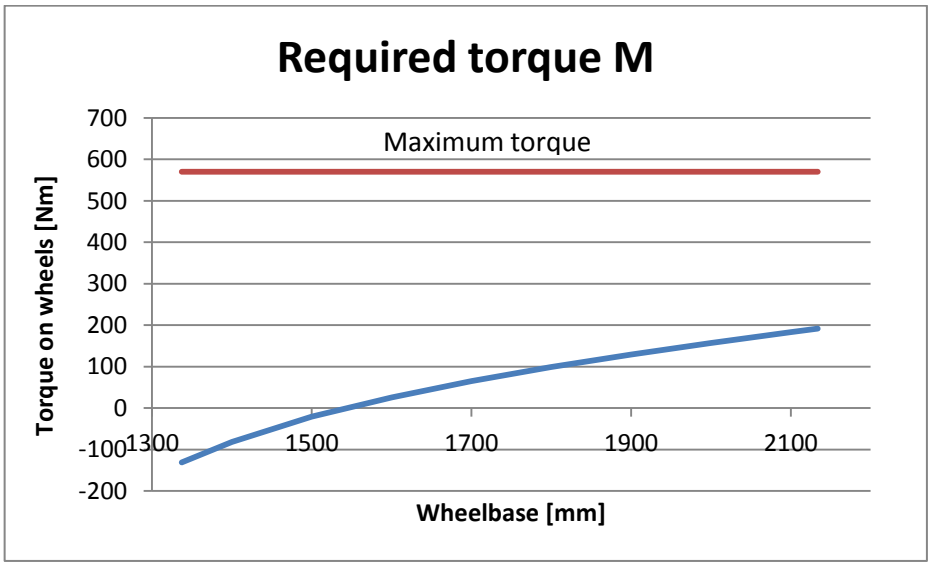

Figure 60 – Required torque on rear wheels delivered by the electric motor. The red line is the maximum torque which can be delivered to the rear wheels.

In figures 61, 62 and 63 there are three positions of the folding mechanism. In figure 61 there is a ride mode which wheelbase is 2134 mm and the length of the vehicle is 2795 mm. The overall length is calculated with the assumption of a front overhang of 100 mm. In figure 62 there is a state during the folding where the wheelbase is 1700 mm. Finally, in figure 63 there is the vehicle depicted in a parking mode in which its length comes to 2068 mm. Originally the task was to keep the length below 2 metres to fit in the width of parking space, but in this case, it exceeds that over 68 mm. As we know, it was not possible to shorten the vehicle even more, because of traction issues. However, if the vehicle park with the front wheels touching the pavement, the front bumper can hang over it and the vehicle can fit in. Otherwise, if there is not such a possibility, the exceeding 68 mm over the parking space won't be really dangerous obstacle in city traffic. It is also important to notice, that the folding mechanism requires in

ride and park modes special locking of the mechanism to provide safe and comfortable ride or stable parking position.

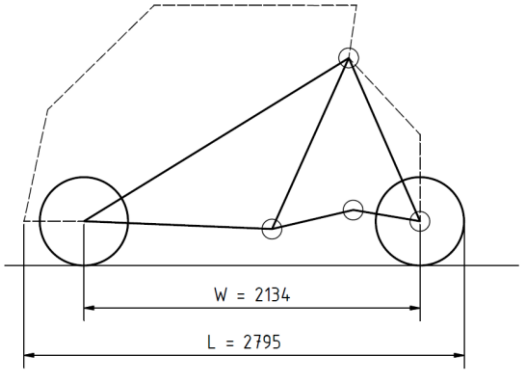

Figure 61 – The ride mode of the vehicle.

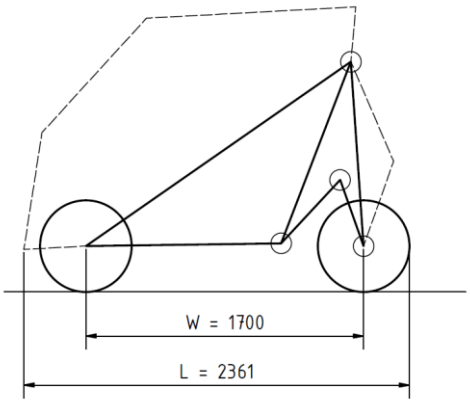

Figure 62 – The vehicle in the middle of the folding.

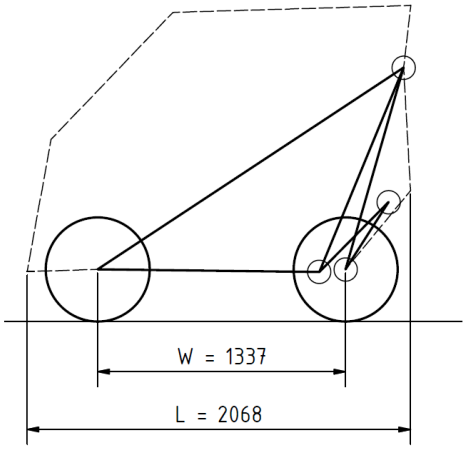

Figure 63 – The park mode of the vehicle.

5. Suspension design

5.1 Suspension kinematics

Camber

According to the standards DIN 70 000, camber is the angle between the wheel centre plane and a vertical to the plane of the road. It is positive if the wheel is inclined outwards and negative when inclined inwards. [8]

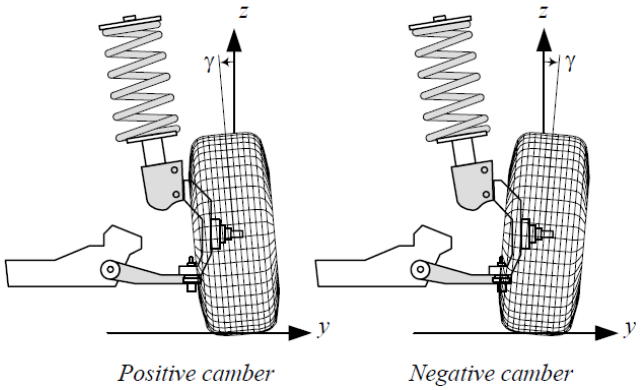

Figure 64 – A positive and negative camber. [4]

To get better lateral tire grip and improve handling, nowadays, modern passenger cars are set to the negative camber even when the vehicle is empty. However, this setting leads to uneven wear of the inner sides of the tires. [8]

In independent wheel suspensions, the wheels incline with the body when the vehicle is cornering. To even this out, the wheels, in bump travel, should go into negative camber and the in rebound travel into positive camber which illustrated in figures 65 and 66. [8]

In figure 67 there is a comparison of different types of rear suspensions in terms of a relation between camber and travel of the wheel. The multi-link independent suspension of the *Mercedes* has a fairly precise camber setting. When the springs compress, the curve is slightly progressive. The multi-link suspension of the *BMW* exhibits a straight-line curve; when the springs deflect in bump travel, the negative camber is less than on *Mercedes*. The double wishbone suspension of the *Honda* has zero camber in the design position, but the wheels take on higher alterations (negative values) when the springs deflect in bump travel than on the two other suspensions. In figure 68 there is a comparison of the front suspensions of *Honda's* double wishbone suspension, 3-series *BMW's* McPherson suspension and the strut damper axle of a *Mercedes*. [8]

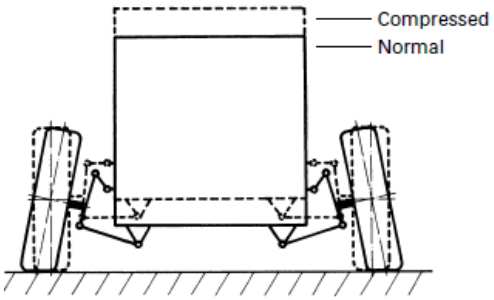

Figure 65 – Behaviour of independent suspension. [8]

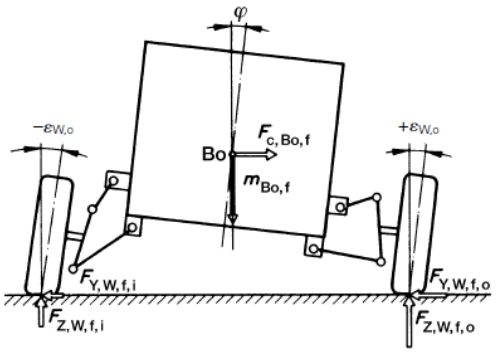

Figure 66 – Behaviour of an independent suspension in a corner. [8]

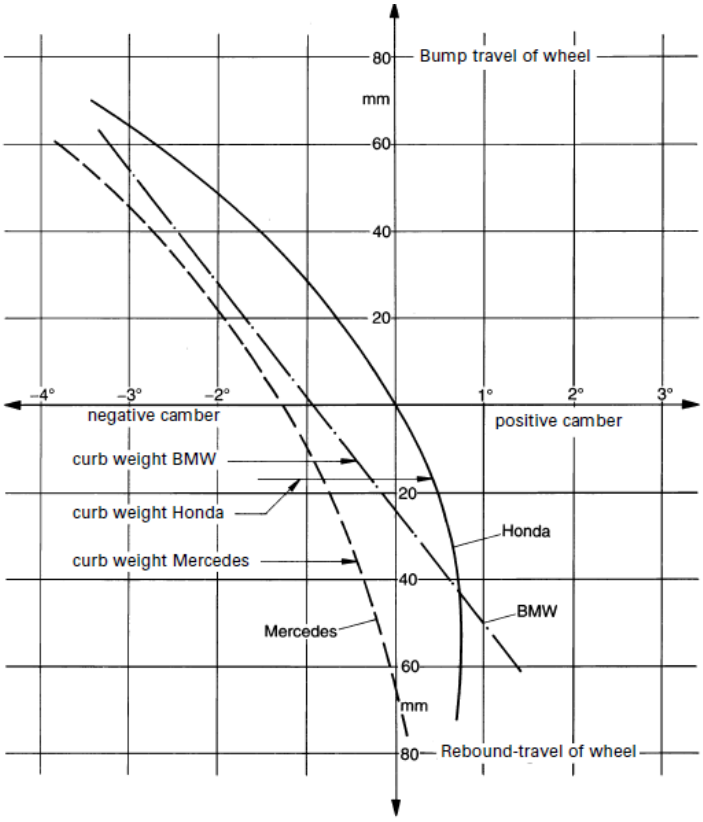

Figure 67 – Camber alteration on the rear double wishbone suspension of a Honda Accord as a function of the wheel travel in comparison with a multi-link suspension of a 3-series BMW and multilink suspension of a Mercedes. [8]

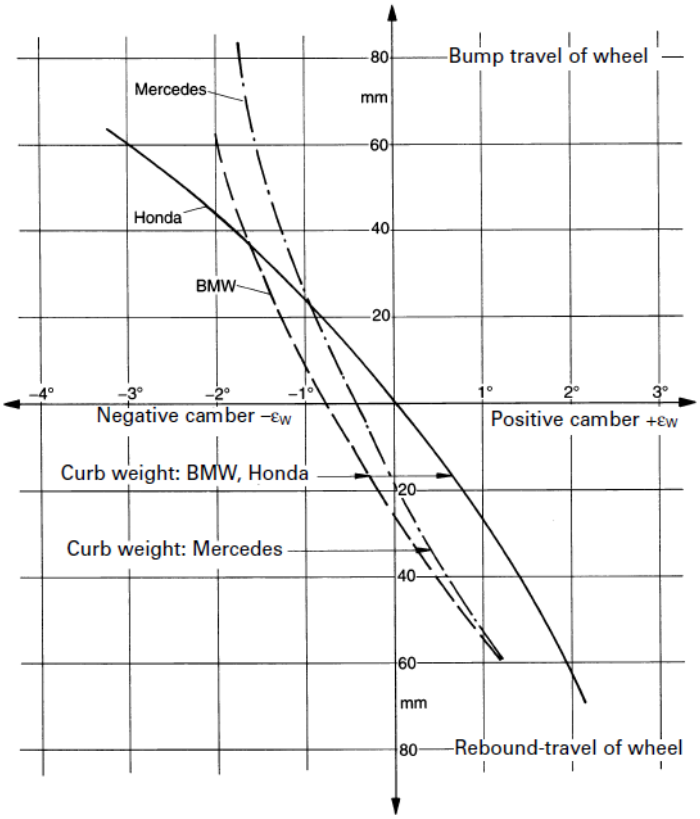

Figure 68 – Camber alteration on the front double wishbone suspension of a Honda Accord as a function of the wheel travel in comparison with McPherson suspension of a 3-series BMW and the strut damper axle of a Mercedes. [8]

Toe

In accordance with standard DIN 70 000, the static toe-in angle δ is the angle that results in a standing vehicle (reference status), between the vehicle centre plane in the longitudinal direction and the line intersecting the centre plane of one left or right wheel with the road plane. It is positive when the front part of the wheel is turned towards the vehicle longitudinal centre plane and negative ("toe-out") when it is turned away. The total toe-in angle delta is obtained by adding the toe-in angle of the right and left wheels. According to DIN 70 020, the total value of toe is sometimes given in millimetres as it is depicted in figure 69. [8]

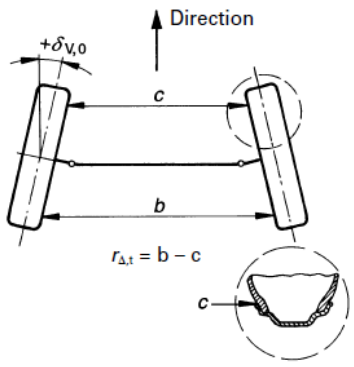

Figure 69 – The toe-in of both wheels in accordance with the German standard DIN 70 020 is the difference in dimension b-c in mm, measured on the rim flanges at the level of the wheel centre. [8]

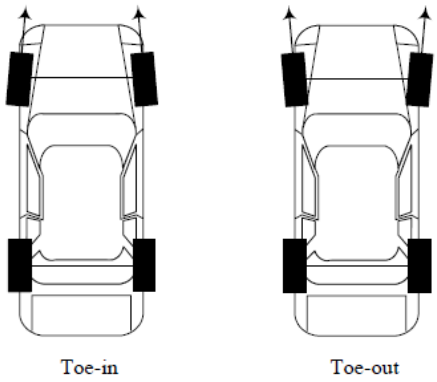

Figure 70 – Toe in and toe out configuration on the front wheels of a car. [4]

Toe setting affects three major performances: tire wear, straight-line stability and corner entry handling. For minimum tire wear, the wheels on a given axle should have zero toe angle. Excessive toe-in causes accelerated wear at the outer side of the tire, while too much toe-out causes higher wear at the inner side. [4]

Toe-in increases the directional stability of the vehicle and toe-out increases steering response. Hence, a toe-in makes the steering function lazy, while a toe-out makes the vehicle unstable.

With four-wheel independent suspensions, the toe may also be set at the rear of the car. Toe settings at the rear have the same effect as they do on the front. Rear toe-in settings result in straight-line stability, better traction out of the corner, more steerability and higher top speed. However, rear-driven sports cars aren't usually set to toe-out in the rear, because of excessive instability.

When driving torque is applied to the wheels, they pull themselves forward and try to create toe-in. Furthermore, a non-driven wheel or a braking wheel will tend to toe-out. [4]

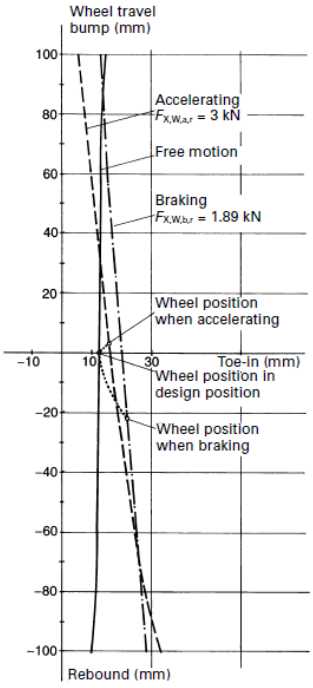

Figure 71 – Kinematic toe-in alteration of one wheel on the multi-link independent rear suspension of the Mercedes Benz S class. [8]

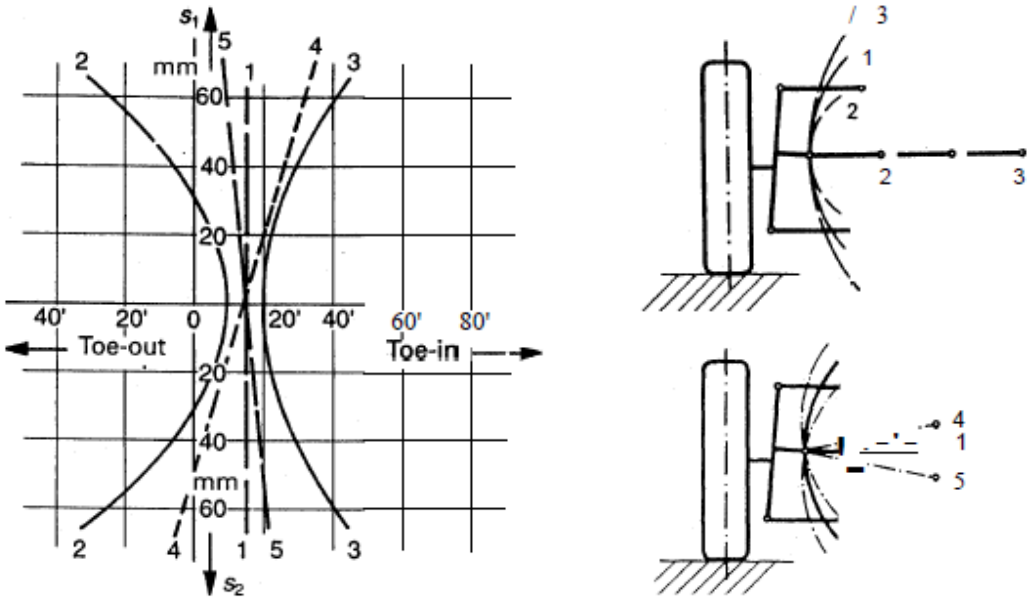

Figure 72 – Possible alteration of toe of one wheel as it travels, due to an incorrect tie rod length or position. [8]

In our car, there will be a MacPherson suspension in both front and rear. However, in the rear, there won't be any steering rod and it will be replaced by an upper arm. The upper arm's length will be able to be adjusted, thus setting the geometry of the rear wheels. The position and length of the upper arm influence the kinematics of the rear wheel in the same manner as the position and length of a steering rod influences the kinematics of front wheels. Because of that, we could use the same theory to find favourable kinematics of the rear wheels. In figure 72 there are shown toe alterations in respect to wheel travel, influenced by different tie rod lengths and positions. [8]

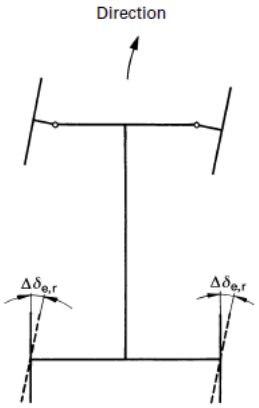

Figure 73 – Reduction of oversteering by toe settings on rear wheels. [8]

To reduce the tendency to oversteer, the rear wheel suspension can be designed so that body roll or lateral force understeering is possible. Under the influence of the body roll (or lateral forces) the compressing wheel on the outer side goes into toe-in and the rebounding one on the inner side goes into toe-out in proportion to the steering angle (figure 73 and figure 74). [8]

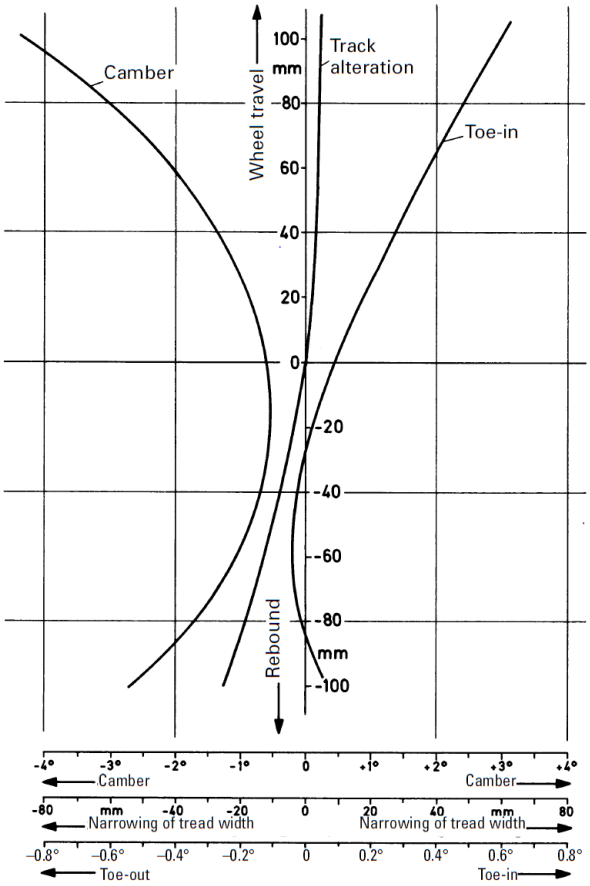

Figure 74 – Kinematic properties of an Audi A6 Quattro (1996) as the rear wheels compress and rebound. Toe-in alteration (of one wheel) which contributes to understeering of the rear axle is clearly visible. [8]

Caster

In accordance with DIN 70 020 (and also DIN 70 000), caster angle τ is the angle between the steering axis *EG* projected onto an *xz* plane and a vertical, drawn through the wheel centre and the kinematic caster trail *r* the distance between the points *K* and *W* on the ground (figure 75). [8]

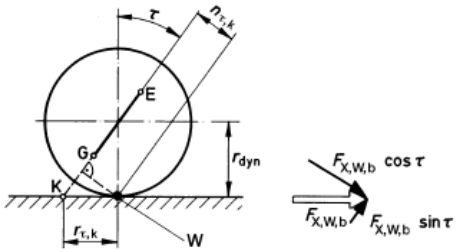

Figure 75 – Illustration of caster angle τ. [8]

In figure 76 there is an explanation of positive of negative caster angle on a front suspension. Negative caster angle helps with a centring of a steering wheel after a turn and makes the front tires straighten quicker. Because of that, it is used to enhance straight-line stability. Most street cars are made with 4-6 degrees negative caster. [4]

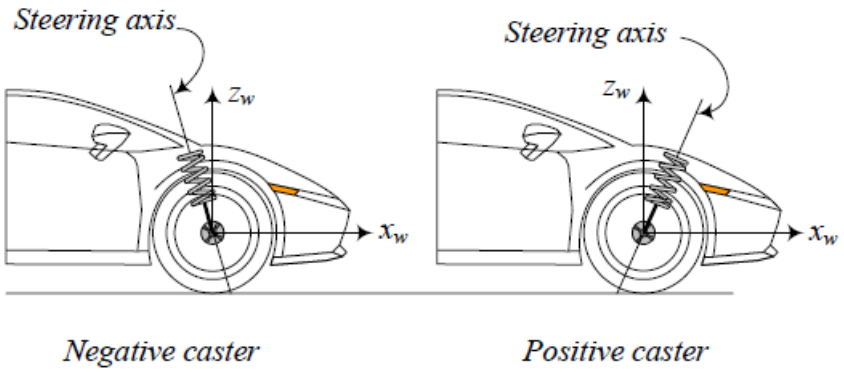

Figure 76 – A positive and negative caster configuration on front wheels of a car. [4]

Assuming a MacPherson suspension on the front, the axis of a spring and damper is the steering axis (figure 76). We can't really talk about caster on the rear MacPherson suspension if the rear wheels are not steerable. However, we can keep that negative caster angle of a shock absorber also in the rear. Because of the so-called wheel recession, the rear wheel centre than travels slightly rearwards as the wheel moves into a bump. This contributes to higher ride comfort. [56]

5.2 Suspension decision

According to the research of small city vehicles, there were following rear suspension systems to choose from: De-Dion, trailing arm, torsion strut and MacPherson. MacPherson suspension was chosen for several reasons.

Advantages

- Lightweight: In order to fit the vehicle in homologation LE it is important to keep the overall weight of the vehicle below 400 kg (without battery).
- Shared parts: In the front, there is going to be used also a MacPherson suspension, which can be built from shared parts from the rear. This can significantly reduce the final price of the vehicle.
- Favourable kinematics: As an independent suspension system it can provide very good performance while cornering and riding over bumps.
- Small: McPherson is really short in a longitudinal direction which can help to extend the overall range of folding mechanism. That's the main reason why other suspension systems were not considered for this vehicle.
- Low unsprung mass: It contributes to a better ride and handling.

Disadvantages

- Complex design: It uses more joints is comparison with other suspension systems which can make it more expensive and less reliable. However, as the parts will be shared with front suspension, the costs can be kept low.
- Height of suspension: As the shock absorber works also as guidance for a wheel, it must be really tall and takes space in a vertical direction. However, there will be a motor placed in between the wheels in a special frame. The motor is small enough and won't be limited by the suspension. The height of the suspension is not a major issue in terms of a range of folding mechanism (as the length of suspension).

A kinematic wire model of the rear McPherson suspension was made in *Catia DMU Kinematics* (more in chapter 5.4). The vertical position of the wheel was set as an independent variable. It was decided to use the total rear wheel travel of 160 mm (80mm in bump and 80mm in rebound) and track width of 1100 mm. In figure 77 there is the final kinematics of the rear McPherson suspension. It was tuned in accordance with the previous research of suspension kinematics.

Camber is set to slightly negative value -0.26° in zero position of the wheel travel. When the wheel travels more in bump, camber is even more negative (up to -2.37°) to get more stability in curves. In the rebound direction, camber changes to positive values (up to 3.14°) to improve cornering stability of the vehicle (figure 66).

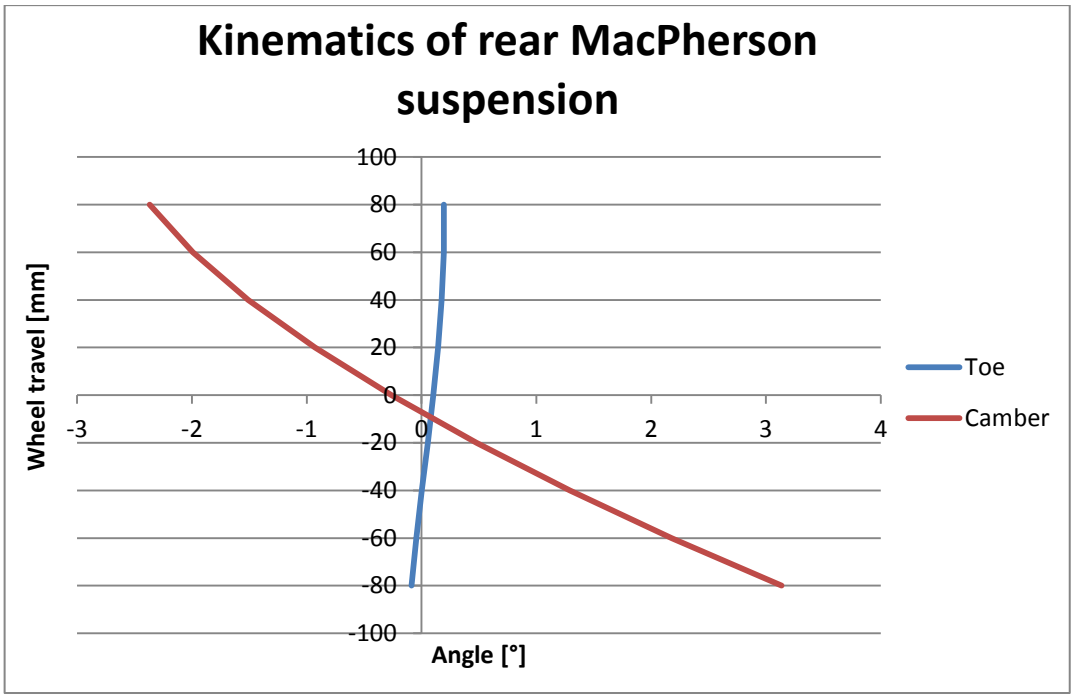

Figure 77 – Kinematics of rear left wheel of designed rear McPherson suspension.

Toe at zero position is set rather positive (0.1°) and further in bump travel, it slowly increases (up to 0.195°). These settings help to get directional stability of the vehicle. In rebound direction it starts to decrease, crossing neutral toe value at -40mm travel and continuing to little positive values of toe-out (up to -0.09°). Getting a little toe-out at the top of the rebound can help to avoid oversteering while cornering (figure 73).

Obtained values of kinematics can vary because of elastokinematics effects. As the suspension parts are deformed while experiencing loads, the angles can be slightly changed. Kinematics of the real suspension is also influenced by manufacturing precision and quality. In the lately coming dynamic tests, we won't take these effects into the account, but it is important to be aware of these phenomena.

Table 10 – Kinematics of rear left wheel of designed rear MacPherson suspension

Travel [mm]	Camber [°]	Toe [°]
80	-2.367	0.195
60	-1.992	0.193
40	-1.508	0.175
20	-0.928	0.144
0	-0.264	0.102
-20	0.478	0.054
-40	1.294	0.003
-60	2.18	-0.046
-80	3.136	-0.088

5.3 Calculation of suspension

5.3.1 Tires

In table 11 there is a comparison of tires of different city vehicles. For our vehicle was decided to use rear tires of *Twizy* (145/80 R 13 75 M) to all four wheels of our vehicle. The reason for the usage of wider tires in front (in comparison with *Twizy*), is to get better cornering ability and more grip while braking (as our vehicle is capable to go faster). In table 12 there is an explanation of tire marking. According to figure 79, the tire with speed index *M* is capable to go up to 130 km/h what is sufficient for our usage. Figure 80 shows maximal wheel loading according to load index and tire pressure. In table 13 there is a summation of the properties of selected tires. Inflation pressure was set according to *Twizy*, 2.3 bar on the front and 2.0 bar on the rear [19]. Nominal tire radius is measured on an unloaded tire and kinematic tire radius is calculated while the tire is rolling and is loaded. Both radii were obtained from tire generator in *CarMaker* as well as tire radial stiffness.

Figure 78 – The rear wheel of Twizy, wearing Continental Conti.eContact 145/80 R 13 75 M [18]

Table 11 – Comparison of tires of different production city cars. [19], [47], [29], [20]

Car	Front tires	Rear tires
Renault Twizy	125/80 R 13	145/80 R 13
Smart ForTwo II	155/60 R 15	175/55 R 15
Smart ForTwo III	165/65 R 15	185/60 R 15
Volkswagen e-Up!	165/65 R 15	165/65 R 15
Jiayuan City Spirit	145/70 R 12	145/70 R 12

Table 12 – Explanation of tire marking of the chosen tire. [8], [4], [1]

175	/65	R	13	75	M
Width of tire [mm]	Aspect ratio of tire height to tire width [%]	Radial construction type	Rim diameter [in]	Load rating	Speed rating

v_{max} in km/h^{-1}	Speed symbol	Identification
80	F	
130	M	
150	P	
160	Q	
170	R	
180	S	
190	T	
210	H	
240	V	
270	W	
300	Y	
over 210	—	VR
over 240	—	ZR (old system)

Figure 79 – Standardized speed categories for radial tires. [8]

Load index	Wheel load capacity in kg with tyre pressure measured in bars										
	1.5	1.6	1.7	1.8	1.9	2.0	2.1	2.2	2.3	2.4	2.5
69	215	225	240	250	260	270	285	295	305	315	325
70	225	235	245	260	270	280	290	300	315	325	335
71	230	240	255	265	275	290	300	310	325	335	345
72	235	250	260	275	285	295	310	320	330	345	355
73	245	255	270	280	295	305	315	330	340	355	365
74	250	260	275	290	300	315	325	340	350	365	375
75	255	270	285	300	310	325	335	350	360	375	387
76	265	280	295	310	320	335	350	360	375	385	400
77	275	290	305	315	330	345	360	370	385	400	412
78	280	295	310	325	340	355	370	385	400	410	425
79	290	305	320	335	350	365	380	395	410	425	437
80	300	315	330	345	360	375	390	405	420	435	450
81	305	325	340	355	370	385	400	415	430	445	462
82	315	330	350	365	380	395	415	430	445	460	475
83	325	340	360	375	390	405	425	440	455	470	487
84	330	350	365	385	400	420	435	450	470	485	500
85	340	360	380	395	415	430	450	465	480	500	515
86	350	370	390	410	425	445	460	480	495	515	530
87	360	380	400	420	440	455	475	490	510	525	545
88	370	390	410	430	450	470	485	505	525	540	560
89	385	405	425	445	465	485	505	525	545	560	580
90	400	420	440	460	480	500	520	540	560	580	600
91	410	430	450	475	495	515	535	555	575	595	615
92	420	440	465	485	505	525	550	570	590	610	630
93	430	455	475	500	520	545	565	585	610	630	650
94	445	470	490	515	540	560	585	605	625	650	670
95	460	485	505	530	555	575	600	625	645	670	690
96	470	495	520	545	570	595	620	640	665	685	710
97	485	510	535	560	585	610	635	660	685	705	730
98	500	525	550	575	600	625	650	675	700	725	750
99	515	540	570	595	620	650	675	700	725	750	775
100	530	560	590	615	640	670	695	720	750	775	800

Figure 80 – Load capacity of a tire according to tire pressure. [8]

Table 13 – Summation of properties of chosen tires.

	Marking	Inflation pressure [bar]	Radial stiffness [N/m]	Nominal tire radius [m]	Kinematic tire radius [m]	Wheel load capacity [kg]	Actual max. load [kg]
Front tire	145/80R13 75 M	2.3	329 129	0.2810	0.2722	360	170
Rear tire	145/80R13 75 M	2.0	311 840	0.2810	0.2717	325	177

5.3.2 Quarter car model

The quarter car model is used to theoretically determine the stiffness of springs and the level of damping of dampers. This calculation comes from the theory of vibration of a system with two masses. It is called the quarter car model because we reckon only with a simplified model of one wheel, its tire and mass of chassis supported by this wheel. The calculation model is depicted in figure 81 where m_1 is mass of unsprung masses (e.g. tire, rim, some parts of suspension system), m_2 is mass of sprung masses (chassis over this wheel), k_{01} is vertical stiffness of tire, k_{12} is vertical stiffness of the suspension spring and b_{12} is damping of the damper. The calculation is performed in the state of a maximal permissible load of the vehicle. Kerb mass and weight of unsprung mass was taken from *Twizy*. [19] Weight distribution was taken from the calculation of the folding mechanism in chapter 4.1.

Table 14 –Input parameters for quarter car model calculation.

Vehicle [19]	
Kerb mass	474 kg
Gross train weight	694 kg
Maximum payload	220 kg
Rear suspension	
Weight on rear (empty)	244 kg
Weight on rear (full load)	354 kg
Unsprung mass [18]	26.7 kg
Sprung mass [18]	152.3 kg
Tire stiffness	311 840 N/m
Front suspension	
Weight on front (empty)	230 kg
Weight on front (full load)	340 kg
Unsprung mass [18]	22.2 kg
Sprung mass [18]	147.8 kg
Tire stiffness	329 129 N/m

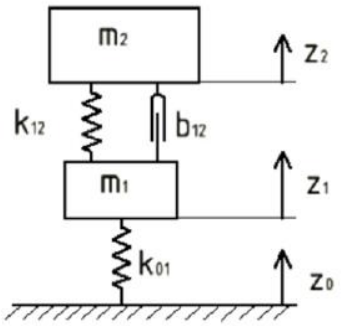

Figure 81 – The vibration system of two masses, z_1 is the position of unsprung mass, z_2 is the position of the sprung mass. [9]

Two differential equations, one for each mass, were obtained using Newton's second law of motion (figure 81).

$$m_1\ddot{z}_1 = k_{12}(z_2 - z_1) + b_{12}(\dot{z}_2 - \dot{z}_1) - k_{01}z_1$$

$$m_2\ddot{z}_2 = -k_{12}(z_2 - z_1) - b_{12}(\dot{z}_2 - \dot{z}_1)$$

We need to transform it into the undampened system (b_{12} = 0) in matrix form in order to get natural frequencies of both masses.

$$\begin{bmatrix} m_1 & 0 \\ 0 & m_2 \end{bmatrix} \cdot \begin{bmatrix} \ddot{z}_1 \\ \ddot{z}_2 \end{bmatrix} + \begin{bmatrix} k_{01} + k_{12} & -k_{12} \\ -k_{12} & k_{12} \end{bmatrix} \cdot \begin{bmatrix} z_1 \\ z_2 \end{bmatrix} = \begin{bmatrix} 0 \\ 0 \end{bmatrix}$$

We simplify it to the following expression.

$$M\ddot{Z} + K\ddot{Z} = 0$$

The natural frequencies are calculated according to this formula.

$$\det(K - \lambda M) = 0$$

$$\begin{vmatrix} k_{01} + k_{12} - \lambda m_1 & -k_{12} \\ -k_{12} & k_{12} - \lambda m_2 \end{vmatrix} = 0$$

$$(k_{01} + k_{12} - \lambda m_1)(k_{12} - \lambda m_2) - k_{12}^2 = 0$$

$$\lambda^2(m_1 m_2) + \lambda(-k_{01}m_2 - k_{12}m_2 - m_1 k_{12}) + k_{01}k_{12} = 0$$

$$k_{12} = \frac{k_{01}\lambda m_2 - \lambda^2 m_1 m_2}{k_{01} - \lambda m_1 - \lambda m_2}$$

There is a substitution for parameter λ:

$$\lambda = 4\pi^2 f_2$$

Where f_2 is the natural frequency of unsprung mass. According to [8] the natural frequency of unsprung mass should be set in these intervals:

- **Front suspension**: 60- 80 min^{-1} = **1 Hz – 1.33 Hz**
- **Rear suspension**:70 -90 min^{-1} = **1.17 Hz – 1.5 Hz**

The natural frequency of the body over the rear axle is chosen to be 10-20% higher than that of the body over the front axle. Thus the vibrating motion resulting from vibration of the front axle caused by unevenness of the road surface is overtaken by more quickly vibrating rear axle. Thus causes the bouncing motion, which is desirable for comfort reasons, instead of pitching motion which is uncomfortable for occupants of the car. [8] For this calculation was chosen a frequency of **1.2 Hz** for the rear and **1 Hz** for the front in the state of the maximal load. This results in spring stiffness of **8906 N/m**

for the rear and **5941 N/m** for the front. The obtained value of spring stiffness is only theoretical and must be recalculated according to the geometry of suspension which will be done only for the rear suspension.

Table 15 – Input parameters for the spring calculation

Distance (fig. 82)	*a*	258 mm
Distance (fig. 82)	*b*	355 mm
Angle of spring axis (fig. 82)	α	14°
Wire diameter	*d*	10 mm
Spring central diameter	*D*	80 mm
Gravitational constant	*g*	9.81 $m.s^{-1}$
Material of spring: Steel *61SiCr7* [49]		
Yield stress	R_m	1550 MPa
Shear modulus	*G*	80 GPa

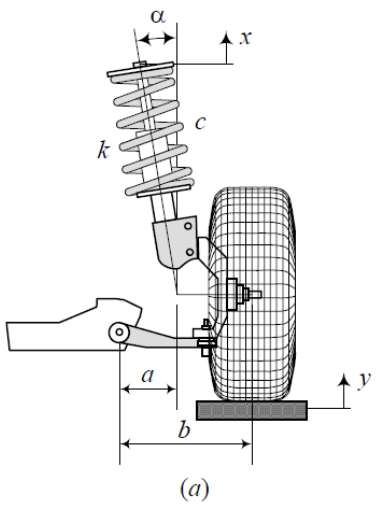

Figure 82 – McPherson suspension and its motion ratio explanation

Motion ratio *M* is a ratio of movement of the spring and wheel (figure 82) and the values were measured from the kinematical model in *Catia*.

$$M = \frac{a}{b} = 0.73$$

The calculation of the spring stiffness comes from an energy balance.

$$\frac{1}{2}kx^2 = const$$

$$k_{12\,M} = \frac{k_{12}}{M^2} = 16862\ N/m$$

Afterwards, the inclination of the spring axis (figure 82) is taken into the account. Then we get final stiffness of the real spring.

$$k_{12\,M\alpha} = \frac{k_{12\,M}}{\cos\alpha} = 17378\ N/m$$

With the usage of material properties of steel *61SiCr7,* we can get a number of active coils *n*. [11]

$$n = \frac{Gd^4}{8D^3 k_{12\,M\propto}} = 11.2 \cong 11$$

Assuming the load of one person (70 kg which is equally distributed to all wheels), we can compute force acting on the spring F_{nom} and shortage of the spring Δx_{nom}.

$$F_{nom} = \frac{m_2 g}{M\cos\alpha} = 1597\ N$$

$$\Delta x_{nom} = \frac{F_{nom}}{k_{12M\alpha}} = 91.9\ mm$$

The sag of the wheel under nominal load (1 person) Δz_2:

$$\Delta z_2 = \frac{\Delta x_{nom}}{M} = 126.5\ mm$$

However, desired sag (rebound) of the wheel is 80 mm (while nominally loaded by 1 person), so we need to calculate the shortage of the spring $\Delta x_{rebound}$ when the wheel position is changed by sag = 80 mm.

$$\Delta x_{rebound} = \frac{sag\ M}{\cos\alpha} = 59.9\ mm$$

Thus to set the rebound from the original value of Δz_2 to desired 80 mm we need to apply a pretension Δx_0 of the spring.

$$\Delta x_0 = \Delta x_{nom} - \Delta x_{rebound} = 32\ mm$$

If the length of installed spring (in maximal rebound) $x_{install}$ = 325mm then the free length of the spring is x_{free}:

$$x_{free} = x_{installed} + \Delta x_0 = 357\ mm$$

We required the bump travel of the wheel of 80 mm, so we need to find the change of the spring length Δx_{bump} accordingly:

$$\Delta x_{bump} = \Delta x_{rebound} = \frac{x_{bump}\ M}{\cos\alpha} = 59.9\ mm$$

Length of the spring while nominally loaded by 1 person x_{design}:

$$x_{design} = x_{free} - \Delta x_{nom} = 265\ mm$$

Length of the spring while the wheel is in the maximal bump position (80 mm):

$$x_{bump} = x_{design} - \Delta x_{bump} = 205\ mm$$

Maximal force in spring while in maximal bump:

$$F_{bump} = k_{12M\alpha}\left(x_{free} - x_{bump}\right) = 2638\ N$$

Shear stress in the spring: [11]

$$\tau_{bump} = \frac{8F_{bump}D}{\pi d^3} = 537\ MPa$$

The highest allowed shear stress [10]:

$$\tau_D = 0.56R_m = 806\ MPa$$

The condition of shear stress safety is satisfied.

$$\tau_D > \tau_{bump}$$

$$806\ MPa > 537\ MPa$$

Check of the minimal geometrical length of the spring:

$$x_{bump} = 205\ mm > nd = 112\ mm$$

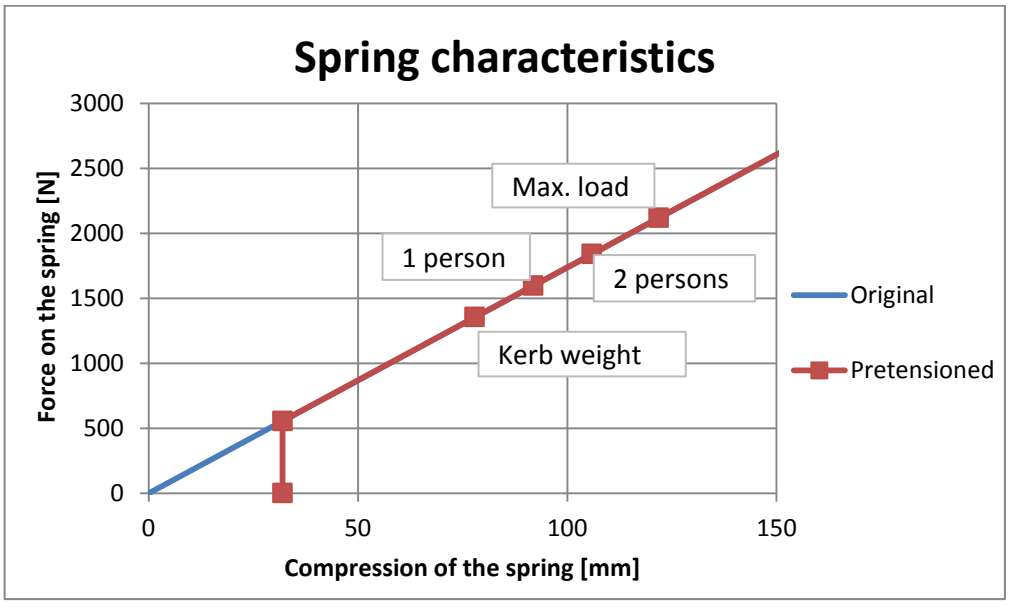

Figure 83 – Theoretical spring characteristics.

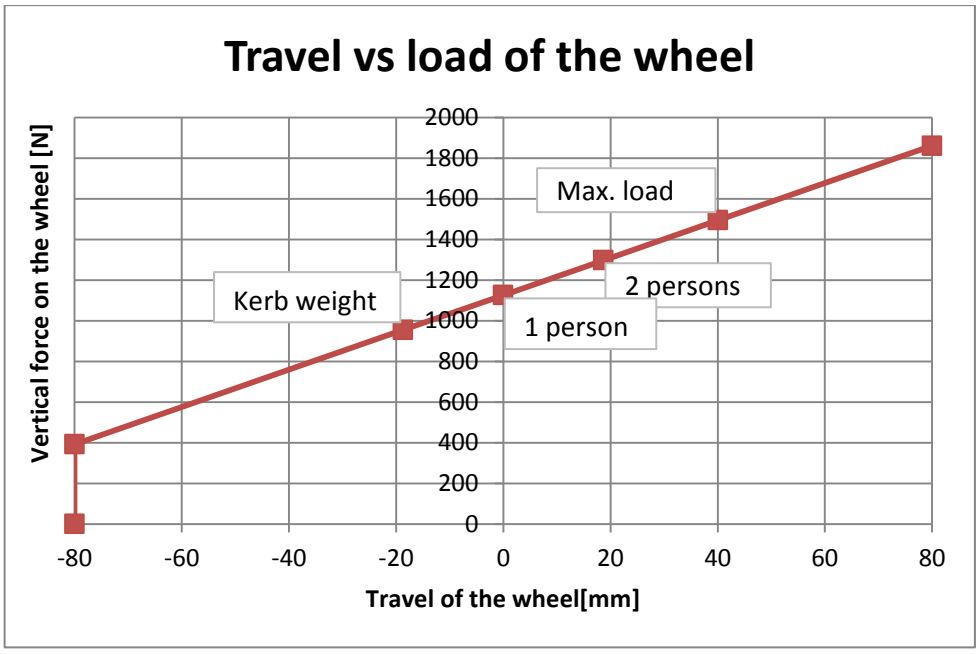

Figure 84 – Theoretical dependency of the load of the vehicle and travel of the wheel.

Damping calculation comes from the equation for a single vibrating mass with damping.

$$m\ddot{x} + b\dot{x} + kx = 0$$

The critical damping ration is achieved when the following formula is equal to zero.

$$D = b^2 - 4km$$

$$b^2 - 4km = 0$$

Critical damping for the rear suspension while fully loaded:

$$b_c = \sqrt{4km} = 2\sqrt{k_{12}m_2} = 2329\ N/(m.s^{-1})$$

Damping ratio was chosen equal to 0.3 while fully loaded:

$$\zeta = \frac{b}{b_c} = 0.3$$

Damping:

$$b = \zeta b_c = 699\ N/(m.s^{-1})$$

Real damping respecting the geometry of the suspension:

$$b_{M\alpha} = \frac{b_{12}}{M^2 \cos\alpha} = 1364\ N/(m.s^{-1})$$

Damping ratio should be set approximately in a range from 0.2 to 0.4 for an empty vehicle and 0.15 to 0.3 for a fully-loaded vehicle. The lower value of damping ratio is used when comfort is

prioritized and the higher ratio contributes to ride safety. [3] As the vehicle is very narrow which can be critical in terms of roll stability we decided for a higher value of critical damping of 0.3 (in the fully loaded state). In table 16 there are summed all calculated values. The natural frequencies of the unsprung masses reach quite high values, because of light weight of it and higher vertical stiffness of the tire. Usually it is set around 10Hz, but it is still acceptable less than 20Hz. [4] However, it can be easily tuned by the application of different tire and inflation pressure.

Table 16 – Calculated values of the suspension system

Rear	
Spring stiffness	8906 N/m (17 378 N/m)
Natural freq. (loaded)	1.2 Hz
Natural freq. (driver only)	1.38 Hz
Unsprung mass nat. freq.	18.1 Hz
Damping	699 N/(m.s^{-1}) (1364 N/(m.s^{-1}))
Damping ratio (full load)	0.3
Damping ratio (driver only)	0.34
Number of active coils	11
Free length	357 mm
Front	
Spring stiffness	5941 N/m
Natural freq. (loaded)	1 Hz
Natural freq. (driver only)	1.16 Hz
Unsprung mass nat. freq.	19.5 Hz
Damping	562 N/(m.s^{-1})
Damping ratio (full load)	0.3
Damping ratio (driver only)	0.347

5.3.3 Straining of the suspension

For the determination of static and dynamic forces acting on joints and silentblocks of suspension was used a simplified kinematic model of the suspension. To evaluate dynamic straining, we assumed the quasistatic load of the suspension according to [12]. The maximal forces acting on the suspension were derived as a multiplication of static vertical force (normal force on the rear wheel while fully loaded). The calculation model was simplified. The shock absorber was assumed as rigid, so we regard the worst case when the wheel is fully compressed. For further simplification, the lower arm of suspension was placed in a horizontal position. All the dimensions were measured directly from *Catia* kinematic model. Six cases, two static and four dynamic, were prepared to evaluate the maximal load of all joints. The results of this analysis should be used for an order of correct silentblocks and joints from the manufacturer.

Table 17 – Quasistatic determination of dynamical forces. [12]

	Mark	Multiplication of static force	Value
Static force	F_z	-	1736 N
Vertical force	$F_{z\,max}$	3x	5209 N
Longitudinal force	$F_{x\,max}$	2x	3473 N
Lateral force	$F_{y\,max}$	2x	3473 N
	M_y	$F_{y\,max}.r_d$	944 Nm
Braking forces	F_{zb}	1.5x	2605 N
	F_{xb}	1x	1736 N
	M_b	$F_{xb}.r_d$	487 Nm

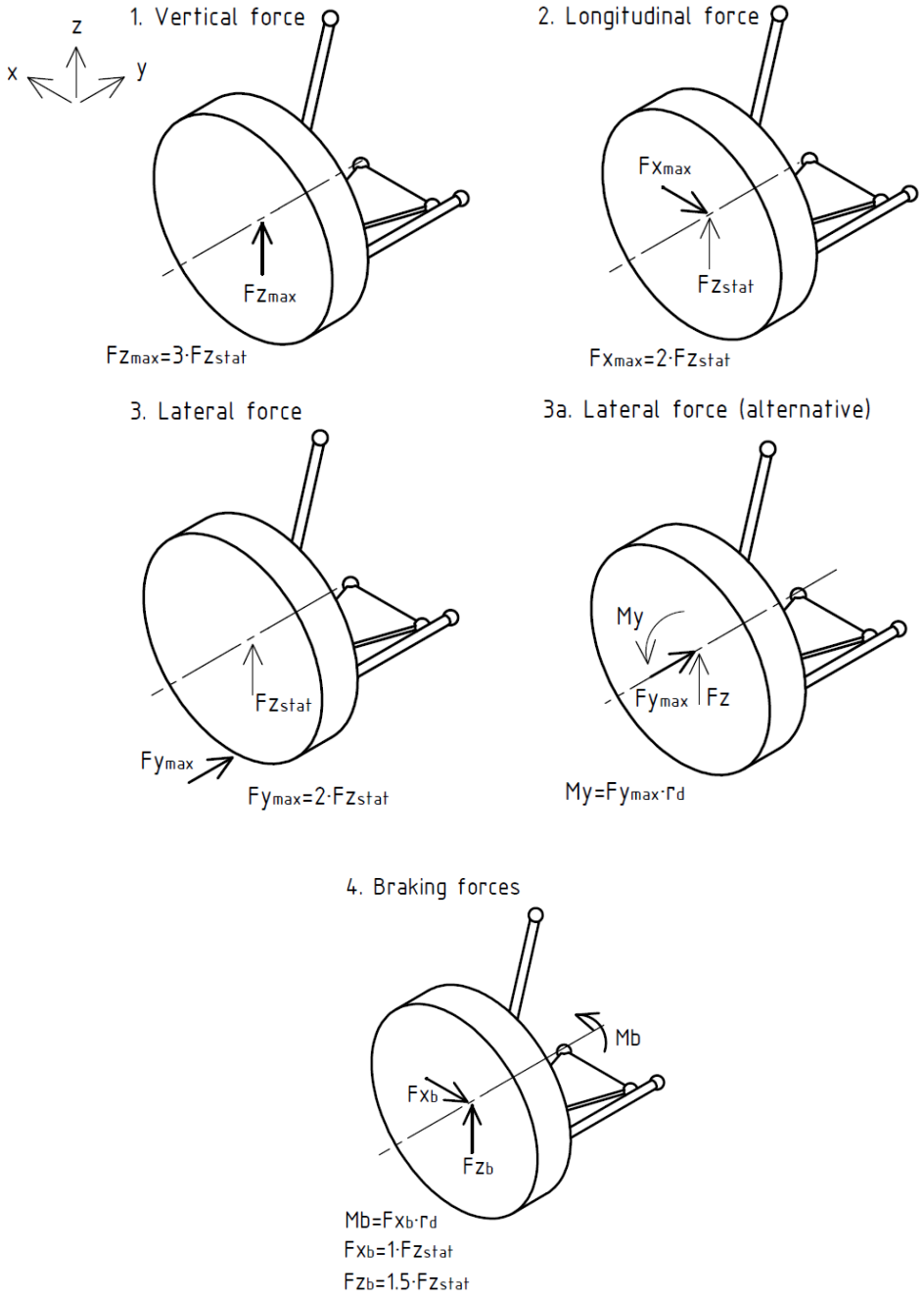

Figure 85 – Explanation of maximal forces acting on the suspension and calculation cases.

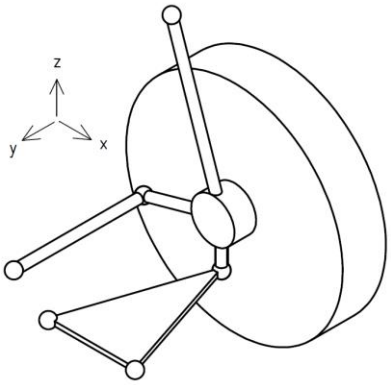

Figure 86 – Calculation model of suspension.

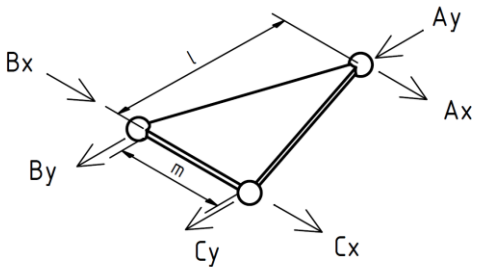

Figure 87 – Lower arm.

$$A_x + B_x + C_x = 0$$

$$A_y + B_y + C_y = 0$$

$$B_x l + B_y \frac{m}{2} + C_x l - C_y \frac{m}{2} = 0$$

$$B_x - C_x = 0$$

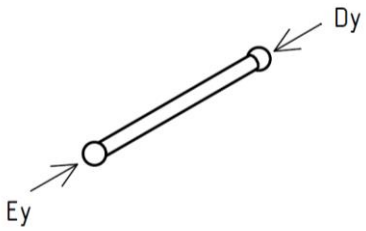

Figure 88 – Upper arm.

$$D_y - E_y = 0$$

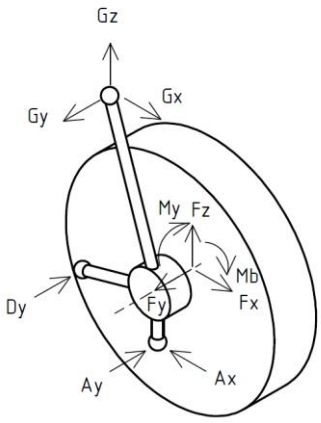

Figure 89 – Knuckle and shock absorber.

$$F_x + G_x - A_x = 0 \quad *$$

$$-D_y + G_y - A_y + F_y = 0$$

$$G_z + F_z = 0 \quad *$$

$$-G_z g_y + A_y a_z + D_y d_z + G_y g_z - M_y = 0$$

$$A_x a_z + G_x g_z + G_z g_x + M_b = 0$$

$$-A_x a_y - D_y d_x + G_x g_y + G_y g_x = 0$$

In case when the rear axle is folded, the normal vertical force changes its direction relative to the suspension system.

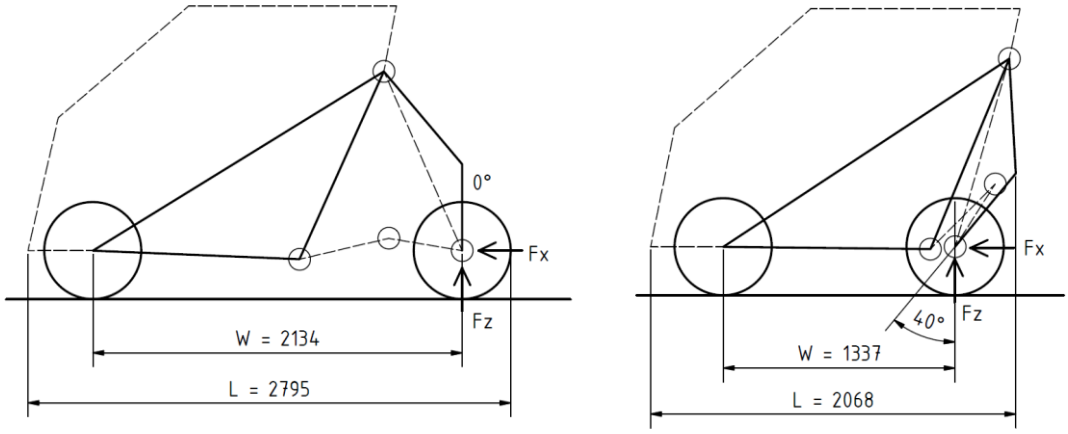

Figure 90 – Demonstration of tilting of the suspension while folded and resulting change of static load.

Two equations of knuckle and shock absorber marked with stars were replaced with the following equations in order to simulate tilt of the suspension while it is folding. The tilt angle α results in 40° in the parking position.

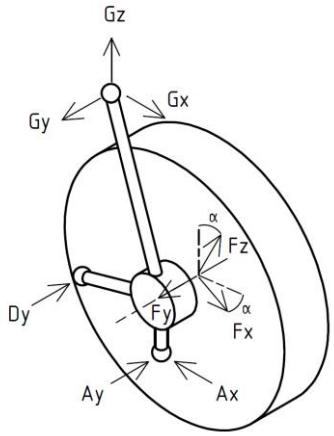

Figure 91 – Modification of equations of knuckle and shock absorber when the suspension is tilted.

$$F_x \cos\alpha + F_z \sin\alpha + G_x - A_x = 0$$

$$G_z + F_z \cos\alpha - F_x \sin\alpha = 0$$

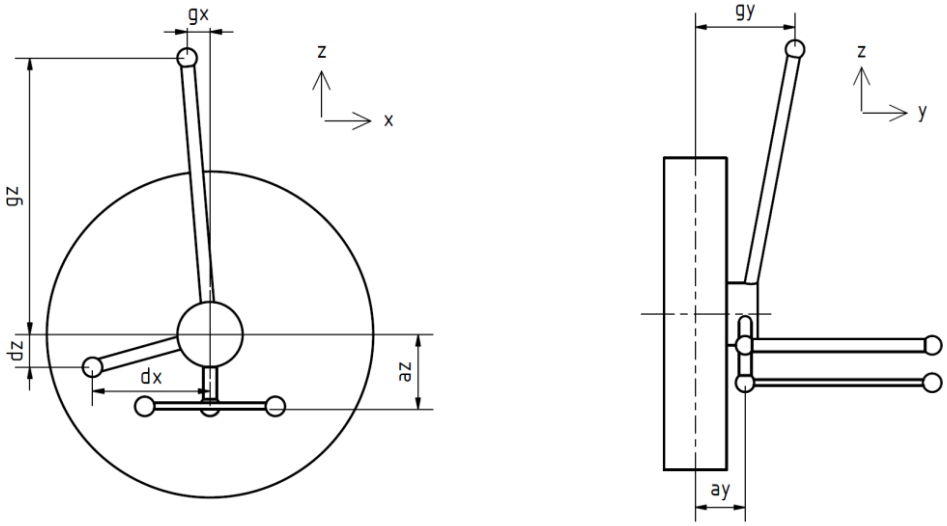

Figure 92 – Geometry of the suspension.

Table 18 – Input parameters [m]

l	0.3
m	0.2
ay	0.045
a_z	0.11
d_x	0.12
d_z	0.06
g_x	0.035
g_y	0.205
g_z	0.424
r_d	0.2717

Table 19 – Resulting static forces.

Static: ride		Static: park	
Load [N]			
Fx	0	*Fx*	0
Fy	0	*Fy*	0
Fz	1736	*Fz*	1736
alpha	0°	alpha	40°
Resulting forces [N]			
Ax	113.7828	*Ax*	973.1803
Ay	-626.683	*Ay*	195.4427
Bx	-56.8914	*Bx*	-486.59
By	484.0155	*By*	1362.049
Cx	-56.8914	*Cx*	-486.59
Cy	142.6672	*Cy*	-1557.49
Dy	-43.8665	*Dy*	-778.897
Ey	-43.8665	*Ey*	-778.897
Gx	113.7828	*Gx*	-142.701
Gy	-670.549	*Gy*	-583.454
Gz	-1736	*Gz*	-1329.85

Table 20 – Resulting dynamic forces.

Max. vertical		Max longitudinal		Braking		Max. lateral	
Load [N]							
Fx	0	*Fx*	-3473	*Fx*	-1736	*Fx*	0
Fy	0	*Fy*	0	*Fy*	0	*Fy*	3473
Fz	5209	*Fz*	1736	*Fz*	2605	*Fz*	1736
				Mb	487 Nm	*My*	974 Nm
Resulting forces [N]							
Ax	341	*Ax*	**-2644**	*Ax*	-2091	*Ax*	114
Ay	-1880	*Ay*	-2729	*Ay*	-894	*Ay*	**3612**
Bx	-171	*Bx*	**1322**	*Bx*	1045	*Bx*	-57
By	1452	*By*	-2601	*By*	**-2689**	*By*	-1635
Cx	-171	*Cx*	**1322**	*Cx*	1045	*Cx*	-57
Cy	428	*Cy*	**5330**	*Cy*	3583	*Cy*	-1977
Dy	-132	*Dy*	**2276**	*Dy*	-117	*Dy*	271
Ey	-132	*Ey*	**2276**	*Ey*	-117	*Ey*	271
Gx	341	*Gx*	**829**	*Gx*	-355	*Gx*	114
Gy	**-2012**	*Gy*	-453	*Gy*	-1011	*Gy*	411
Gz	**-5209**	*Gz*	-1736	*Gz*	-2605	*Gz*	-1736

5.3.4 Bearing calculation

In the hub of the wheel will be used double row angular contact ball bearing *SKF 3207*. This type of bearing is often used for this automotive application, because of its durability and ability to bear high axial forces. To begin the calculation of the bearing, it's necessary to determine forces acting on it. For this purpose, we use the previous quasistatic estimation of dynamic forces according to table 17. Maximal radial force can be obtained as a vector addition of maximal vertical and longitudinal forces. An axial force F_a is equal to lateral force.

$$F_r = \sqrt{F_z^2 + F_x^2} = 6261\ N$$

$$F_a = F_y = 3473\ N$$

Note: We assume constant maximal radial and maximal axial load of the bearing (according to table 17). In reality, the loads in different directions vary during the ride. In order to get more accurate estimation, there must be implemented a more advanced model of load fluctuations. However, with this approach, we can guarantee the obtained result of bearing's life because we were assuming the worst case of loading. It's also important to be aware of the fact that evaluated values of acting forces on the wheels (in table 17), were only guessed (according to [12]) and can be exceeded in some rare occasions during the ride.

The ratio of axial and radial force will determine the next step of the calculation. In our case the ratio *Fa/Fr* = 0.55 which is less than *e* = 0.8, thus we will continue with the second formula. [50]

$$\frac{F_a}{F_r} \leq e \ \rightarrow P = F_r + Y_1 F_a$$

$$\frac{F_a}{F_r} > e \ \rightarrow P = XF_r + Y_2 F_a = 8969\ N$$

Where *P* is equivalent dynamic load and *e*, Y_1, Y_2, *X* are calculation factors. The final step is to determine the approximate value of the bearing life according to the following relations:

$$L_{10} = \left(\frac{C}{P}\right)^p = 72.85\ 10^6 revolutions$$

$$L_{km} = 2\pi r L_{10} \cong \mathbf{128\ 400\ km}$$

Where L_{10} is basic rating life (at 90% reliability; millions of revolutions), L_{km} is basic rating life (at 90% reliability; thousands of kilometres), *C* is basic dynamic load rating [kN], *P* is equivalent dynamic bearing load, *p* is exponent for the life equation (= 3 for ball bearings). [50]

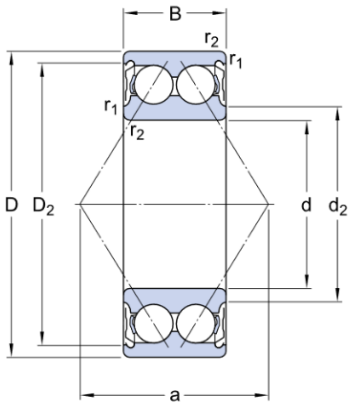

Figure 93 – SKF 3207 A-2Z. [50]

Table 21 – Basic parameters of SKF 3207 A-2Z. [50]

d	35 mm
D	72 mm
B	27 mm
C	40 kN
e	0.8
X	0.63
Y1	0.78
Y2	1.24
rpm_{max}	9000 rpm

5.4 Catia model

CATIA is an engineering and design software for product 3D CAD design. It is used to design, simulate, analyse, and manufacture products in a variety of industries including aerospace, automotive, consumer goods, industrial machinery and much more. [57]

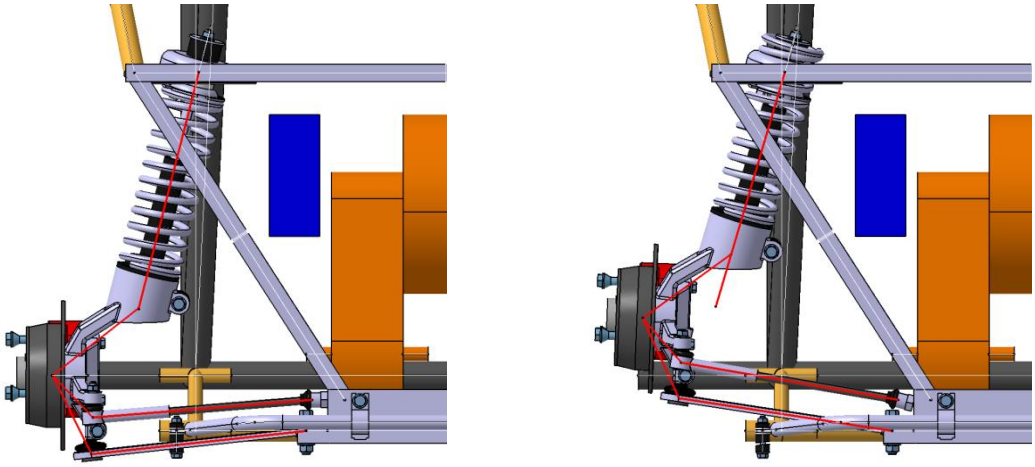

Figure 94 - Kinematic model of the suspension in Catia (red lines represent the wire model).

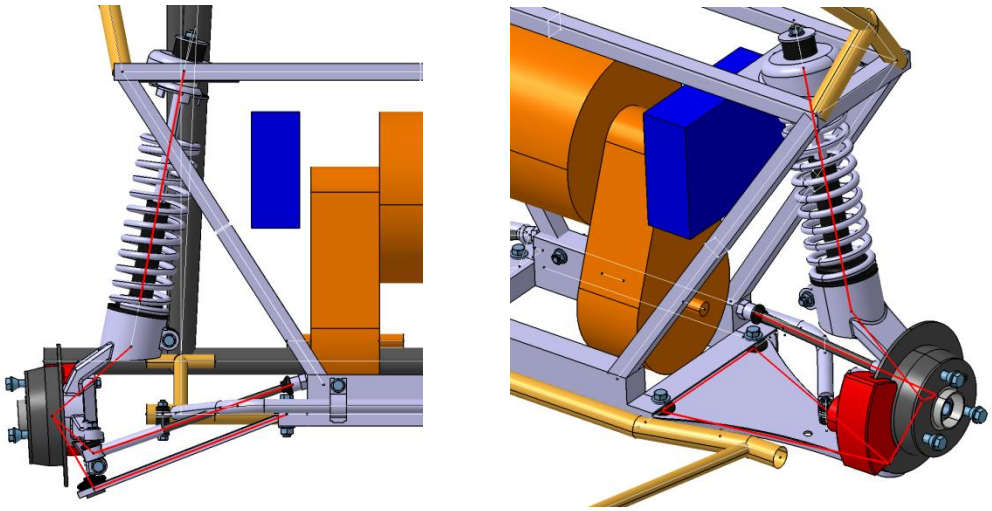

Figure 95 – Kinematic model of the suspension in Catia (red lines represent the wire model).

The process of modelling started with the construction of a wire model of the parts of the suspension system of the rear left wheel. All constraints and joints between the parts were defined in *DMU Kinematics* in *Catia*. This allowed us to inspect and tune kinematics of the rear wheel. The vertical position of the rear wheel was set as a variable in the range from -80 to 80 mm, simulating the wheel travel. Afterwards, the geometry was mirrored to simulate the right rear wheel too, respecting decided wheel track of 1100 mm. Both wire models of the rear suspension were connected to the symbolic wire model of the chassis of the vehicle. Another variable of changing wheelbase (from 1337 mm to 2134 mm) was defined to simulate the folding mechanism. The kinematic model of the vehicle has 3 degrees of freedom: rear left, rear right suspension and folding mechanism. On the wire models of the parts of the suspension system were built bodies, representing the volume of the structure. Appling dress-up option, different parts can be connected together as one kinematic object.

The design of the rear MacPherson suspension was inspired by *Renault Twizy*. The priority of the design was to keep it as cheap as possible, simple and reliable. Major parts of the suspension (in terms of kinematics) are the lower arm, upper arm, casing (knuckle) and shock absorber. The upper arm length can be adjusted to set the correct toe angle. The shock absorber consists of combined coil spring and damper. The knuckle houses the bearing downloaded from the SKF library. The hub is pressed into the inner diameter of the bearing. The brake disc is secured with the hub by 1 small screw. The wheel is attached to the hub by three bolts. The rim and tire have the same size as *Twizy's*. The brake calliper model is only symbolical as it will be ordered from external manufacturers. The decision of final calliper also influences the final choice of the brake disc and mountings for the calliper on the knuckle. The frame was designed as narrow as possible to allow high range of the folding mechanism. The lower part of the frame holds lower arms and is made to be as stiff as possible. To the upper part of the frame are welded forged brackets for the shock absorber. In the middle of the frame is located electric motor with drive shafts and inverter. Their design is only representative just to verify if they fit in the frame, as they will be bought from an external supplier. The chassis and detailed design of the folding mechanism was not solved in this thesis, so they are represented by simplified structure to show the possible size of the vehicle. All bolts and nuts were downloaded from an online library [54].

Figure 96 – Render of the folding mechanism, park mode length is 2110mm, ride mode length is 2810 mm.

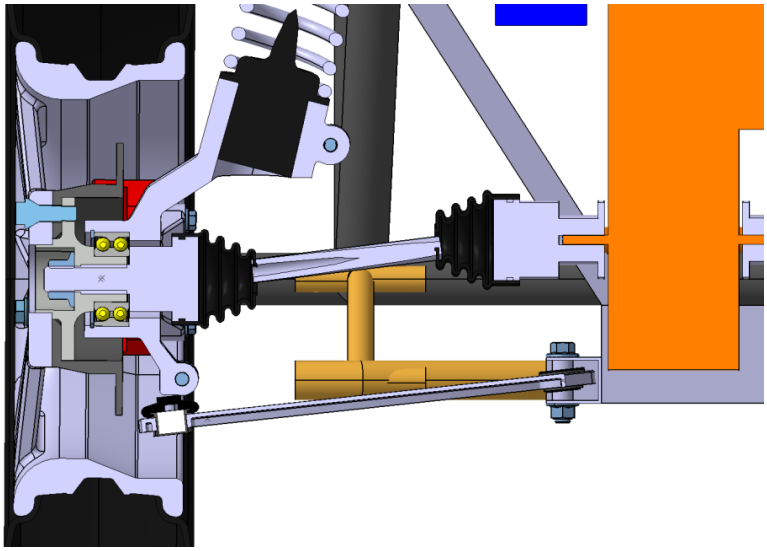

Figure 97 – Cross-section of the rear left wheel.

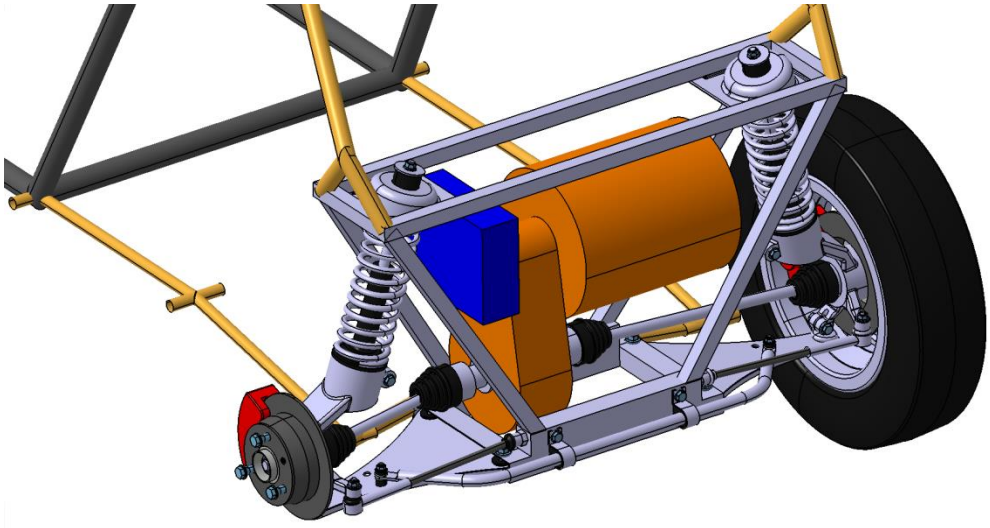

Figure 98 – Rear suspension.

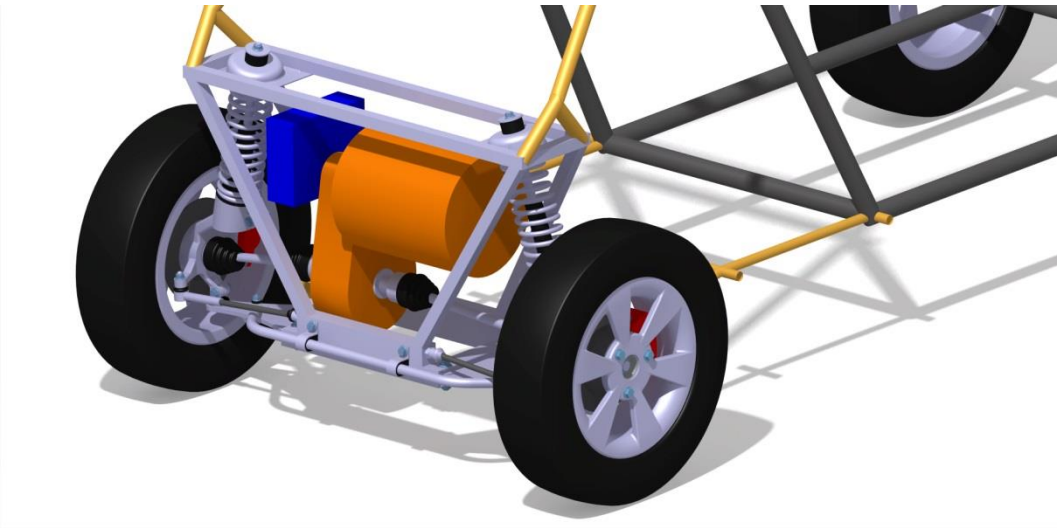

Figure 99 – Render view on the rear suspension.

6. Simulation of dynamic tests

CarMaker was developed by *IPG Automotive* as a simulation solution specifically for the testing of passenger cars and light-duty vehicles. Using this software, the real-world test scenarios can be modelled, including the entire surrounding environment, in the virtual world. Powerful and real-time capable models for vehicles, roads, drivers and traffic make this possible. *CarMaker* is an open integration and test platform and can be applied throughout the entire development process – from model- to software- to hardware- to vehicle-in-the-loop. *CarMaker* can bring significant savings in cost and time for the development of a vehicle. [53]

6.1 Vehicle dynamics fundamentals

Before starting any dynamical tests, we need to define some terms from vehicle dynamics. In figure 100, there is a definition of the coordinate system of the vehicle according to SAE (Society of Automotive Engineers), which is going to be used in the test in *CarMaker*.

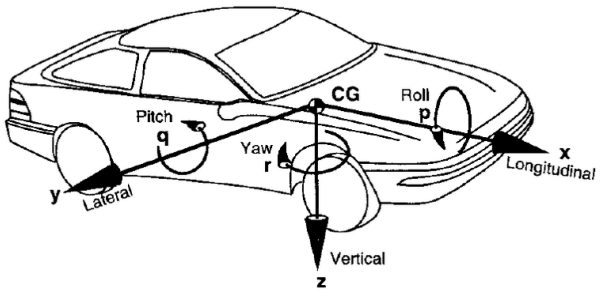

Figure 100 – Definition of a coordinate system in vehicle dynamics according to SAE. [51]

During many tests, we will also measure the **side slip angle** of the tire. Side slip angle is the angle between the direction in which a wheel is pointing and the direction in which it is actually

travelling (figure 101). According to SAE, side slip angle is considered positive if the tire is slipping to the right. It can be calculated from the longitudinal and lateral velocity of the wheel.

$$\alpha = -arctan\left(\frac{v_y}{|v_x|}\right)$$

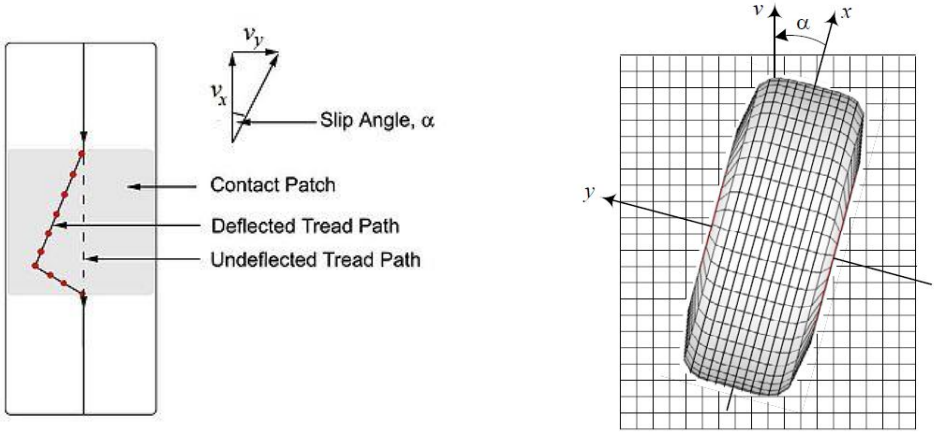

Figure 101 – Side slip angle is the angle between the velocity vector and the x-axis measured about the z-axis. [52], [4]

6.2 CarMaker vehicle set –up

Kinematic properties of the rear MacPherson suspension has to be transformed into text-type *.skc* file which is used in *CarMaker* to define kinematics of a suspension. For our purpose is used simplified description where we don't consider elastokinematics, antiroll bar behaviour and some other parameters. Parameters which were measured in *Catia* (on the left rear wheel) and written in *.skc* file are: toe angle r_z, camber angle r_x, longitudinal translation t_x, lateral translation t_y and wheel compression t_z (all angles are in radians and translations in meters). A spin of the wheel r_y was not considered.

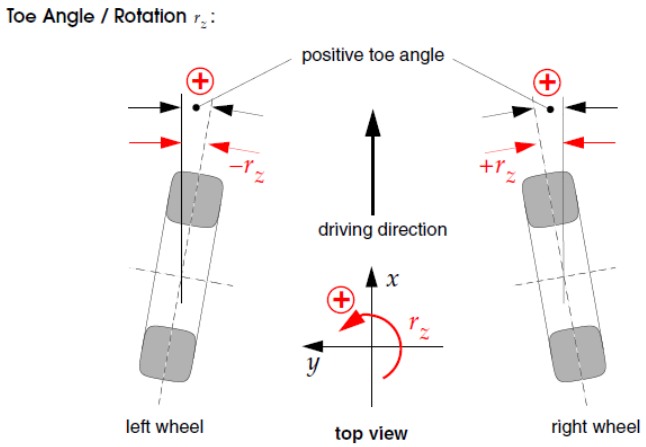

Figure 102 – Toe angle r_z. A positive toe angle at the right wheel carrier equals a positive rotation r_z. [53]

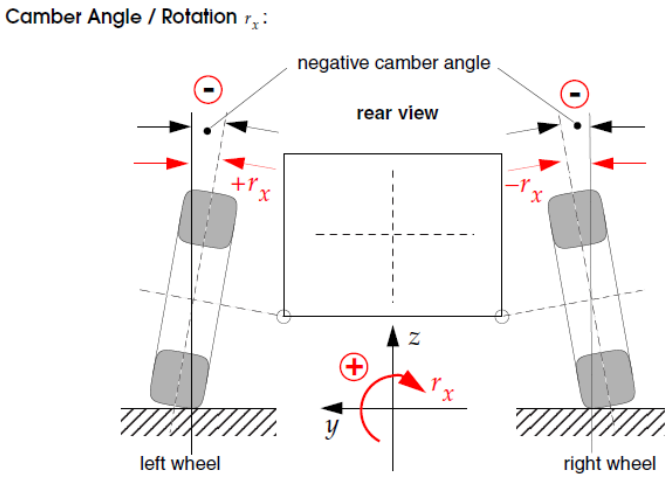

Figure 103 – Camber angle r_x. A positive camber angle at the right wheel carrier equals a positive rotation r_x. [53]

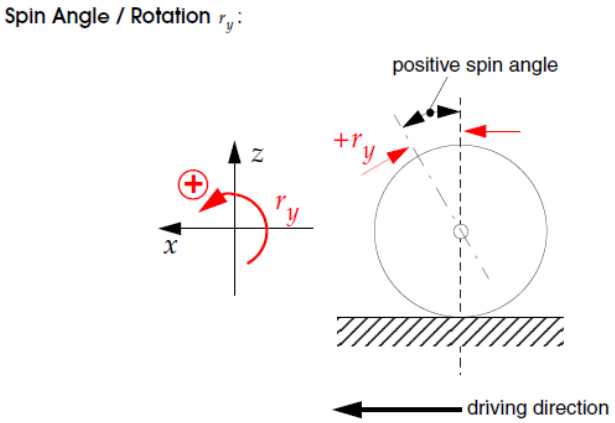

Figure 104 – Spin angle r_y. A positive spin angle equals a positive rotation r_y. [53]

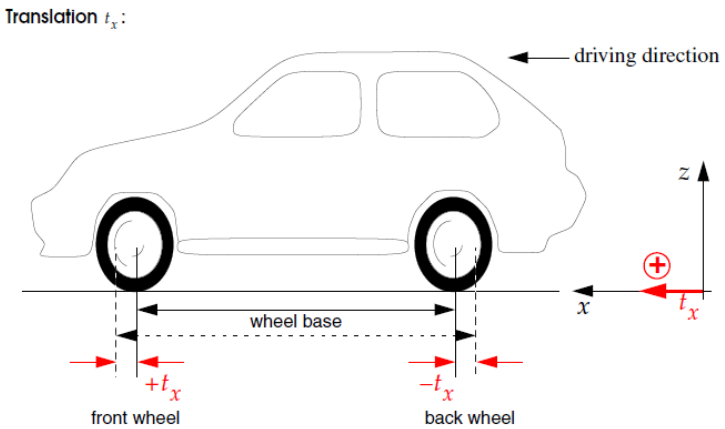

Figure 105 – Longitudinal translation t_x. The translations t_x of front and back wheel are parametrized independently. The change of wheelbase is a result of both, the change of the front and the back wheel. [53]

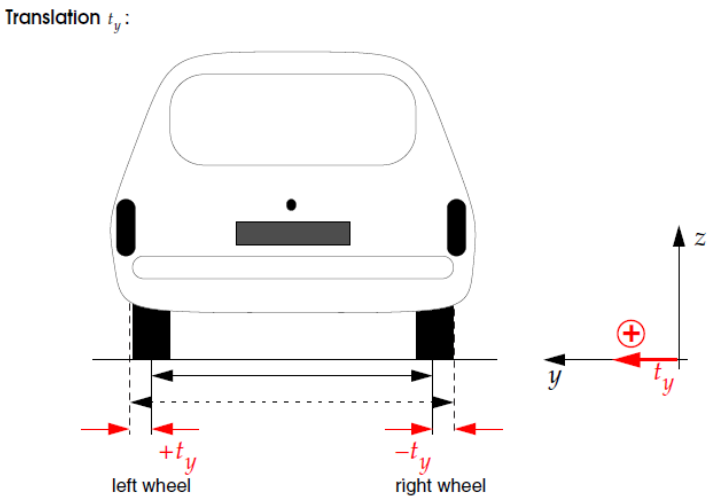

Figure 106 – Lateral translation t_y. The translations t_y of left and right wheel are parametrized independently. The change of wheel track is a result of both, the change of the left and the right wheel. [53]

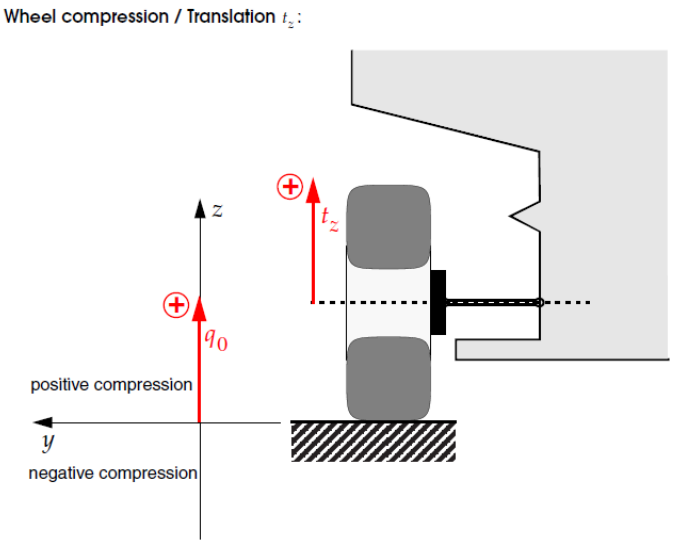

Figure 107 – Wheel compression t_z. Positive wheel compression tz is defined in an upward direction. Usually, translation t_z = 0 equals the position in vehicles design configuration. [53]

In table 22 there is a parameterization of the previously designed rear MacPherson suspension. The only variable in the description is the wheel compression. On the front was used a front MacPherson suspension from an example in CarMaker. As it is a front suspension, the description is much more complicated, as a two-variable map (wheel compression and steering rod position as variables). In figure 108 there are depicted some parameters to make a comparison with the rear suspension. We can notice similar camber behaviour but the alterations are smaller. Toe keeps slightly positive along most of the wheel travel, but surprisingly it changes to toe-out from 60 mm to 80 mm of travel. This is very rare setting which can lead to some instability when a bump is hit. After trying first tests with previously theoretically-calculated values, the suspension was tuned to get better results.

- Springs were stiffened at all the wheels to get more stability in corners, but it negatively influences overall comfort. However, natural frequency of the unsprung mass still satisfies previously mentioned limits in all loadings (table 24).

- Anti-roll bars virtual stiffness were generated according to the input parameters. These original values must have been increased on both front and rear. It radically reduced the roll of the chassis and helped with the roll stability which is critical for a short wheel track vehicle.
- Damping was adjusted according to the stiffer springs. For safety reasons was chosen higher damping ratio which again negatively decreases ride comfort.

All the input parameters into the *CarMaker* model are summed in table 23. Very important parameter, CG (centre of gravity) of the vehicle, was estimated according to the weight distribution which was previously calculated. The height of CG was generated by *CarMaker* with consideration of typical values for small cars. As we don't know the detailed construction of the vehicle, this rough estimation is enough at this point of development of the vehicle. However, the final position of CG can radically change the vehicle's stability and ability in corners.

Table 22 – SKC parameterization of the rear MacPherson suspension.

travel	*comp*	*tx*	*ty*	*tz*	*rx*	*ry*	*rz*
-80	0	2.06E-03	-1.27E-02	-8.00E-02	-5.47E-02	0.00E+00	1.54E-03
-60	1	1.89E-03	-7.86E-03	-6.00E-02	-3.80E-02	0.00E+00	8.03E-04
-40	2	1.72E-03	-4.23E-03	-4.00E-02	-2.26E-02	0.00E+00	-5.24E-05
-20	3	1.53E-03	-1.78E-03	-2.00E-02	-8.34E-03	0.00E+00	-9.42E-04
0	4	1.31E-03	-4.75E-04	0.00E+00	4.61E-03	0.00E+00	-1.78E-03
20	5	1.06E-03	-2.83E-04	2.00E-02	1.62E-02	0.00E+00	-2.51E-03
40	6	7.63E-04	-1.19E-03	4.00E-02	2.63E-02	0.00E+00	-3.05E-03
60	7	4.14E-04	-3.18E-03	6.00E-02	3.48E-02	0.00E+00	-3.37E-03
80	8	0.00E+00	-6.28E-03	8.00E-02	4.13E-02	0.00E+00	-3.40E-03

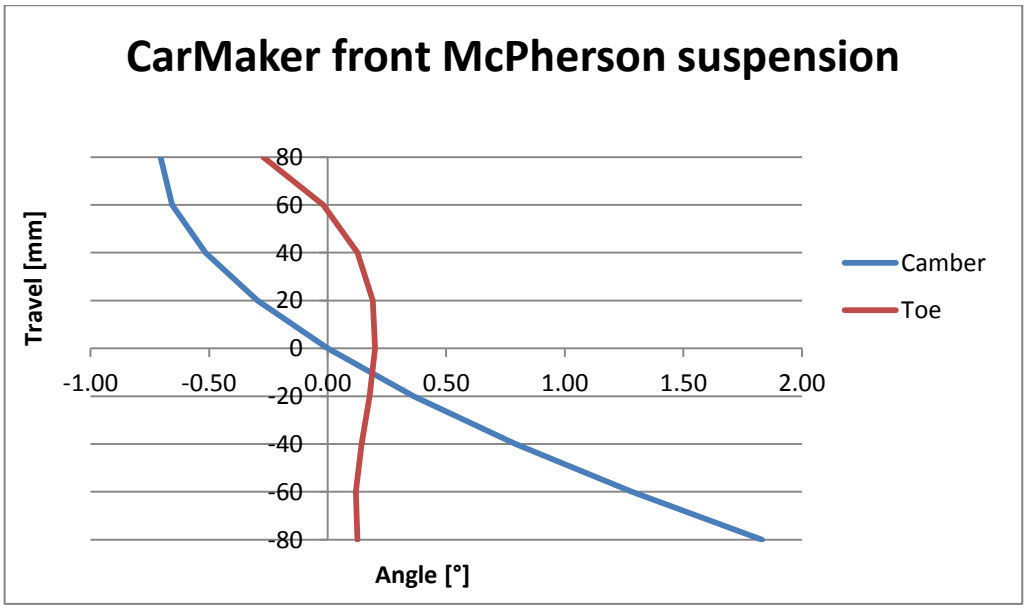

Figure 108 – Kinematics of the front McPherson suspension when wheel compression and position of steering rod are in a neutral position. [53]

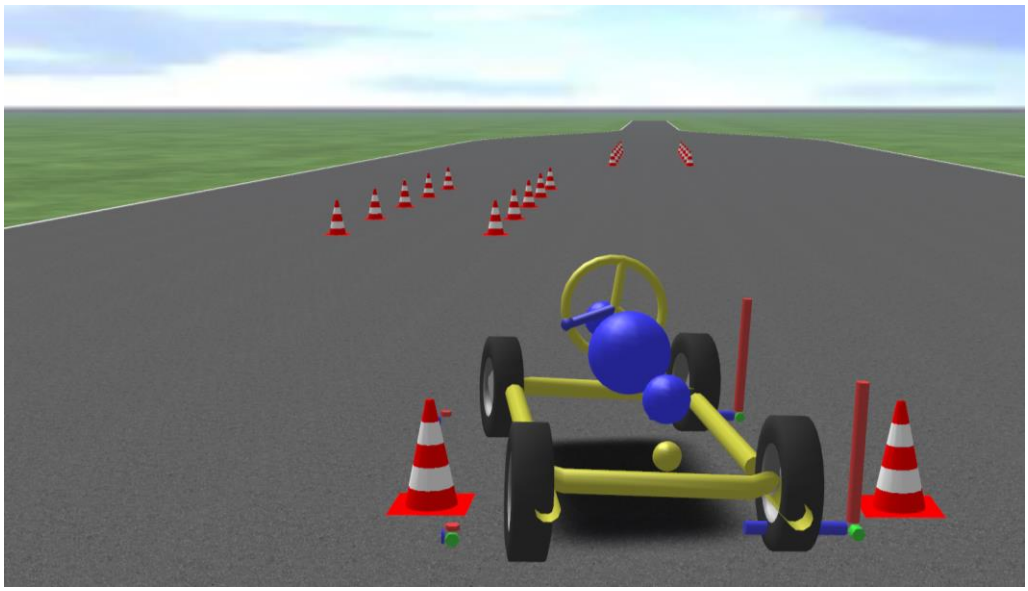

Figure 109 - CarMaker simulation during the VDA test with our vehicle.

Table 23 – Summation of the most important input parameters in the *CarMaker* model

Vehicle class	small car
Driving axle	rear
Tires front	145/80 R13 (2.3 bar)
Tires rear	145/80 R13 (2 bar)
Unloaded weight	474 kg
Vehicle length	2030 mm
Vehicle width	1350 mm
Vehicle height	1450 mm
Wheelbase	2134 mm
Track width (front and rear)	1100 mm
Drag coefficient	0.5
Nominal power	15 kW
Max. Torque	43 Nm
Gear ratio	11.87
Centre of gravity position (measured from the ground in the middle of rear track width)	x = 1.045 m, y = 0 m, z = 0.551 m

Table 24 – Suspension input values in CarMaker model.

Front suspension	Original value	Tuned value
Spring stiffness	5941 N/m	7426 N/m (1.25x)
Sprung Nat. freq. (loaded)	1 Hz	1.12 Hz
Sprung nat. freq. (driver)	1.16 Hz	1.29 Hz
Damping	562 N/(m.s-1)	724 N/(m.s-1)
Damping ratio (full load)	0.3	0.346
Damping ratio (driver)	0.347	0.4
Stabilizer	4476 N/m	10 295 N/m (2.3x)
Rear suspension		
Spring stiffness	8906 N/m	9797 N/m (1.1x)
Natural freq. (loaded)	1.2 Hz	1.26 Hz
Natural freq. (driver only)	1.38 Hz	1.45 Hz
Damping	699 N/(m.s-1)	848 N/(m.s-1)
Damping ratio (full load)	0.3	0.347
Damping ratio (driver)	0.34	0.4
Stabilizer	1865 N/m	7959 N/m (4.2x)

6.3 CarMaker tests

6.3.1 Acceleration and top speed test

The first test compared the previously made longitudinal dynamics calculation with *CarMaker* simulation. According to table 25, the theoretical calculation was really close to the simulation and proved a high-quality estimation of all parameters. Only in the estimation of acceleration 0 – 100 km/h, there is a significant difference of almost 10 seconds. This can be caused by more advanced aerodynamic model in the software and a bigger increment in the numerical method of theoretical calculation.

Table 25 – Comparison of dynamic properties of the previously performed theoretical calculation, CarMaker test and Renault Twizy.

Test	Theoretical calculation	CarMaker	Renault Twizy
0-50 km/h	5.7 s	5.7 s	6.1 s (0-45 km/h)
0-80 km/h	15.6 s	15.4 s	-
0-100 km/h	37.8 s	47.1 s	-
30-60 km/h	5.4 s	5.1 s	8.1 s
0-50 m	6.1 s	6 s	6.6 s
Top speed	102.7 km/h	101.5 km/h	80 km/h

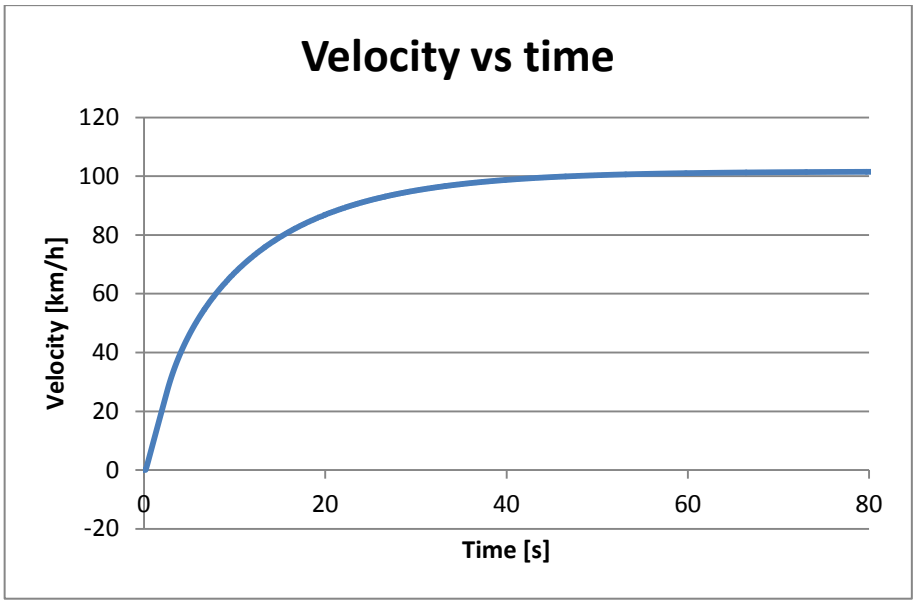

Figure 110 – Vehicle velocity with respect to time.

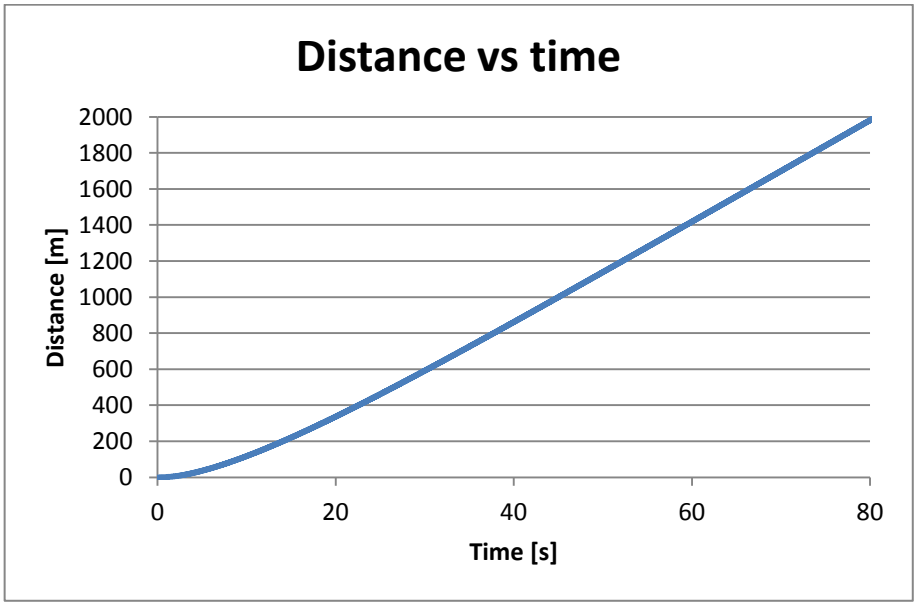

Figure 111 – Vehicle distance with respect to time.

6.3.2 Braking test

The vehicle accelerated to 100 km/h on a straight road and then started to brake at a certain point (without considering a reaction time of a driver). The stopping distance of the vehicle was **45.3 metres**. The vehicle was not equipped with ABS system and the brake pedal was pressed in that manner to get maximal tire grip without any tire slip.

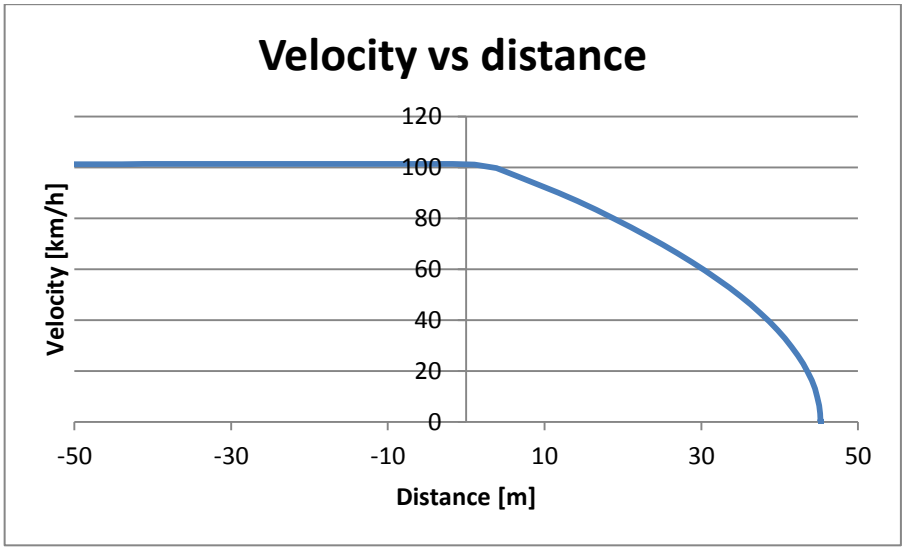

Figure 112 – Vehicle velocity with respect to distance.

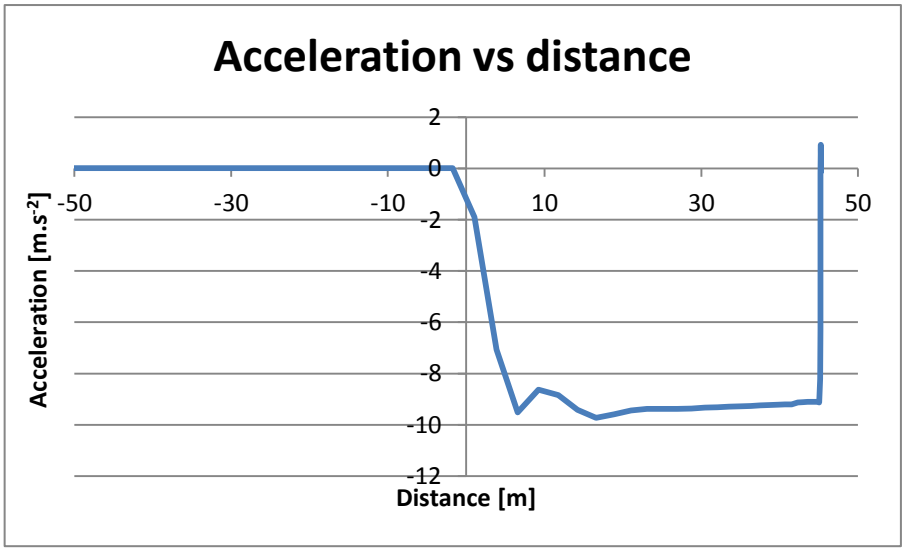

Figure 113 – Vehicle longitudinal acceleration with respect to distance.

6.3.3 ISO 3888-1 – Double lane change

This test should prove roll stability of the vehicle in case of a lane change or overtaking manoeuvre. In figure 113 there is a scheme of the test track symbolized with pylons on the plane road. The vehicle successfully passed this test at speed of **92 km/h** what was the highest speed achieved by the vehicle on the test track. The vehicle was very stable during the test, kept the contact of all four wheels with the road. Side slip angle of the rear wheels was slightly higher than front wheels. This shows a little oversteering tendency of the vehicle.

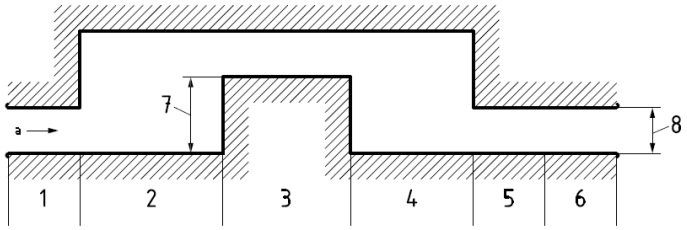

Key

1 section 1
2 section 2
3 section 3
4 section 4
5 section 5
6 section 6
7 lane offset
8 width
a Driving direction.

Dimensions in metres

Section	Length	Lane offset	Width
1	15	—	1,1 × vehicle width + 0,25
2	30	—	—
3	25	3,5	1,2 × vehicle width + 0,25
4	25	—	—
5	15	—	1,3 × vehicle width + 0,25
6	15	—	1,3 × vehicle width + 0,25

Figure 114 – Scheme of the double lane change test. [13]

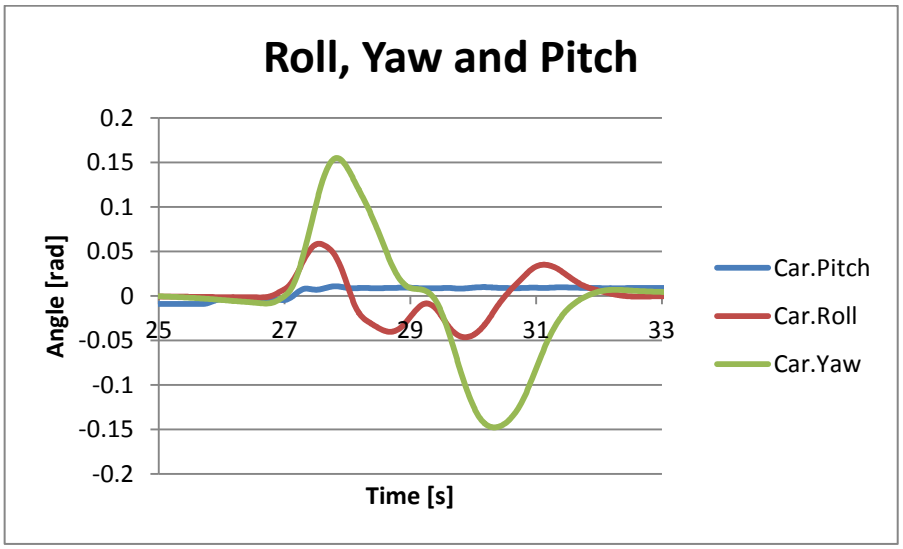

Figure 115 – Roll, yaw and pitch during the double lane change test.

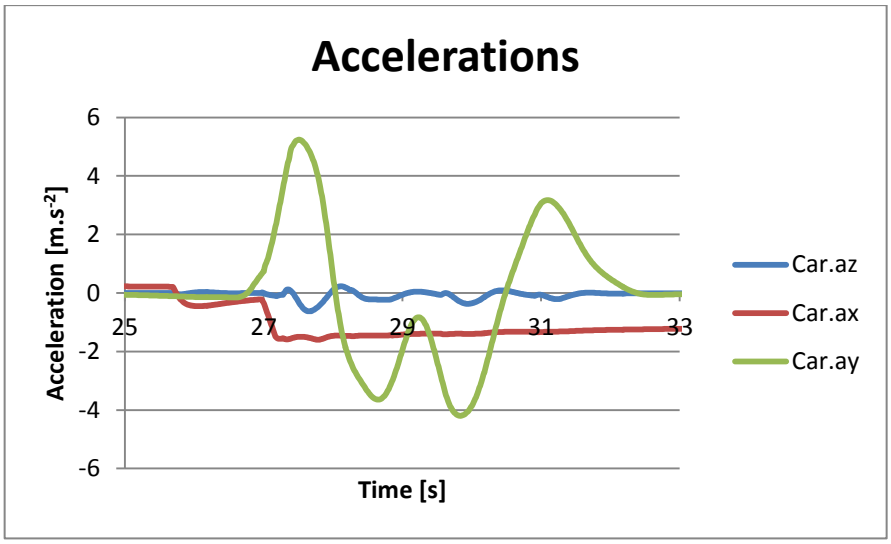

Figure 116 - Lateral, longitudinal and vertical accelerations during the double lane change test.

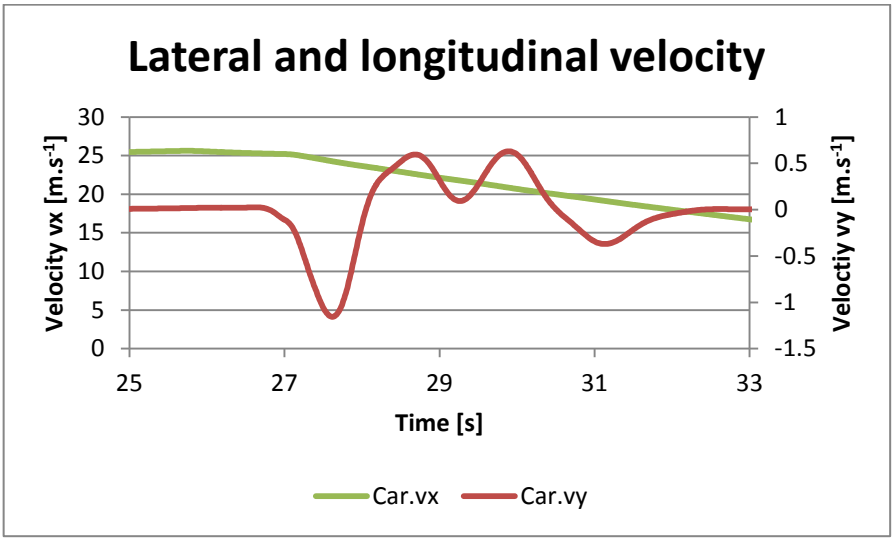

Figure 117 – Lateral and longitudinal velocity during the double lane change test.

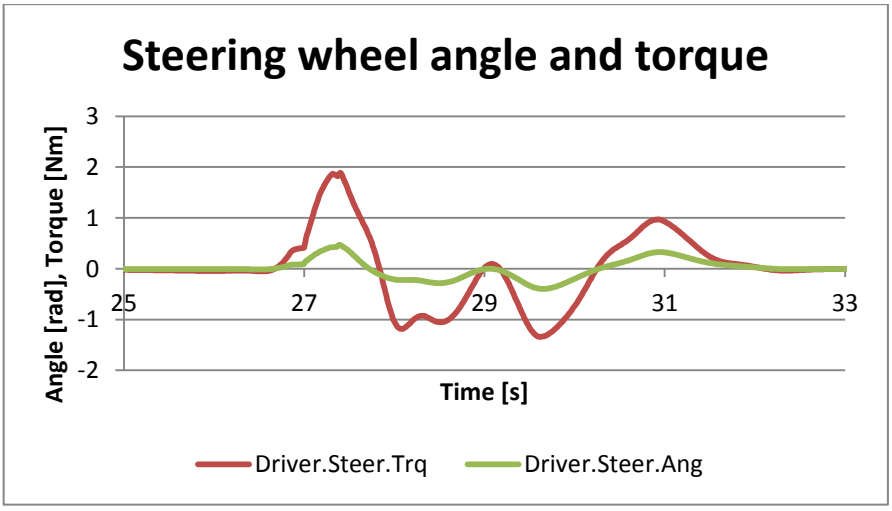

Figure 118 – Steering wheel angle and torque during the double lane change test.

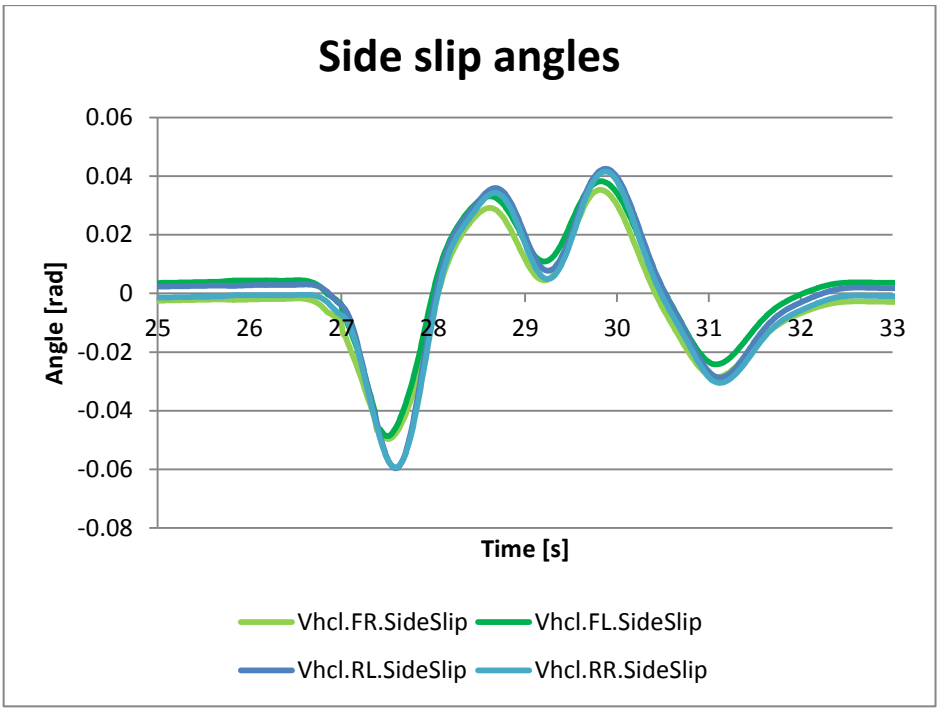

Figure 119 – Sideslip angles of all wheels during the double lane change test.

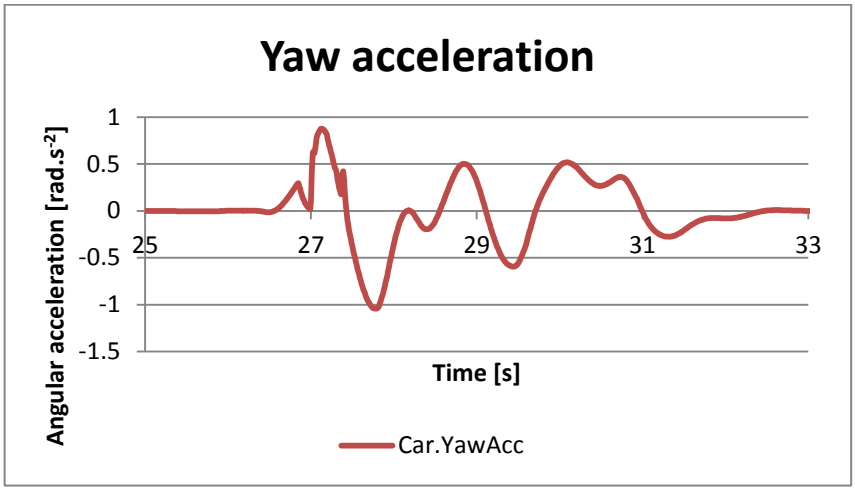

Figure 120 – Yaw acceleration during the double lane change test.

6.3.4 ISO 3888-2 – Obstacle avoidance

This test (sometimes is called VDA or moose test) simulates obstacle avoidance of the vehicle in case of an emergency situation and should prove roll stability of the vehicle. In figure 120 there is a scheme of the testing track. The vehicle successfully did this test at a speed of **53 km/h** without hitting any pylon. It was achieved thanks to stiffer springs and higher damping ratio of the dampers. Anti-roll bars were significantly stiffened because roll-over stability is crucial for short track width vehicle. Originally the rear stabilizer had a stiffness of 42% of the front one. After tuning, the ratio changed to 77%. Relatively stiffer rear anti-roll bar leads to a more oversteering tendency of the vehicle, but there wasn't any critical oversteering slide during any tests and it significantly helped to overall rolling stability of the vehicle. At the speed of 57 km/h, the roll-over came. Unfortunately, to successfully pass this test the vehicle must go at least 60 km/h. As this vehicle will be certified as a quad, it doesn't need to pass it. However, in terms of safety it would be recommended to apply an additional electronic stability programme (ESP).

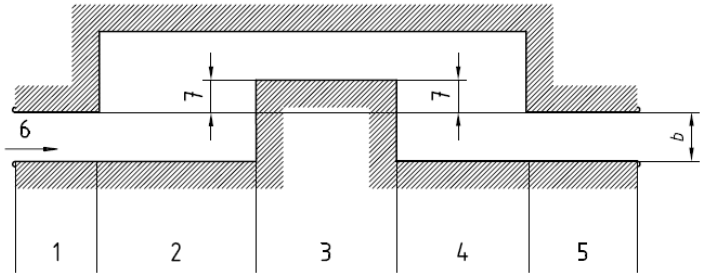

Key

1	Section 1
2	Section 2
3	Section 3
4	Section 4
5	Section 5
6	Driving direction
7	Lane offset

Dimensions in metres

Section	Length	Lane offset	Width b
1	12	—	1,1 × vehicle width + 0,25
2	13,5	—	—
3	11	1	vehicle width + 1
4[a]	12,5	—	—
5	12	—	1,3 × vehicle width + 0,25, but not less than 3 m

[a] To ensure high lateral accelerations at the end of the track, section 4 is 1 m shorter than section 2.

Figure 121 – Scheme of the obstacle avoidance test. [14]

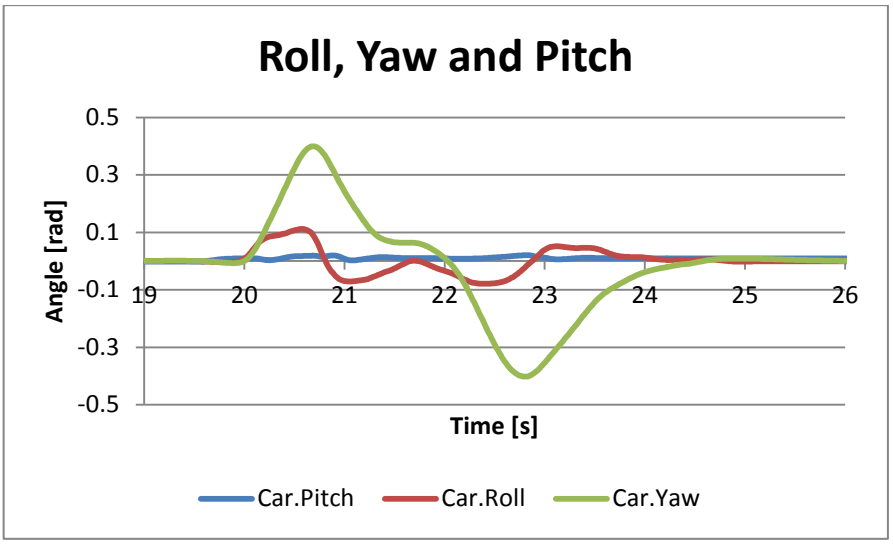

Figure 122 – Roll, yaw and pitch during VDA test.

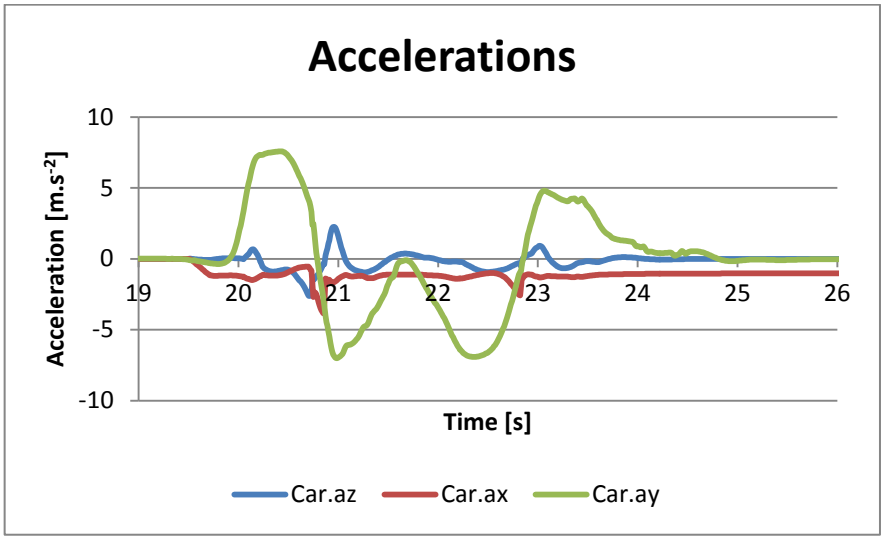

Figure 123 – Longitudinal, lateral and vertical accelerations during VDA test.

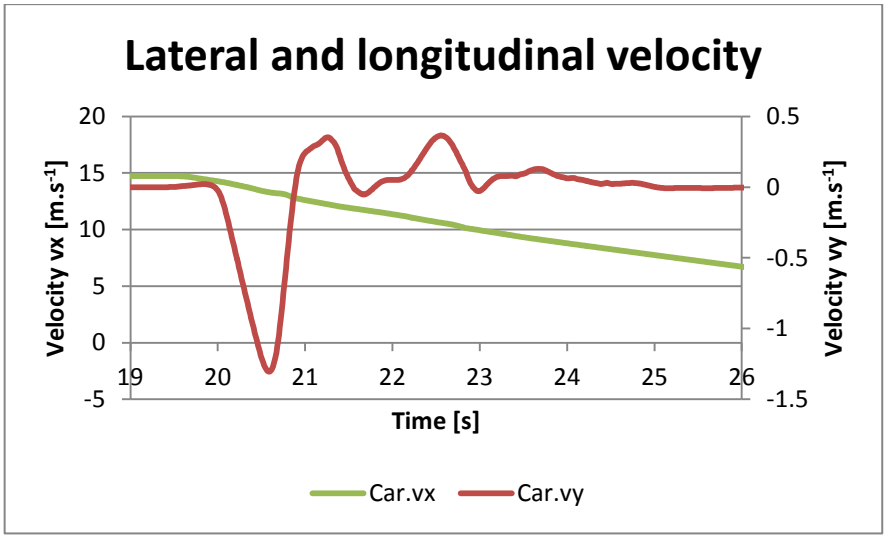

Figure 124 – Lateral and longitudinal velocity during VDA test.

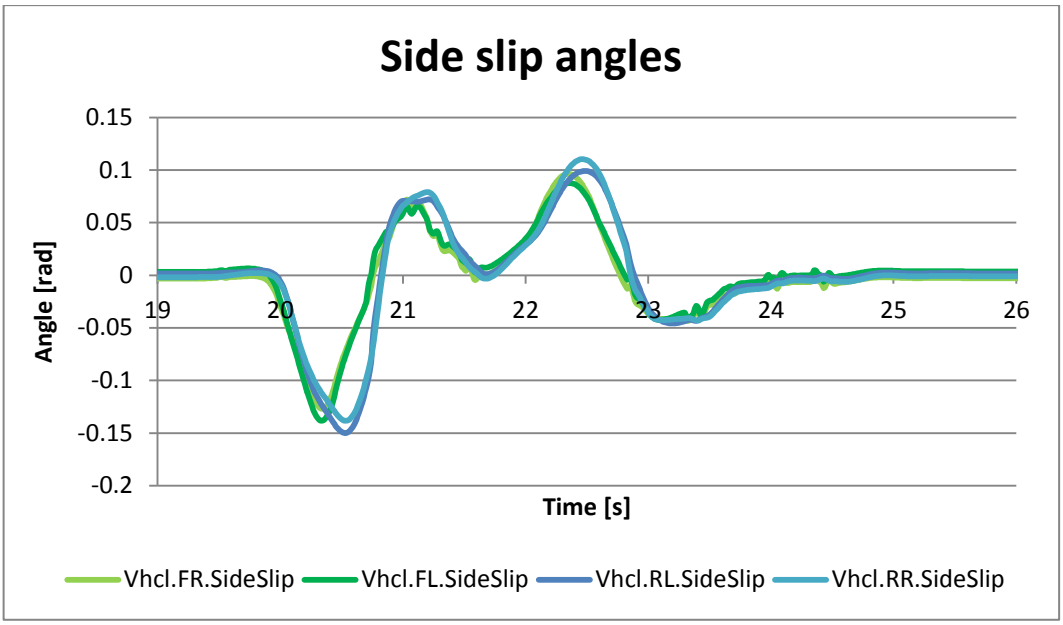

Figure 125 – Side slip angles of all tires during VDA test.

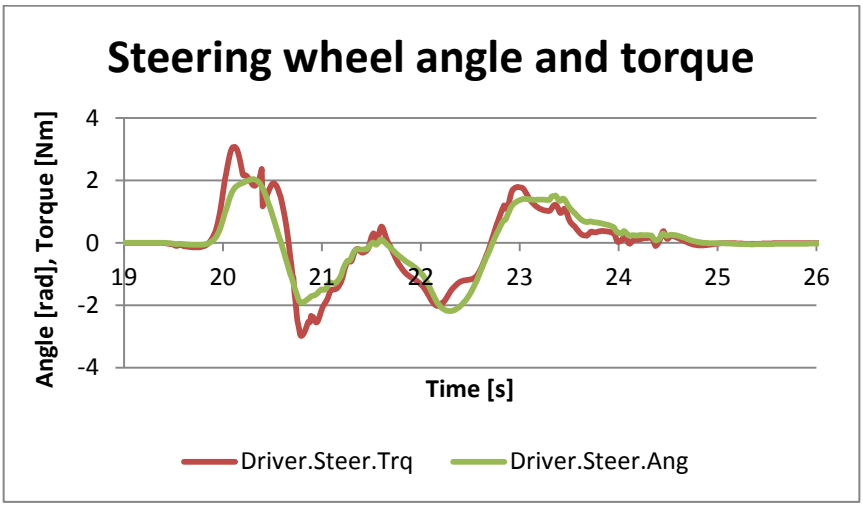

Figure 126 – Steering wheel angle and torque during the VDA test.

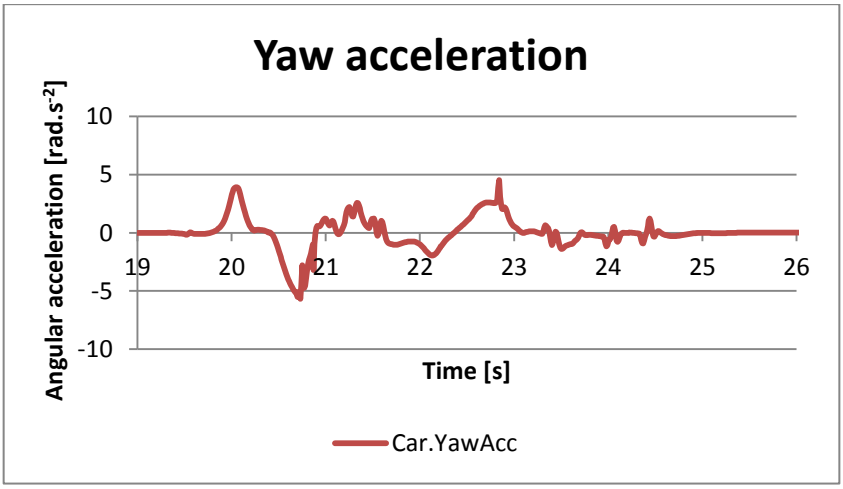

Figure 127 – Yaw acceleration during the VDA test.

6.3.5 ISO 4138 – Steady-state circular driving behaviour (open-loop)

For this test was used a constant radius method with a circular track with a radius of 42 metres. The velocity of the vehicle was increasing that slowly, that we can consider every moment as a single steady state. It is not a representation of rear driving condition, but it is useful for obtaining measures of vehicle steady-state behaviour resulting from several specific types of control inputs under controlled test conditions. The vehicle couldn't reach the point of losing the grip and it stopped to accelerate at speed of 59 km/h. The reason for this is unknown as other example vehicles with the same driver settings reached the limit of the grip. However, according to figure 127, showing side slip angles, we might assume the loss of grip close to the ending velocity as the sideslip angles started to decrease rapidly. We can also notice again slightly oversteering behaviour of the car as the sideslip angles of the rear wheels are greater than front ones and if the test continued, probably oversteering slide would occur.

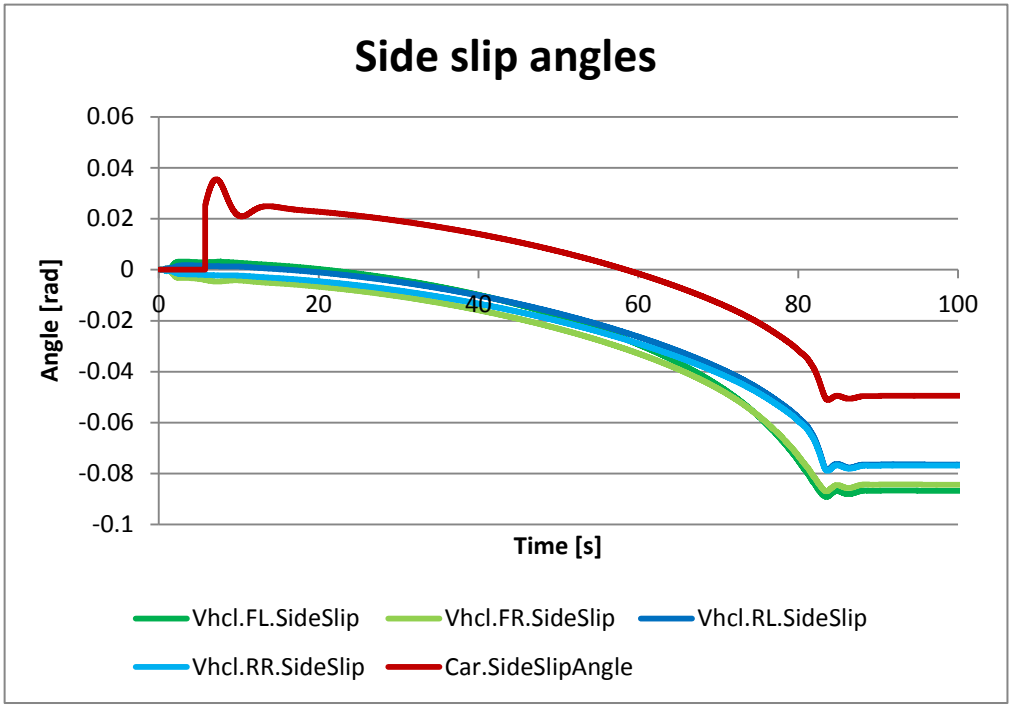

Figure 128 – Side slip angles during the steady-state circular driving test.

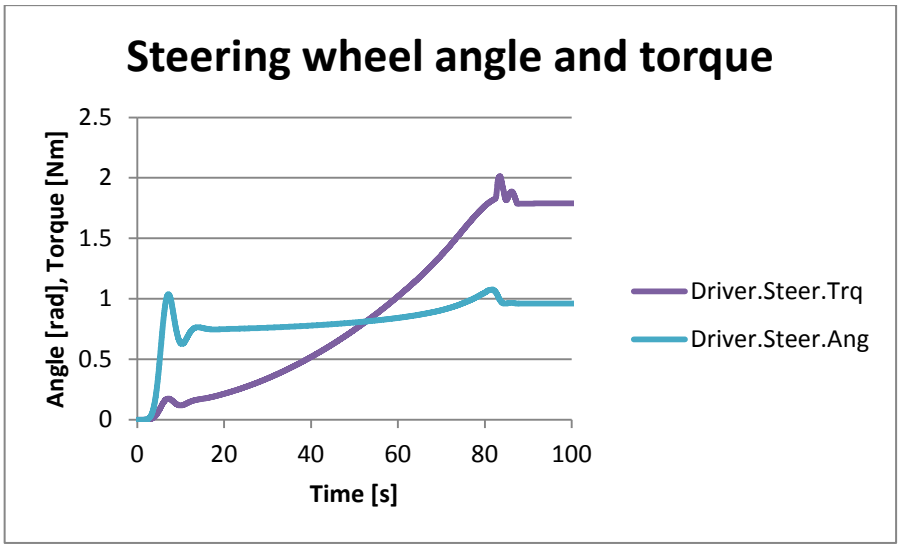

Figure 129 – Steering wheel angle and torque steady-state circular driving test.

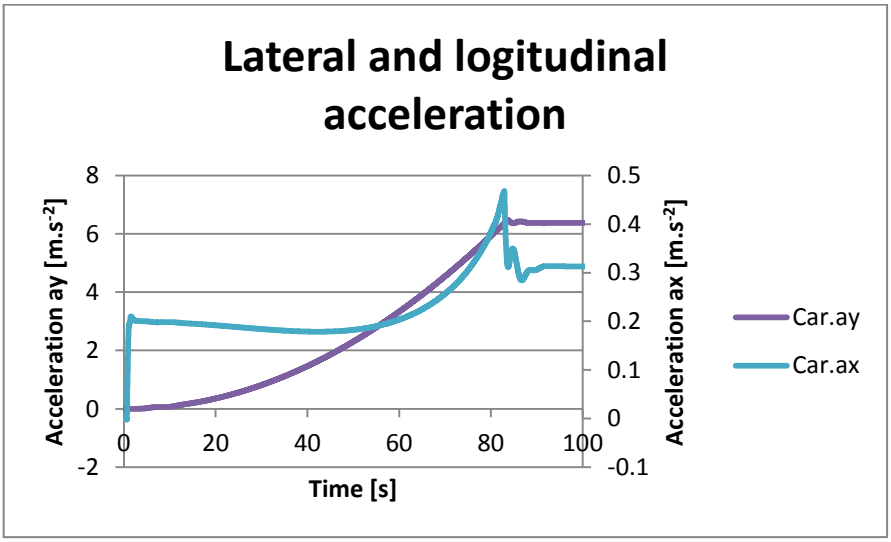

Figure 130 – Lateral and longitudinal acceleration steady-state circular driving test.

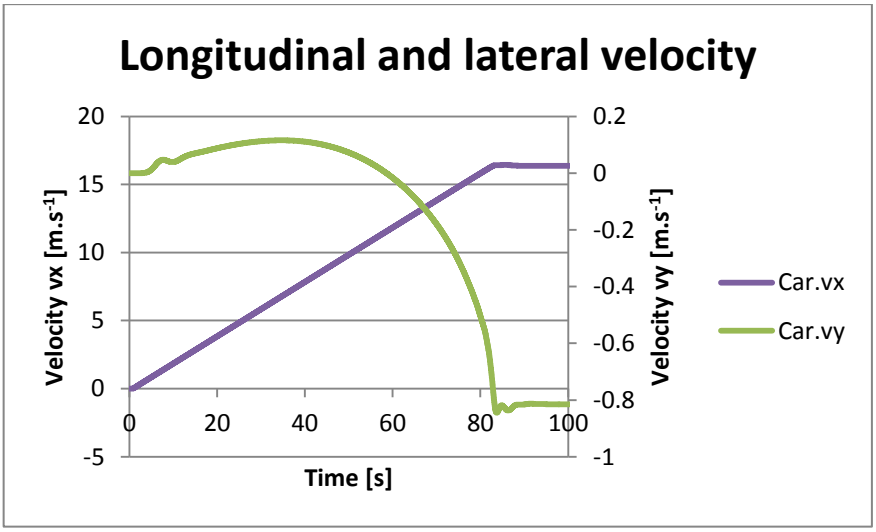

Figure 131 – Longitudinal and lateral velocity steady-state circular driving test.

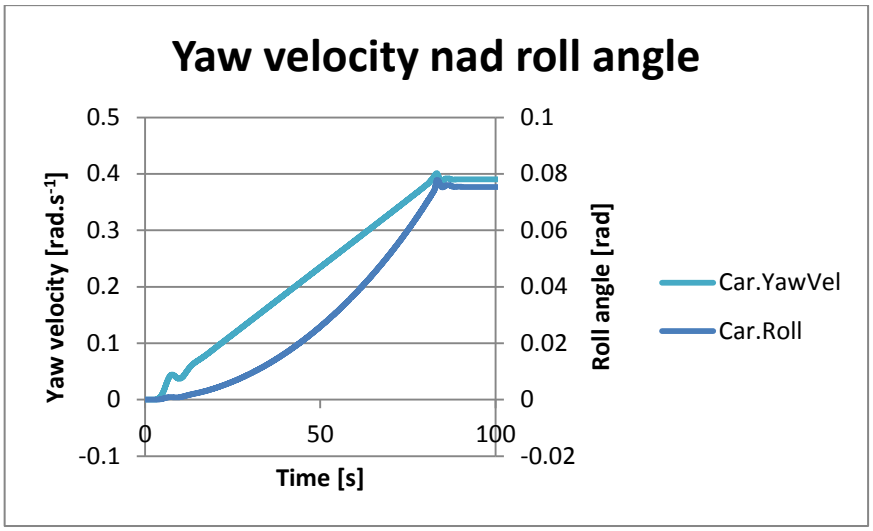

Figure 132 – Yaw velocity and roll angle steady-state circular driving test.

6.3.6 ISO 7975 – Braking in turn (open-loop)

The purpose of this test is to examine the effect of braking while steady-state cornering. A track with a radius of 100 metres was used for this test. The initial longitudinal velocity was 72 km/h and the brake distance measured 32.8 m. The brake pedal was fully pressed by the driver to simulate an emergency braking. According to figure 131 understeer occurred as the front wheels got locked because they reached much higher sideslip angle than rear ones. The vehicle was not equipped with ABS, otherwise, the slip wouldn't happen and it would be stopped faster with the controllable direction of the front wheels. However, this understeering behaviour is desirable, because is safer than oversteering slip.

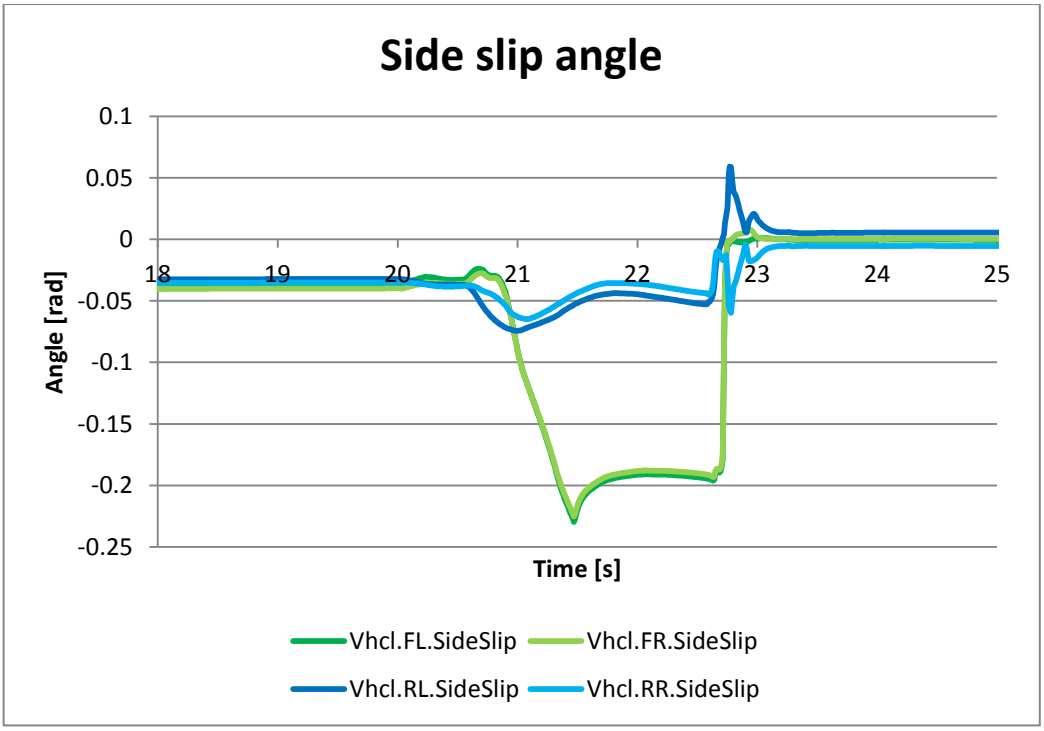

Figure 133 – Side slip angles during the corner braking test

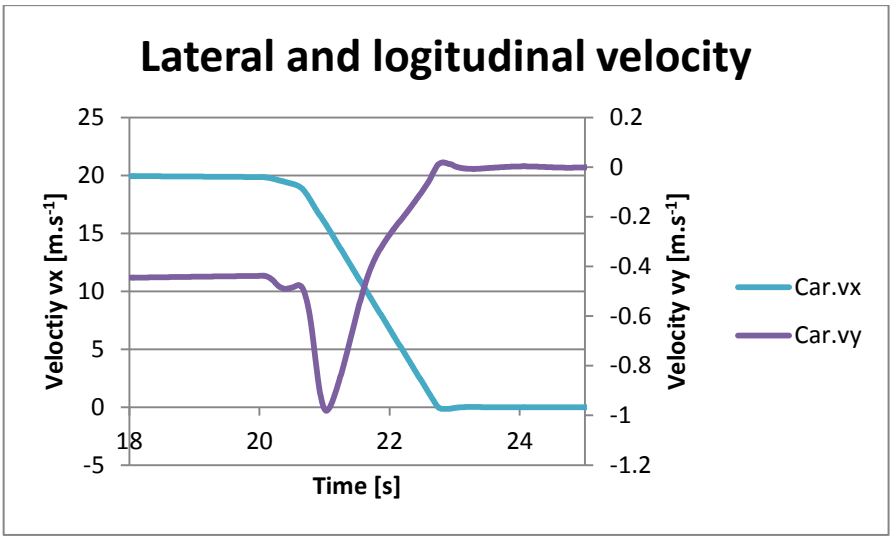

Figure 134 – Lateral and longitudinal velocity corner braking test.

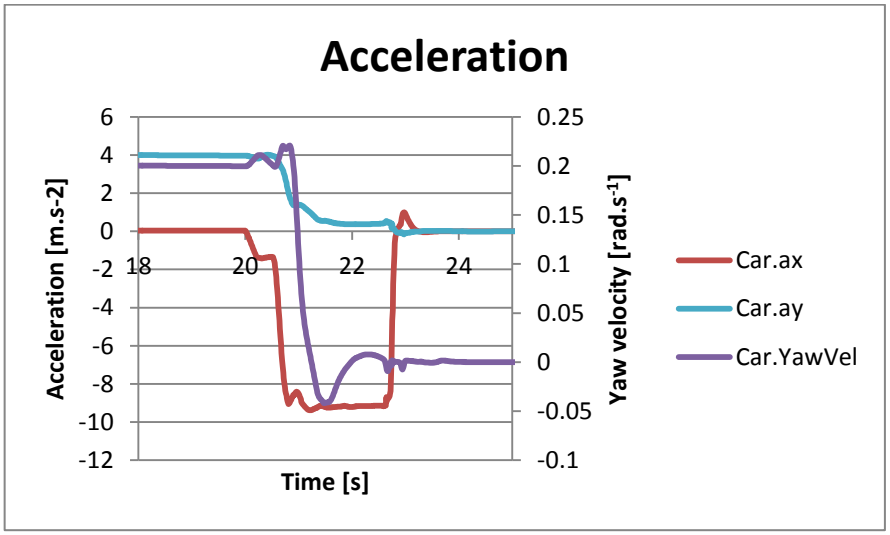

Figure 135 – Longitudinal and lateral accelerations and yaw velocity corner braking test.

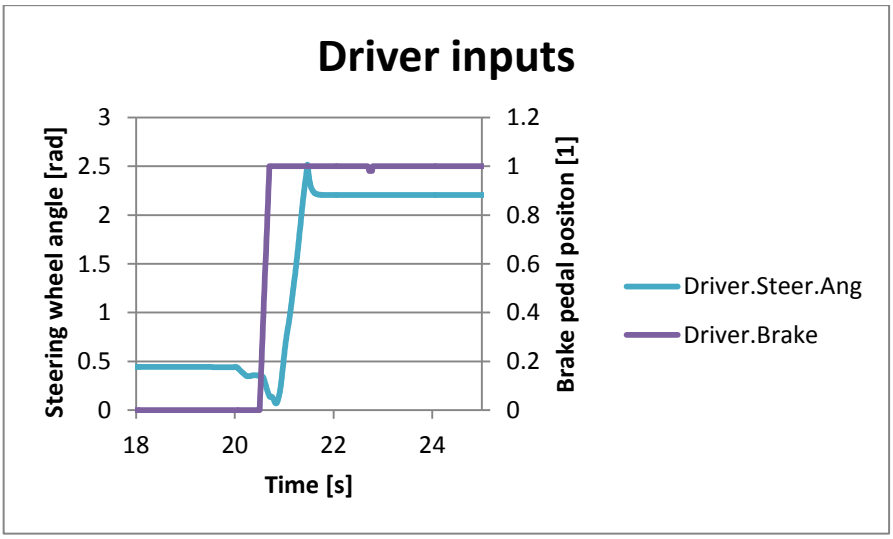

Figure 136 – Driver inputs: Steering wheel angle and brake pedal position during the corner braking test.

6.3.7 ISO 8725 – Transient open-loop response method with one-period sinusoidal input

The objective of the test is to determine the transient response behaviour of a vehicle subjected to one period of sinusoidal input in the steering wheel (0.5 Hz) which is similar to what is used in real traffic during lane change manoeuvers. The initial velocity is 100 km /h. Important criteria are:

- Time lags between steering-wheel angle, lateral acceleration and yaw velocity.
- Response of lateral acceleration to steering-wheel angle.
- Response of yaw velocity to steering-wheel angle.

The vehicle showed a good performance, kept stable during the whole test. All of the wheels kept in contact with the road. Its behaviour was slightly oversteering, because of higher stiffness of the rear stabilizer, but it didn't result in any indications of dangerous slip situation.

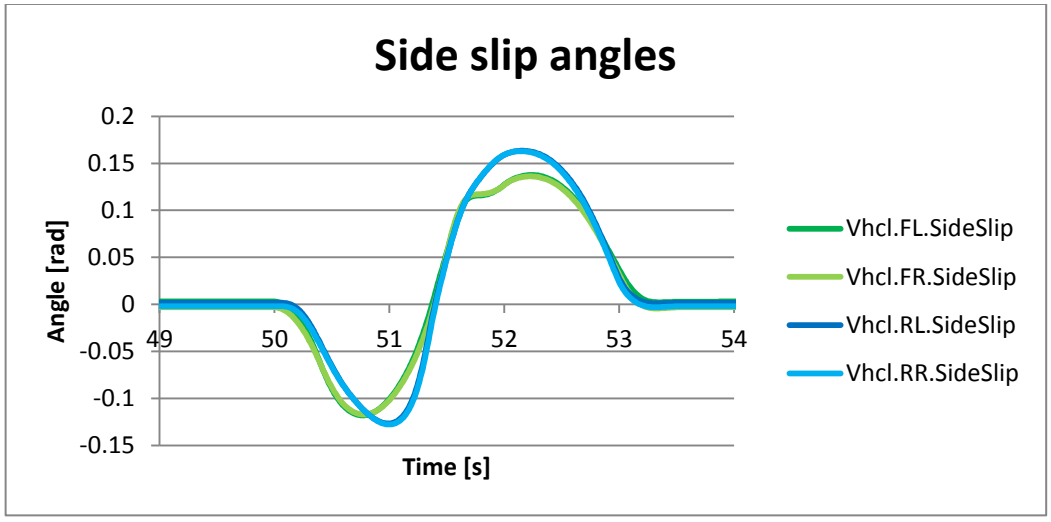

Figure 137 – Sideslip angles of all wheels during transient open-loop response method with one period sinusoidal input.

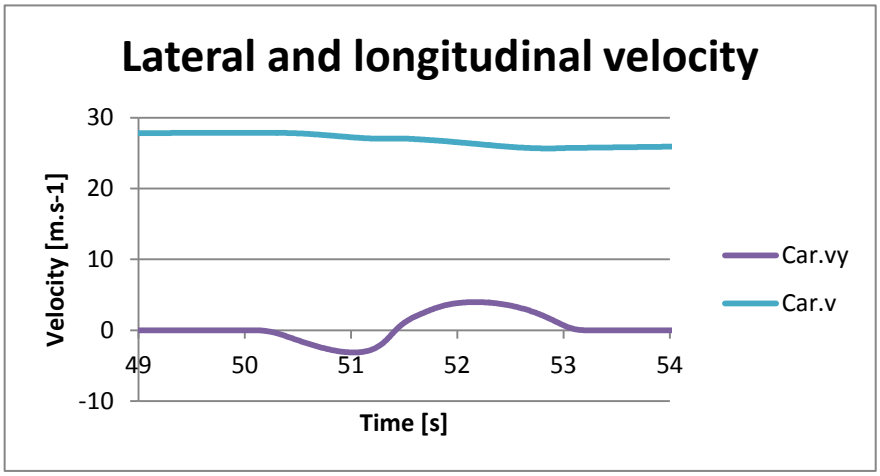

Figure 138 – Lateral and longitudinal velocity during transient open-loop response method with one period sinusoidal input.

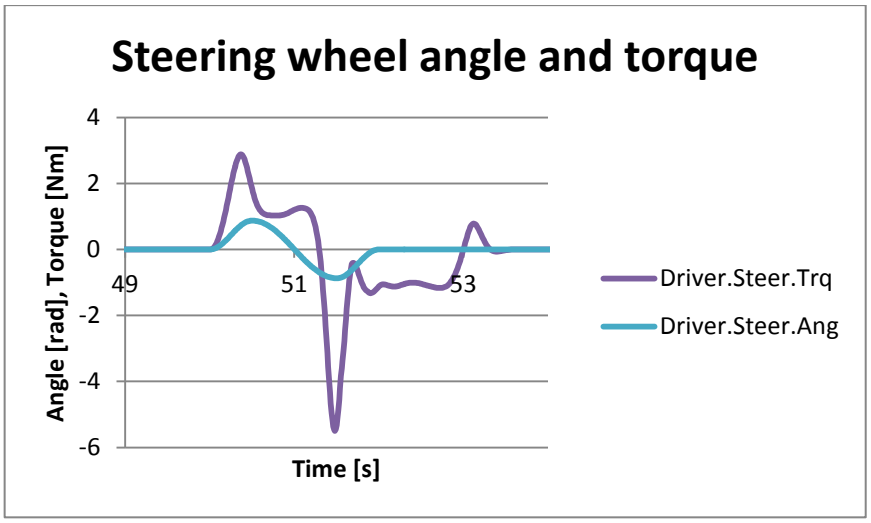

Figure 139 – Steering wheel angle and torque during transient open-loop response method with one period sinusoidal input.

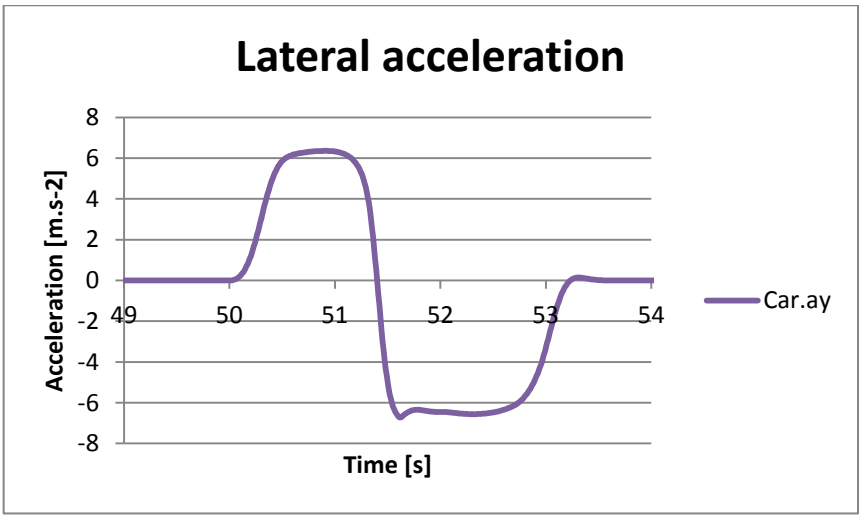

Figure 140 – Lateral acceleration during transient open-loop response method with one period sinusoidal input.

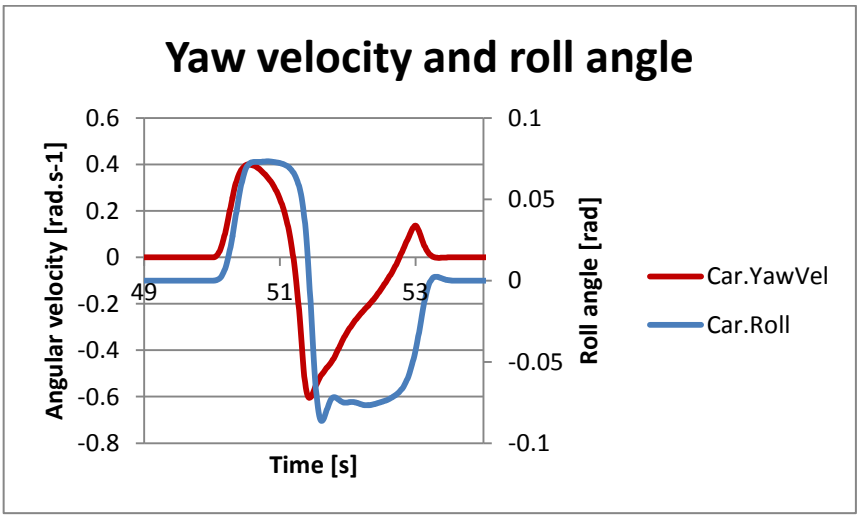

Figure 141 – Yaw velocity and roll angle during transient open-loop response method with one period sinusoidal input.

6.3.8 Bump test

In the following test, the vehicle had to run over a 5 cm tall bump and 8cm tall kerb (while going up the pavement). The velocity was set to **15 km/h**. The main objective was to prove the cushioning behaviour of the suspension system. There were five sensors on the vehicle measuring acceleration and change of vertical position:

- RW: Sensor on the rear wheel (unsprung mass representation)
- R: Sensor on the chassis just above the rear wheel (sprung mass representation)
- CG: Sensor on the chassis, located in the centre of gravity
- FW: Sensor on the front wheel (unsprung mass representation)
- F: Sensor on the chassis just above front wheel (sprung mass representation)

Bump geometry:

- Ramp-up: 0.2 m
- Plateau: 0.4 m
- Ramp-down: 0.2 m
- Bump height. 0.05 m

Kerb geometry:

- Kerb height: 0.08 m
- Vertical (90° angle with the road)

Bump

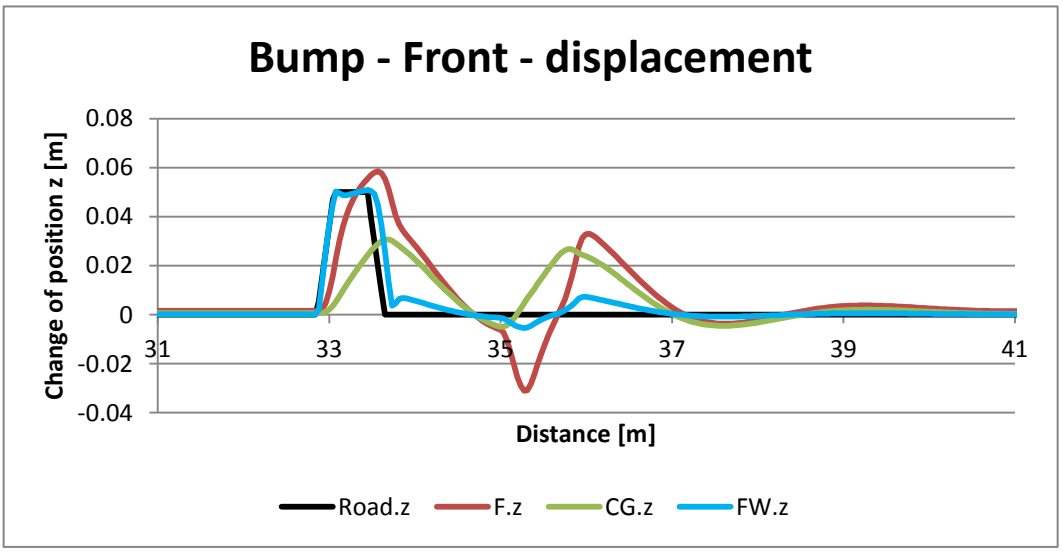

Figure 142 – Bump – change of vertical position on the front.

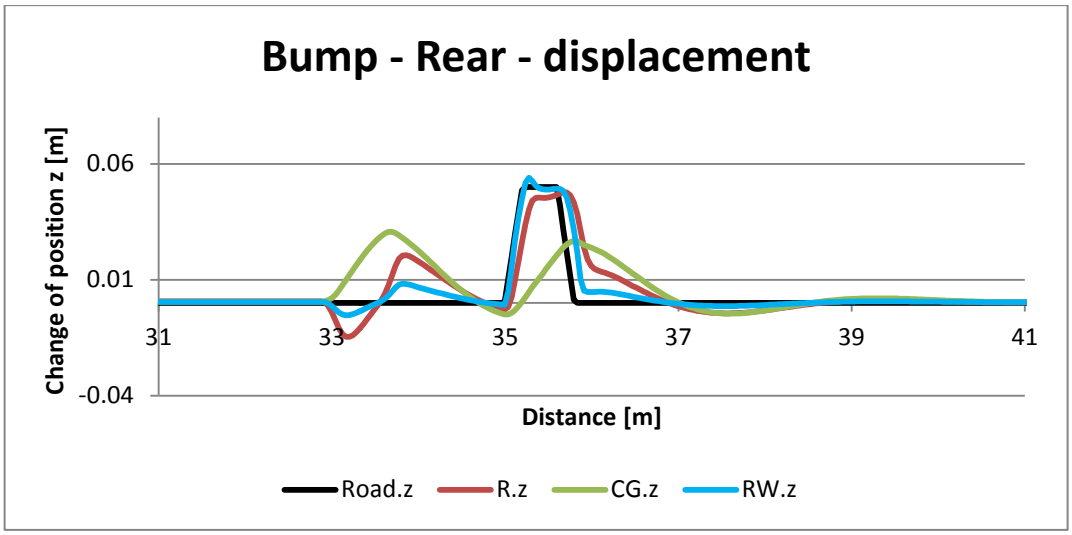

Figure 143 – Bump – change of vertical position on the rear.

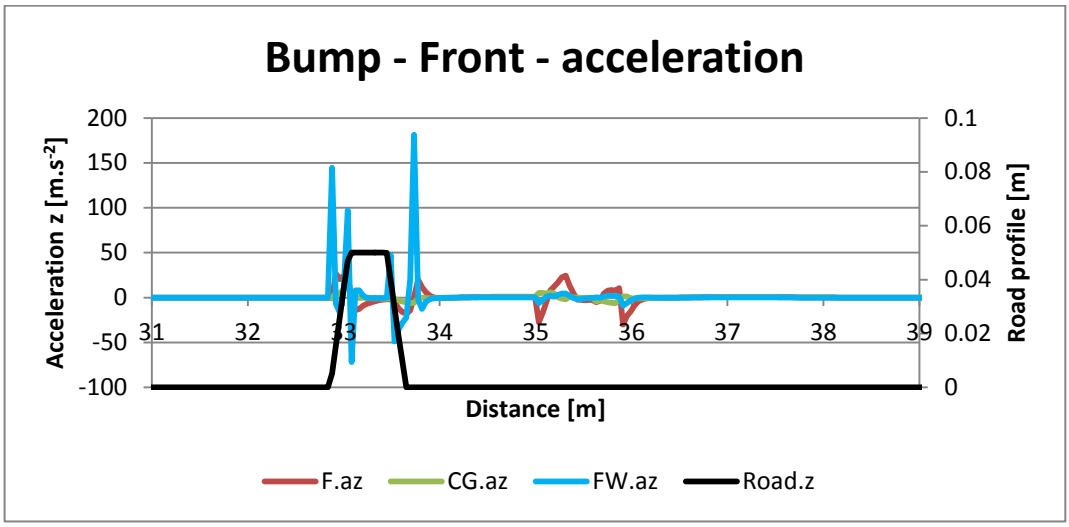

Figure 144 – Bump - vertical acceleration on the front.

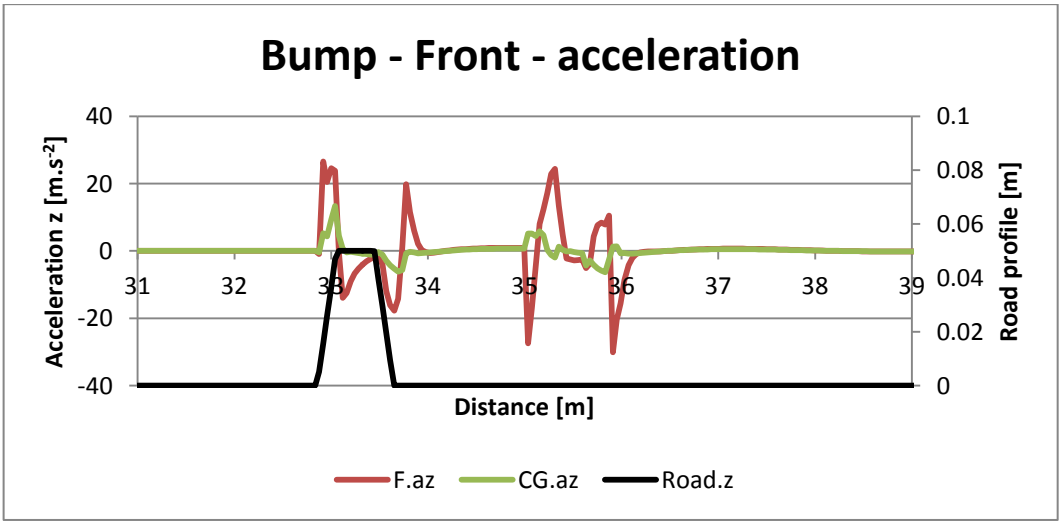

Figure 145 – Bump – vertical accelerations on the front.

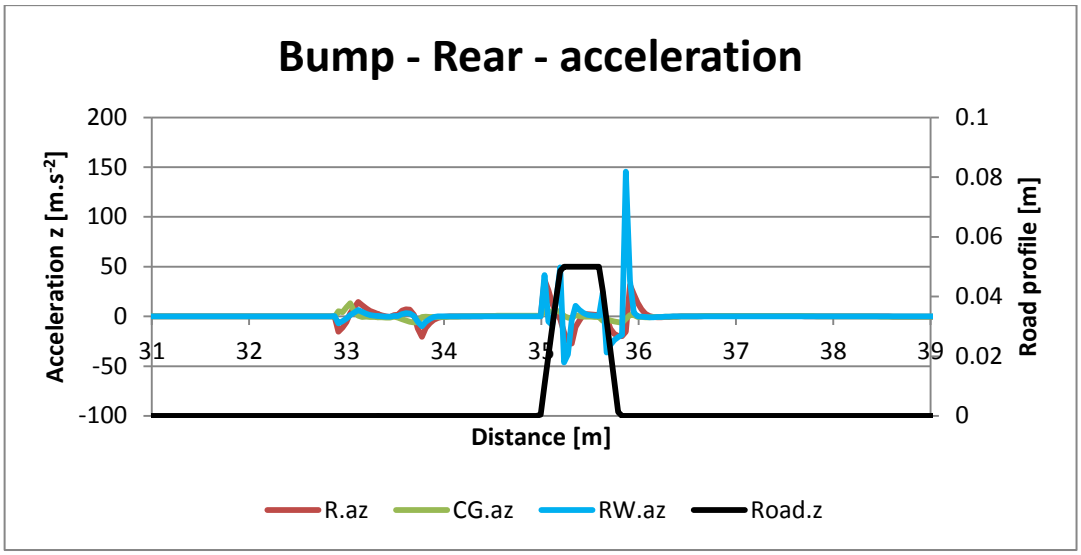

Figure 146 – Bump – vertical accelerations on the rear.

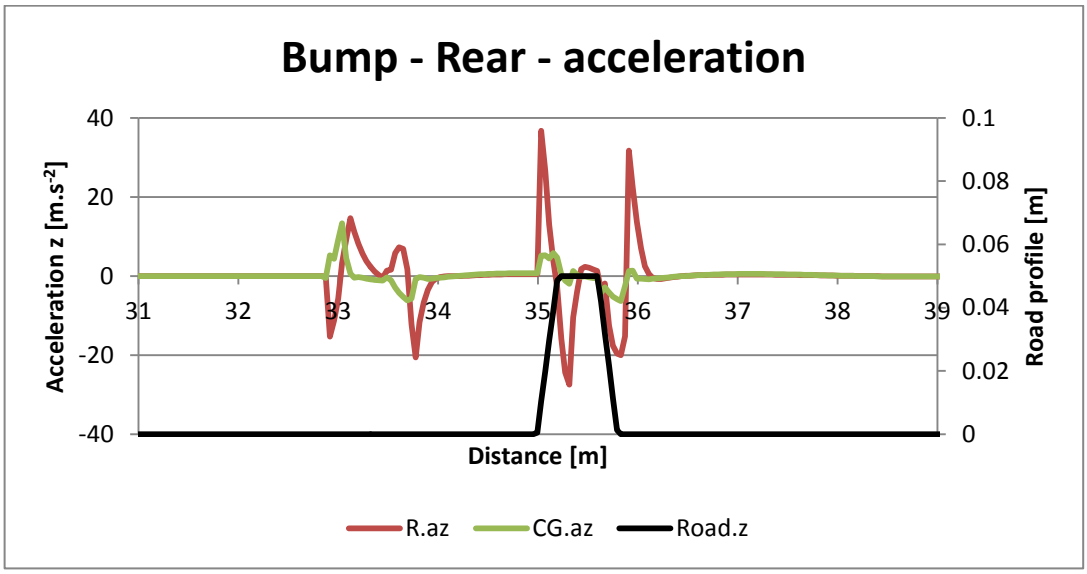

Figure 147 – Bump – vertical accelerations on the rear.

Kerb

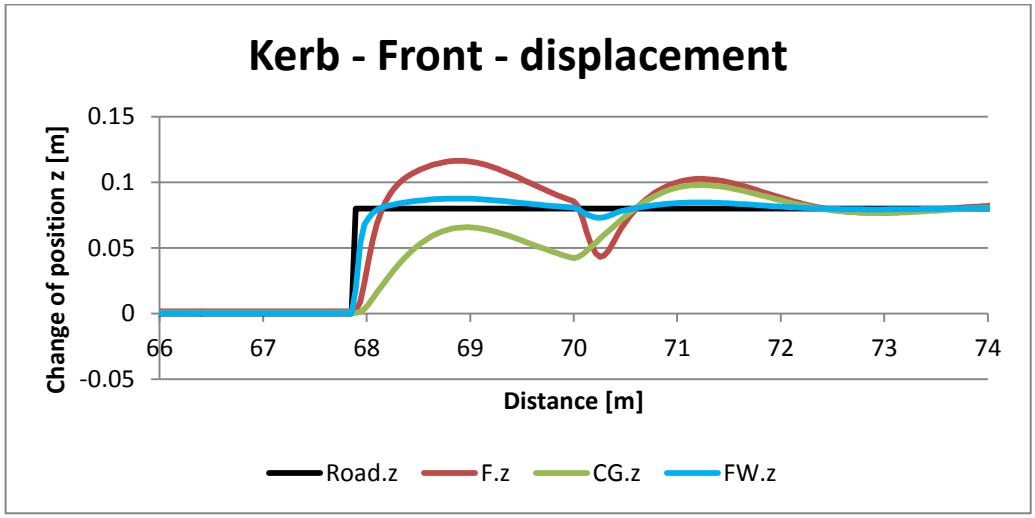

Figure 148 – Kerb – change of vertical position on the front.

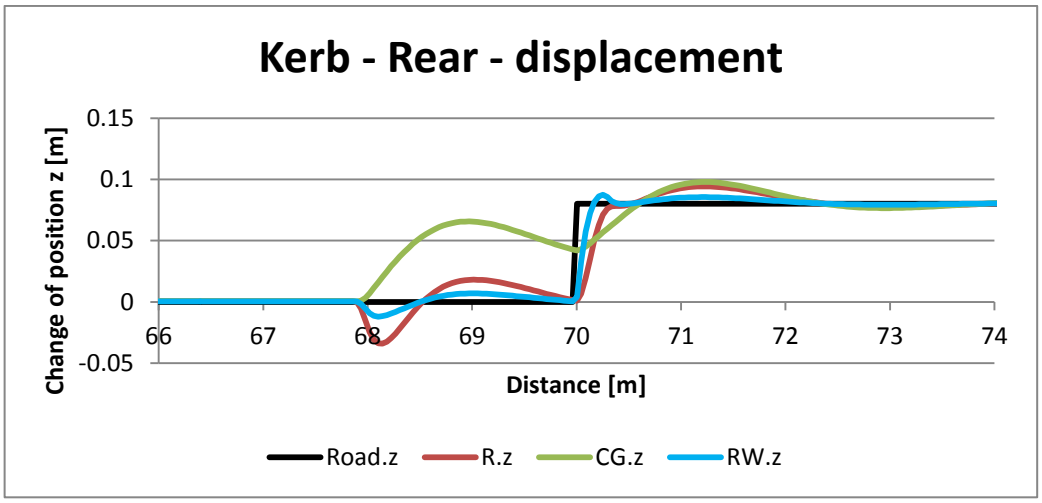

Figure 149 – Kerb – change of vertical position on the rear.

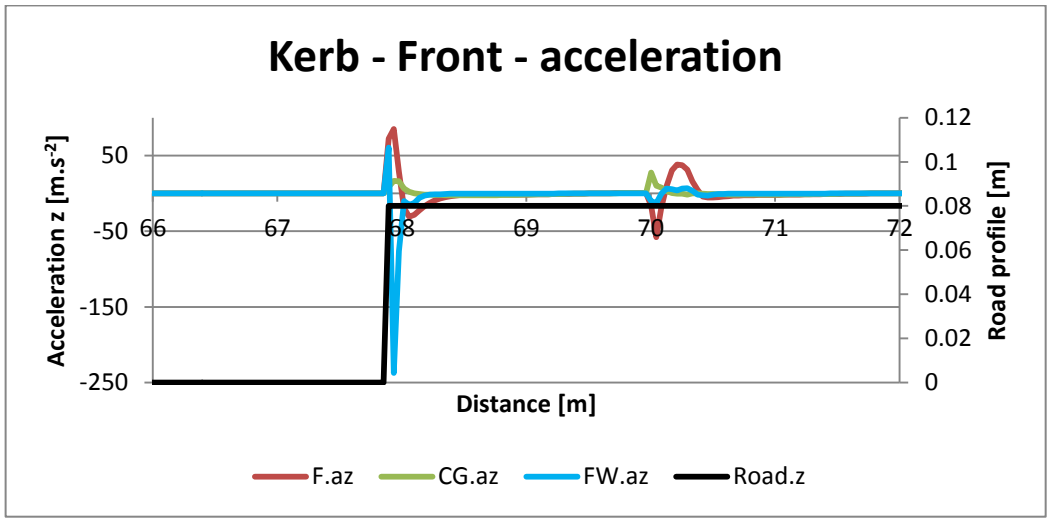

Figure 150 – Kerb – accelerations on front

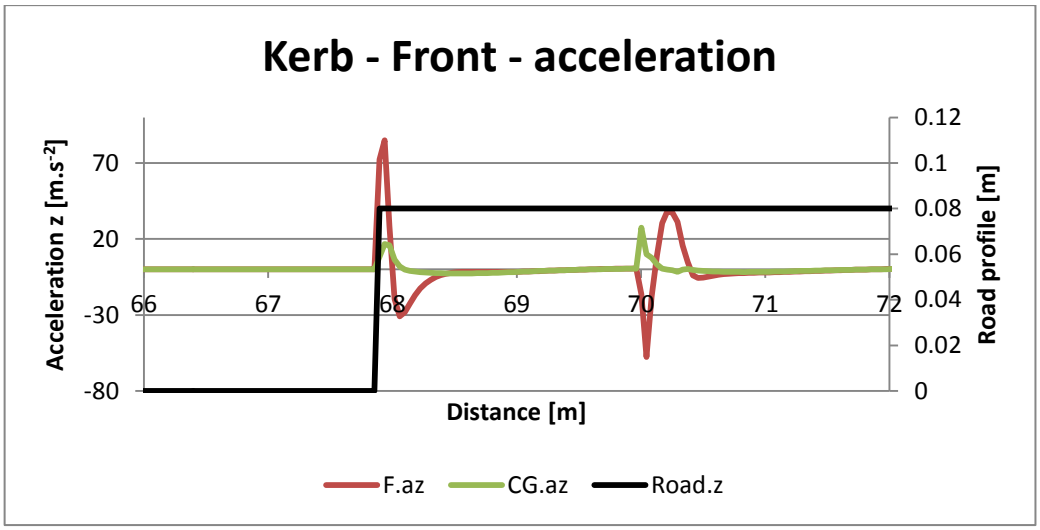

Figure 151 – Kerb – accelerations on the front.

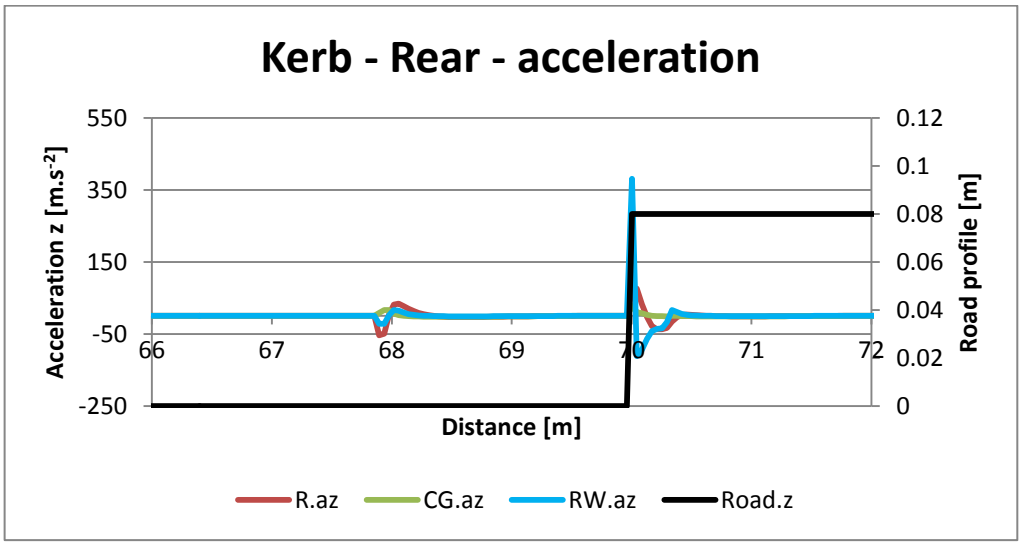

Figure 152 – Kerb – accelerations on the rear.

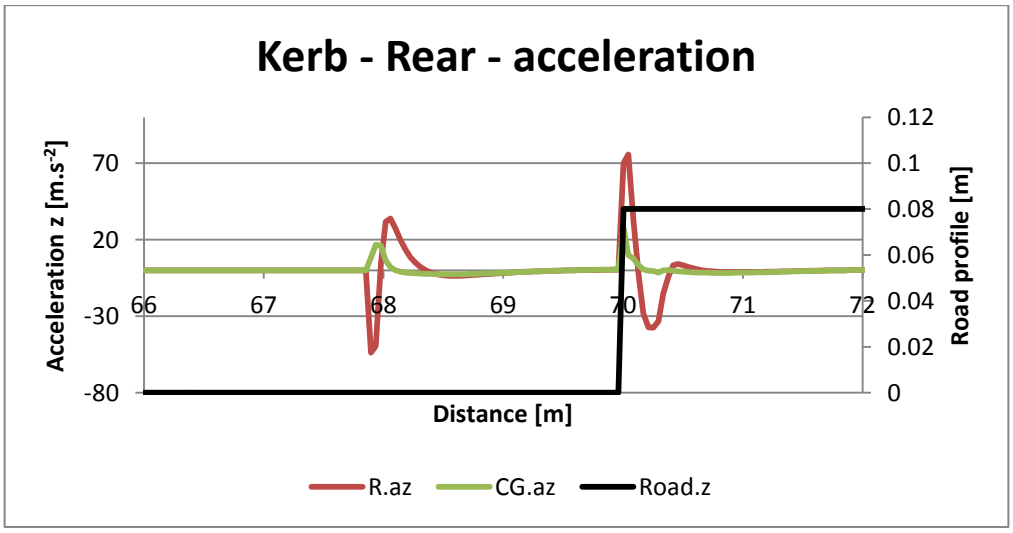

Figure 153 – Kerb - accelerations on the rear.

6.3.9 Wave test

Purpose of this test was to prove cushioning properties of the suspension system while riding on sinusoidal bumps (a height of 5 cm) on the straight road. The same sensors were used as for the previous bump test. Following figures show change of vertical position of the front wheel, front of the chassis and centre of gravity. Four different scenarios were applied for this test (table 26). In figure 154 there is excitation frequency (1 Hz) close to the natural frequency of the chassis and displacement of the chassis is the highest. As the excitation frequency is decreasing, the suspension functioning is getting more obvious. Figure 157 shows very good performance of the suspension system which was achieved thanks to the long wheelbase. On the other hand, it could have been even better if softer springs and lower damping ratio were used as originally calculated.

Table 26 – Four types of wave tests.

Type	Wavelength [mm]	Velocity [km/h]	Excitation freq. [Hz]
Wave W 8km/h	2134 (wheelbase)	8	1
Wave W/2 8 km/h	1067 (wheelbase/2)	8	2
Wave W 32 km/h	2134 (wheelbase)	32	4
Wave W/2 32 km/h	1067 (wheelbase/2)	32	8

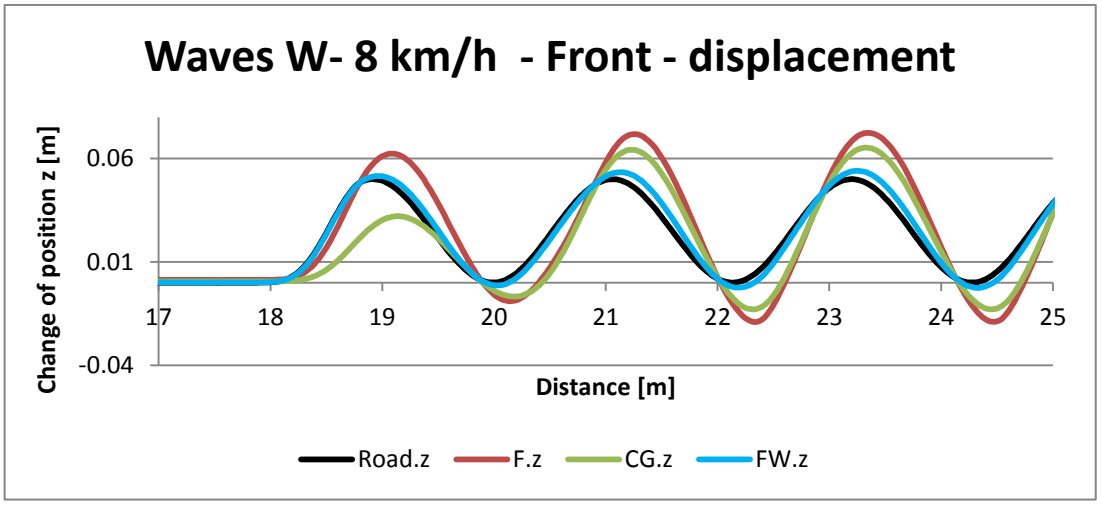

Figure 154 – Waves W 8km/h, change of vertical position on the front.

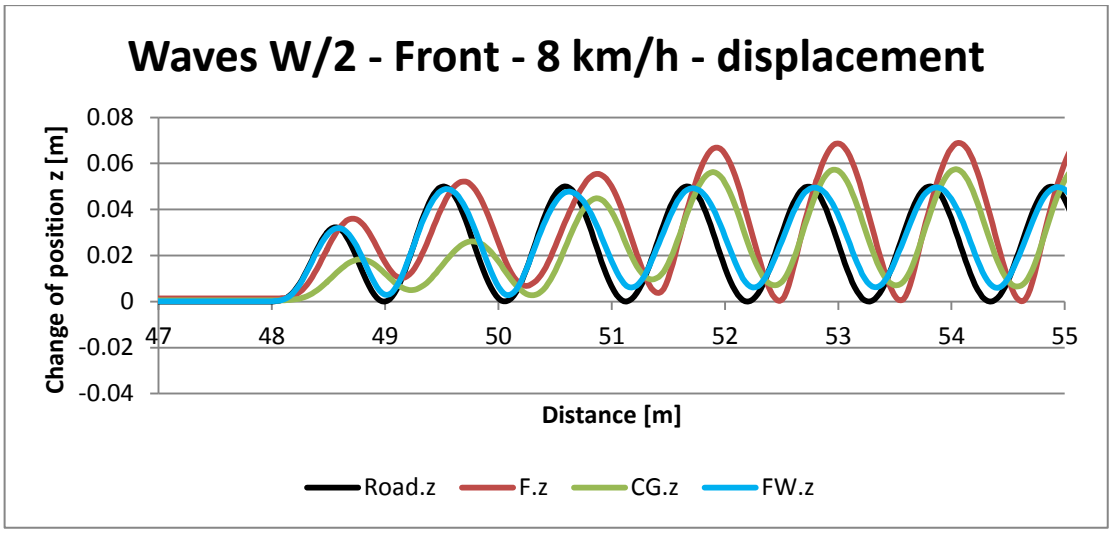

Figure 155 – Waves W/2 8km/h, change of vertical position on the front.

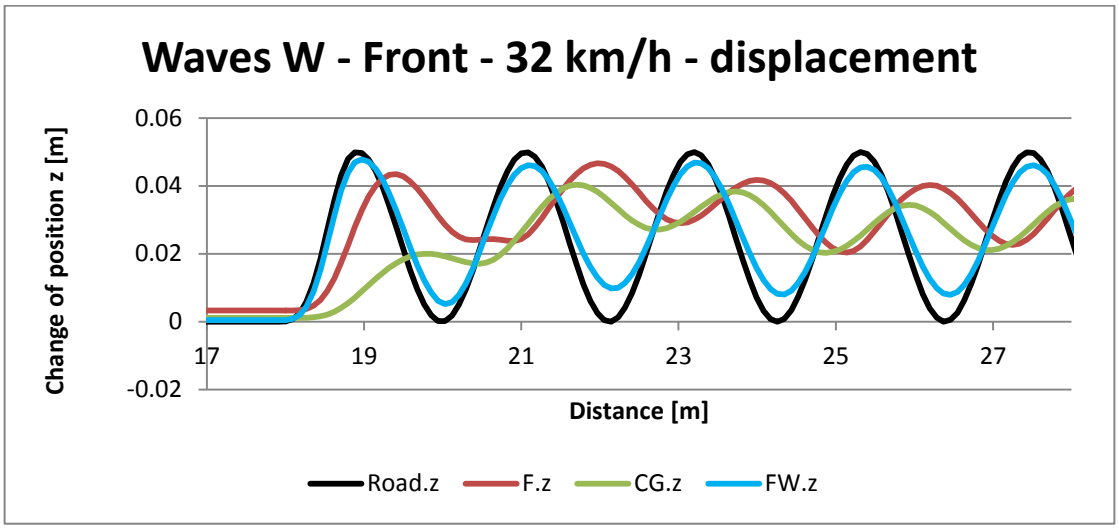

Figure 156 – Waves W 32 km/h, change of vertical position on the front.

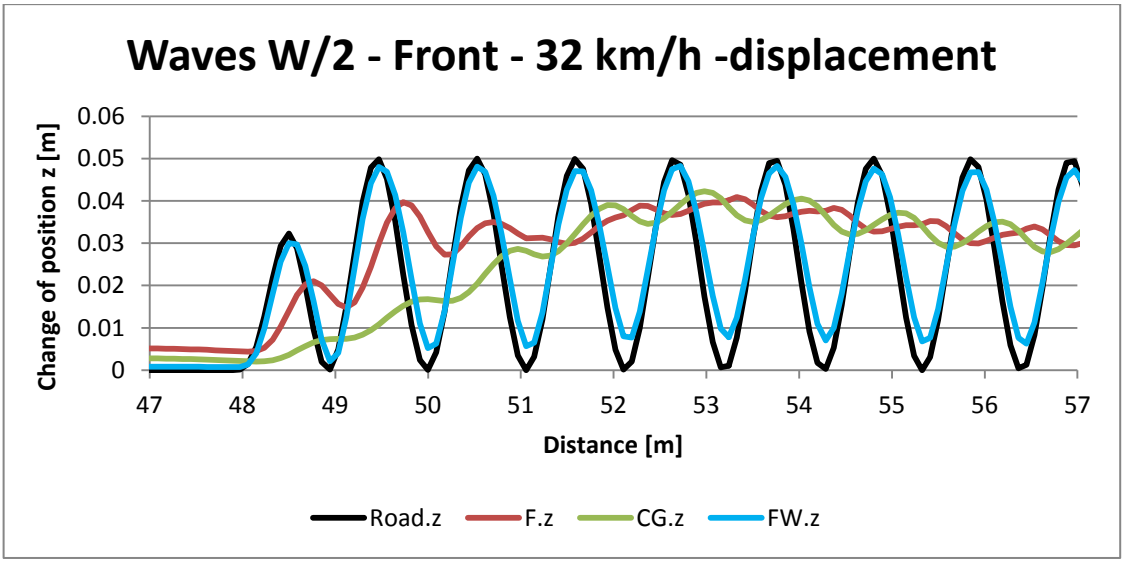

Figure 157 – Waves W/2 32 km/h, change of vertical position on the front.

7. Conclusion

The task of this thesis was to design a rear suspension for a small city electric car. The vehicle is meant to be autonomous and should be used in a car sharing programme. To meet strict space requirements the rear axle needs to be foldable.

At first, research on small city vehicles was made what showed there never has been a production foldable vehicle available in the market. Because of that, we had to find inspiration in non-foldable production cars and foldable prototypes. The closest production vehicle to our vehicle is *Renault Twizy* which became the main inspiration and competitor of our vehicle.

Required maximal velocity of the vehicle is at least 100 km/h, according to the task. As the vehicle is intended to be homologized as a quad, it can be equipped with a motor of the maximal nominal power of only 15 kW. Assuming some simplified estimations of the calculation, it was proved, that this power is enough to go even 102.7 km/h. The results also showed that the acceleration of the vehicle (0-45km/h; 4.9s) should be slightly better as it boasts a higher power than *Twizy* (0-45 km/h; 6.1s).

The folding mechanism was designed to be as simple as possible, thus it is actuated by rear wheels powered by the traction electric motor. The calculation proved the possibility of this concept where tire grip is the most crucial parameter. The shortest length of the vehicle in parking mode was 2110 mm (according to CAD model) which is acceptable in case of perpendicular parking in parallel parking space with a width of 2 metres.

Taking into account previous research of small city vehicles it was decided to use a rear MacPherson suspension which can be also seen in *Twizy*. The main reason for this decision was small longitudinal space requirements, low weight and the possibility of sharing of some of the parts with the front MacPherson suspension, thus saving overall manufacturing costs. Theoretical calculations of spring stiffness and design, damper, bearing and silentblocks straining were performed. All of the obtained information was implemented in a CAD model in *Catia*, showing the conceptual design of the rear suspension. The vehicle track width was chosen 1100 mm to fit two vehicles in one lane. The kinematic model was assembled in order to get and tune kinematics of the rear suspension.

CarMaker software was used to test the dynamic properties of the vehicle. The calculated values of the suspension system were applied as an input in the software. Also, the kinematics derived in *Catia* were rewritten into text *.skc* file to import designed kinematics of the rear wheels. As we don't know anything about the rest of the car, some of the input parameters must have been approximately estimated. The tests were made according to ISO standards for passenger cars. Satisfactory results were achieved in most of the tests, but the obstacle avoidance test (VDA) revealed the weakness of a short-track vehicle, rollover stability. The suspension must have been stiffened, the damping ratio was increased and antiroll bars stiffness was enhanced. This contributed to the successful passing of the VDA test at the speed of 53 km/h. However, at higher speeds above 56 km/h dangerous rollover came which must be eliminated by electronic stability programme to improve the safety of this vehicle. On the other hand, those tunings negatively influenced the comfort of the ride. In the remaining tests the vehicle behaved stable, slightly

oversteering, but under control in every situation. The longitudinal ride stability was enhanced by a long wheelbase, provided by the folding mechanism. As the input parameters will be more exactly specified during further development, the dynamic test of the vehicle can significantly change. According to the tests, we can confirm that the vehicle with this conception can work and can achieve good dynamic properties despite the short track width. However, roll stability is still critical and must be supported by electronic systems.

Why a foldable car has never been produced? Maybe it has been caused because of its complexity and high manufacturing costs. Maybe the folding mechanism hasn't brought convincing benefits over conventional cars. We need to know the answer to this question if we want to bring something completely new to the market. If we want to apply a foldable design to a vehicle it has to bring significant advantages over a similar car, in our case *Renault Twizy*. Both of them can carry two persons seated in a longitudinal line. The shortest achievable length of the vehicle is 2110 mm (*Twizy* 2337 mm) which makes it easier to park everywhere. The maximal length reaches 2810 mm. Unfolding opens large boot space for luggage or packages. The much longer wheelbase of 2134 mm (Twizy 1686 mm) can offer enhanced longitudinal stability and comfort of the ride. However, the decisive parameter is bending and torsional stiffness of the folding mechanism. It also must be reliable and cheap to manufacture.

Small electric cars can be the future of city mobility. In comparison with larger electric cars, they can be significantly cheaper as they only need a small reasonable-priced battery which is currently the most expensive part of electric vehicles. Electric energy consumption is also lower as they are lightweight. Electric vehicles are not suitable for long journeys, because in that case, it must have a large battery which is heavy, expensive and it takes a long time to charge it.

Autonomous driving is today's trend in automotive development. This feature would widen a range of possible usages of the vehicle. It can be then used as autonomous delivery, taxi or the user would choose between autonomous or non-autonomous driving while it is shared via car sharing programme. However, autonomous driving has been being developed for many years and it is still struggling with application to production cars.

The sales of Twizy haven't reached expected values. Actually, it doesn't offer much more than a scooter motorcycle, but for more than four-times higher price (comparison with Honda PCX 125 equipped with an internal combustion engine). Twizy also can't bring the comfort of a car during rainy or winter days. If we want to make our car more successful, it has to be comfortable for passengers in all seasons. Nowadays, it is still more advantageous for an end customer to own a standard car powered by an internal combustion engine, mainly because of the price and practical reasons.

European cities are planning to ban cars with internal combustion engines in their centres. If it happens, it can cause a rise in the category of small electric city vehicles. Our vehicle can then serve in car sharing programme in the city centre. As the larger electric vehicles are and will be expensive, people would rather keep their more universal cars with ICE and use a shared electric vehicle in the city centre. Symbiosis with public transportation in car sharing programme is a must. However, it is important to be aware of the fact, that the success of such a vehicle is strongly dependent on future regulations.


TWIZY


e-business services

References

Literature

[1] VLK, František. *Podvozky motorových vozidel*. 2. vyd. Brno: František Vlk, 2003. 392 s. ISBN 80-239-0026-9.

[2] HLINOVSKÝ, Bc. Tomáš. *Optimal Control of Mathematical Model of the Electrovehicle*. Prague, 2015. Master thesis. ČTU in Prague, Faculty of Electrical Engineering.

[3] VLK, František. *Dynamika motorových vozidel*. 2. vyd. Brno: František Vlk, 2003. ISBN 80-239-0024-2.

[4] JAZAR, Reza N. *Vehicle Dynamics: Theory and Applications*. 2008. ISBN 978-0-387-74244-1.

[5] The Czech Republic. Act no.56/2001, Zákon o podmínkávh provozu vozidel na pozemních komunikacích.. Available from: https://www.psp.cz/sqw/sbirka.sqw?cz=56&r=2001

[6] *ČSN 73 6056: Odstavné a parkovací plochy silničních vozidel*. 2011.

[7] *ČSN 73 6101: Projektování silnic a dálnic*. 2018.

[8] REIMPELL, Jornsen, Helmut STOLL a Jurgen BETZLER. *The Automotive Chassis: Engineering Principles*. 2001. ISBN 0-7506-5054-0.

[9] VALDECKÝ, Marek. *Návrh podvozku osobního automobilu*. 2016. Master thesis. CTU in Prague.

[10] BUDYNAS, Richard G., NISBETT, J. Keith, SHIGLEY, J. Edward. Shigley's mechanical engineering design. 10th edition. New York, NY: McGraw-Hill Education, 2015. ISBN 0073398209

[11] MICHALEC, Jiří, a kol.: *Pružnost a pevnost II*, Vydavatelství ČVUT, Praha 1994.

[12] APETAUR, Milan, HANKE, Miroslav, KEJVAL, Zdeněk, ROST, Milan. Karosérie. Praha: Editační středisko ČVUT, Praha 1, Husova 5, 1985.

[13] *ISO 3888-1-2018: Passenger cars - Test track for a severe lane-change manoeuvre, Part 1: Double lane-change*.

[14] *ISO 3888-2:2002: Passenger cars - Test track for a severe lane-change manoeuvre - Part 2: Obstacle avoidance*.

[15] *ISO 4138:2012: Passenger cars - Steady-state circular driving behaviour - Open-loop test methods*.

[16] *ISO 7975:2006: Passenger cars - Braking in a turn - Open-loop test method*.

[17] *ISO 8725:1988: Road vehicles - Transient open-loop response test method with one period of sinusoidal input*.

Internet

[18] *A2mac1.com - Automotive benchmarking* [online]. [cit. 2019-08-15]. Available from: www.a2mac1.com

[19] *TWIZY/Electric/Renault UK* [online]. [cit. 2019-08-15]. Available from: https://www.renault.co.uk/vehicles/new-vehicles/twizy.html

[20] *Nanjing Jiayuan Special Electric Vehicles Manufacture Co., Ltd: Jianyuan City Spirit* [online]. [cit. 2019-08-15]. Available from: http://www.jiayuan-ev.com/english/pro/detail.aspx?mtt=1&id=87

[21] *VXT: eCHOICE 2* [online]. [cit. 2019-08-15]. Available from: https://vxt.cz/echoice-osobni/

[22] *Re.volt/ carsharing revolution* [online]. [cit. 2019-08-15]. Available from: https://revolt.city/

[23] *Smart fortwo/ smart Česká republika* [online]. [cit. 2019-08-15]. Available from: https://www.smart.com/cz/cs/index/smart-fortwo-453.html

[24] *Auto.cz: Smart Fortwo 1.0 (52 kW) – Skořápka do města* [online]. [cit. 2019-08-15]. Available from: https://www.auto.cz/smart-fortwo-1-0-52-kw-skorapka-do-mesta-85704

[25] *Auto.cz: Smart ForTwo (1998 - 2007): Mikroexperiment* [online]. [cit. 2019-08-15]. Available from: https://www.auto.cz/smart-fortwo-1998-2007-mikroexperiment-1583

[26] *Alfa Romeo 159 (1950)* [online]. [cit. 2019-08-15]. Available from: https://i.pinimg.com/originals/4a/8b/69/4a8b69dda8df811244b36df1ce32d406.jpg

[27] *Life axle with leaf springs* [online]. [cit. 2019-08-15]. Available from: https://www.counterman.com/counter-view-live-axle/

[28] *Alfa Romeo De Dion rear axle* [online]. [cit. 2019-08-15]. Available from: http://www.movitcars.com/images/alf6ha.jpg

[29] *Volkswagen ČR: e-up! - Modely* [online]. [cit. 2019-08-15]. Available from: https://www.volkswagen.cz/e-up

[30] *Auto.cz: Volkswagen e-Up! – Dává smysl?* [online]. [cit. 2019-08-15]. Available from: https://www.auto.cz/volkswagen-e-up-dava-smysl-82531

[31] *DTV: Theme: Suspension – Not Quite De Dion* [online]. [cit. 2019-08-15]. Available from: https://driventowrite.com/2016/03/08/suzuki-suspension-not-quite-de-dion/

[32] *MIT Media Lab: Overview CityCar* [online]. [cit. 2019-08-15]. Available from: https://www.media.mit.edu/projects/citycar/overview/

[33] *Hiriko presentation* [online]. [cit. 2019-08-15]. Available from: https://www.slideshare.net/GorkaEspiau2/hiriko-presentation-2-11?from_action=save

[34] *EL PAIS: The failed electric car that cost the Spanish government €17 million* [online]. [cit. 2019-08-15]. Available from: https://elpais.com/elpais/2015/04/07/inenglish/1428404457_818634.html

[35] *Wikipedia: Hiriko* [online]. [cit. 2019-08-16]. Available from: https://en.wikipedia.org/wiki/Hiriko

[36] *Renault Zoom Electric City Car Concept 1992* [online]. [cit. 2019-08-16]. Available from: http://www.autoconcept-reviews.com/cars_reviews/renault/renault-zoom-concept-1992/cars_reviews-renault-zoom-concept-1992.html

[37] *Diseno-Art: Renault Zoom/Concept Cars* [online]. [cit. 2019-08-16]. Available from: http://www.diseno-art.com/encyclopedia/concept_cars/renault_zoom.html

[38] *Wikipedia: Renault Zoom* [online]. [cit. 2019-08-16]. Available from: https://en.wikipedia.org/wiki/Renault_Zoom

[39] *Walzel, Bernhard & Brunner, Helmut & Hirz, Mario. (2016). NEW FOLDABLE URBAN CAR CONCEPT.* [online]. [cit. 2019-08-16]. Available from: https://www.researchgate.net/publication/308898621_NEW_FOLDABLE_URBAN_CAR_CONCEPT

[40] *SEAT: Seat Minimó* [online]. [cit. 2019-08-16]. Available from: https://www.seat.com/company/news/cars/seat-minimo-mwc.html

[41] *Casple-Podadera Folding city car* [online]. [cit. 2019-08-15]. Available from: https://wordlesstech.com/casple-podadera-folding-city-car/

[42] *Prestige electric cars: Casple-Podadera* [online]. [cit. 2019-08-16]. Available from: https://www.prestigeelectriccar.com/en/articles/711/Casple-Podadera_

[43] Zechmair, Derrick & Steidl, Kurt. (2012). *Why the Induction Motor Could be the Better Choice for Your Electric Vehicle Program.* World Electric Vehicle Journal. 5. 546-549. 10.3390/wevj5020546.

[44] *Alibaba.com: Electric Car Motor Power 15kW Ac Induction Motor* [online]. [cit. 2019-08-16]. Available from: https://www.alibaba.com/product-detail/electric-car-motor-power-15kw-ac_60021760877.html?spm=a2700.7724857.normalList.22.23782451iVzc4u

[45] *Bosch Rexroth AG: High-speed asynchronous motors* [online]. [cit. 2019-08-16]. Available from: https://www.boschrexroth.com/en/xc/products/product-groups/electric-drives-and-controls/motors-and-gearboxes/high-speed-motors/1mb

[46] *Renault Česká Republika: Brozura Twizy* [online]. [cit. 2019-08-16]. Available from: https://www.renault.cz/content/dam/Renault/CZ/pdf/brochures/twizy-brochure.pdf

[47] *Daimler Global Media Site* [online]. [cit. 2019-08-16]. Available from: https://media.daimler.com/marsMediaSite/en/instance/ko/Start.xhtml?oid=4836258

[48] *Project Gutenberg Self-Publishing: Automobile drag coefficients* [online]. [cit. 2019-08-16]. Available from: http://self.gutenberg.org/articles/automobile_drag_coefficients

[49] Material data sheet: Steel grade 61SiCr7. Ovako.com [online]. [cit. 2019-08-16]. Available from: http://steelnavigator.ovako.com/steel-grades/61sicr7/

[50] *SKF Česká republika: Kuličková ložiska s kosoúhlým stykem, dvouřadá - 3207 A-2Z* [online]. [cit. 2019-08-16]. Available from: https://www.skf.com/cz/products/bearings-units-housings/ball-bearings/angular-contact-ball-bearings/double-row-angular-contact-ball-bearings/double-row/index.html?designation=3207%20A-2Z

[51] Development of an internal combustion engine fuel map model based on on-board acquisition - Scientific Figure on ResearchGate. Available from: https://www.researchgate.net/figure/SAE-Coordinate-system-adopted-by-Gillespie-1992_fig41_312577762 [accessed 16 Aug, 2019]

[52] *Wikipedia: Sideslip angle* [online]. [cit. 2019-08-16]. Available from: https://en.wikipedia.org/wiki/Slip_angle

[53] *IPG Automotive: CarMaker documentation* [online]. [cit. 2019-08-16]. Available from: https://ipg-automotive.com/products-services/simulation-software/carmaker/

[54] *TraceParts* [online]. [cit. 2019-08-18]. Available from: https://www.traceparts.com/en

[55] *Auto.cz: Renault Twizy Urban* [online]. [cit. 2019-08-19]. Available from: https://www.auto.cz/renault-twizy-urban-zivot-v-bubline-125145

[56] *Suspension designer: Kinematic wheel recession* [online]. [cit. 2019-08-19]. Available from: https://www.suspensiondesigner.com/kpi-kinematic-wheel-centre-recession/

[57] *3DS: Catia V5* [online]. [cit. 2019-08-19]. Available from: https://academy.3ds.com/en/software/catia-v5-student-edition

List of abbreviations

ICE	Internal combustion engine
UK	The United Kingdom
ABS	Anti-lock Brake System
CV	Constant velocity (joint)
VW	Volkswagen
MIT	Massachusetts Institut of Technology
EU	The European Union
PMSM	Permanent magnet synchronous motor
AC	Alternating current
DC	Direct current
ČSN	Česká technická norma
ISO	International Organization for Standardization
DIN	Deutsches Institut für Normung
CAD	Computer aided design
CG	Centre of gravity
ESP	Electronic stability programme
VDA	Verband der deutschen Automobilindustrie

Attachments

1. CAD Model
2. Excel calculations
3. CarMaker simulations
4. Electronic version of the thesis